NON-DESTRUCTIVE EVALUATION OF MULTI-LAYERED GFRP COMPOSITE STRUCTURES USING LOW FIELD NMR

A dissertation work submitted in partial fulfilment of the requirements for the award of the degree of

DOCTOR OF PHILOSOPHY

in

MECHANICAL ENGINEERING

by

SANJAYA KUMAR SAHOO

(Roll No. 701617)

Supervisor:

Dr. R. NARASIMHA RAO

(Professor)

Co-Supervisor:

Dr. MANOJ KUMAR BURAGOHAIN

(Scientist "G", ASL, DRDO, Hyderabad)

DEPARTMENT OF MECHANICAL ENGINEERING

NATIONAL INSTITUTE OF TECHNOLOGY

WARANGAL

JULY 2021

NON-DESTRUCTIVE EVALUATION OF MULTI-LAYERED GFRP COMPOSITE STRUCTURES USING LOW FIELD NMR

A dissertation work submitted in partial fulfilment of the requirements for the award of the degree of

DOCTOR OF PHILOSOPHY

in

MECHANICAL ENGINEERING

by

SANJAYA KUMAR SAHOO

(Roll No. 701617)

Supervisor:

Dr. R. NARASIMHA RAO

(Professor)

Co-Supervisor:

Dr. MANOJ KUMAR BURAGOHAIN

(Scientist "G", ASL, DRDO, Hyderabad)

DEPARTMENT OF MECHANICAL ENGINEERING

NATIONAL INSTITUTE OF TECHNOLOGY

WARANGAL

JULY 2021

DEPARTMENT OF MECHANICAL ENGINEERING
NATIONAL INSTITUTE OF TECHNOLOGY
WARANGAL – 506004, INDIA

CERTIFICATE

This is to certify that the work presented in the thesis entitled **"NON-DESTRUCTIVE EVALUATION OF MULTI-LAYERED GFRP COMPOSITE STRUCTURES USING LOW FIELD NMR"** which is being submitted by **Mr. Sanjaya Kumar Sahoo (Roll No. 701617),** is a bonafide work submitted to National Institute of Technology, Warangal in partial fulfilment of the requirement for the award of the degree of **Doctor of Philosophy** in **Mechanical Engineering.**

To the best of our knowledge, the work incorporated in the thesis has not been submitted to any other university or institute for the award of any other degree or diploma.

Prof. R. Narasimha Rao
Thesis Supervisor
Professor
Department of Mechanical Engineering
National Institute of Technology
Warangal, India – 506004.

Dr. Manoj Kumar Buragohain
Thesis Co-Supervisor
Scientist "G"
Advanced Systems Laboratory
Defence R & D Organisation
Hyderabad, India – 500058.

Prof. A. Kumar
Chairman, DSC
Professor and Head
Department of Mechanical Engineering
National Institute of Technology
Warangal, India – 506004.

Approval Sheet

This Thesis entitled **Non-Destructive Evaluation of Multi-layered GFRP Composite Structures using low field NMR** by **Sanjaya Kumar Sahoo** is approved for the degree of Doctor of Philosophy

Examiners

……

……

Supervisor

…….

…….

Co-Supervisor

…….

…….

Chairman

……..

……..

Date:

Place:

Declaration

This is to certify that the work presented in the thesis entitled **Non-Destructive Evaluation of Multi-layered GFRP Composite Structures using low field NMR** is a bonafide work done by me under the supervision of **Dr. R. Narasimha Rao**, Professor, Mechanical Engineering Department and co-supervision of **Dr. Manoj Kumar Buragohain**, Scientist "G", Advanced Systems Laboratory, DRDO, Hyderabad and was not submitted elsewhere for the award of any degree.

I declare that this written submission represents my ideas in my own words and where others' ideas or words have been included, I have adequately cited and referenced the original sources. I also declare that I have adhered to all principles of academic honesty and integrity and have not misrepresented or fabricated or falsified any idea/ data/ fact/ source in my submission. I understand that any violation of the above will be a cause for disciplinary action by the Institute and can also evoke penal action from the sources which have thus properly cited or from whom proper permission has not been taken when needed.

……..

(Signature)

Sanjaya Kumar Sahoo

(Name of the Student)

701617

(Roll Number)

Date:……..

DEDICATED

TO

MY BELOVED PARENTS,

TEACHERS

&

THE ALMIGHTY

Acknowledgements

First of all, I would like to express my deepest regards and immense gratitude to my supervisors **Prof. R. Narasimha Rao** and **Dr. Manoj Kumar Buragohain** for their earnest involvement, constant encouragement, active guidance and permanent impulse at all the stages of my work.

I would like to express my special thanks to **Dr. Kuchipudi Srinivas** for providing the invaluable opportunity to work on single-sided NMR as well as theoretical support and useful discussions during the last four years. Many thanks also for carefully reading and correcting this work.

I would like to thank all the members of doctoral scrutiny committee, **Prof. N. Selvaraj**, **Prof. V. Suresh Babu** and **Prof. N. Narasaiah** for their valuable time and suggestions to improve my work. Thanks to the chairman of doctoral scrutiny committee **Prof. A. Kumar** and former chairmen **Prof. R. Narasimha Rao**, **Prof. N. Selvaraj**, **Prof. P. Bangaru Babu**, **Prof. S. Srinivasa Rao** for sparing their valuable time to review, verify and approve semester progress reports.

I am very much thankful to **CPDC team**, **Shri Deo Kumar Verma**, SFC, Jagdalpur and **Shri V. L. N. Rao**, M/s PEL, Pedakandukur who prepared samples in a very short time and professionally. I am highly obliged to recognize the timely testing support by **NDE Division/CPDC**, **NDED/DRDL**, **SITAR Group/ASL**, Hyderabad.

I wish to thank especially **Dr. Ch Sri Chaitanya** and **other research scholars** who had always been so kind to me and took special interest to solve my problems. Perhaps words are not enough to acknowledge their help during the last four years.

I wish to thank **Head, HRDG** and **Director, ASL** for their motivation, support and timely processing of my work.

I am very much grateful to **Shri S. M. Gajbhiye** for the help concerning the computer related problems and **Shri V. Kalyan Chakravarty** for many hours of fruitful discussions. Special thanks to **Abhijith, Kamlesh, Praveen, Srinivas, Madhukar, my tennis friends** and **other colleagues** for their timely help I needed.

At the end, I want to say the biggest thanks in this world for those who gave me the strength to survive, the power to move on, the reason to love: my late mother **Smt. Kumudini Sahoo** and my late father **Shri Radhashyam Sahoo**. I am also deeply thankful to my brothers late **Shri Bijaya Kumar Sahoo** and **Shri Ajaya Kumar Sahoo**, sisters **Smt. Nalini Prava Sahoo** and **Smt. Jhunu Sahoo**, mother-in-law **Smt. Anasuya Sahoo**, brother-in-law **Shri Surya Prakash Sahoo,** aunt **Dr. Lalita Manjari Sahoo** and their families for their moral support and inspiration throughout this work without which I would not have been able to reach this stage.

The last thoughts are for my wife **Dibyasikha**, my sons **Arnav** and **Arnesh**. I did not find the right words and perhaps the words I have are not enough to express my thanks to you. Thus, I only say thank you for everything.

Sanjaya Kumar Sahoo

Contents

List of Figures

List of Tables

List of Abbreviations and Symbols

NDE	:	Non-destructive Evaluation
NDT	:	Non-destructive Testing
NMR	:	Nuclear Magnetic Resonance
SRM	:	Solid Rocket Motor
GFRP	:	Glass Fibre Reinforced Polymer or Plastics
UV	:	Ultraviolet
RF	:	Radio Frequency
LPT	:	Liquid Penetrant Testing
MPT	:	Magnetic Particle Testing
ECT	:	Eddy Current Testing
AET	:	Acoustic Emission Testing
IRT	:	Infrared Thermography
IR	:	Infrared Radiation
UT	:	Ultrasonic Testing
RT	:	Radiographic Testing
MeV	:	Million electron Volts
AUS	:	Acousto-Ultrasonic Scanning
CT	:	Computed Tomography
MWNDE	:	Microwave NDE
Hz	:	Hertz
KHz	:	Kilohertz
MHz	:	Megahertz
A^0	:	Angstrom
lux	:	Unit of illuminance
mm	:	Millimetres
cm	:	Centimetres
km	:	Kilometres
µm	:	Micrometres
nm	:	Nanometres

ms	:	Milliseconds
μs	:	Microseconds
g	:	Gram (unit of weight)
cc	:	Cubic centimetre
cP	:	Centipoise
^{0}C	:	Degree Celsius
K	:	Kelvin
PoP	:	Plaster of Paris
CNC	:	Computer Numerical Control
MRI	:	Magnetic Resonance Imaging
MOUSE	:	Mobile Universal Surface Explorer
FID	:	Free Induction Decay
B_0	:	Static magnetic field vector
B_1	:	Radio Frequency magnetic field vector
CPMG	:	Carr-Purcell-Meiboom-Gill
ΔE	:	Energy level difference
k	:	Boltzmann constant
h	:	Planck's constant
ω	:	Larmor or precession angular frequency
γ	:	Gyromagnetic ratio of nucleus
T_2	:	Transverse relaxation time

Abstract

The application of composite materials in components and structures has evolved due to the need to reduce structural weight and improve performance. Other attributes of composite materials, such as corrosion resistance, excellent surface profiles, enhanced fatigue resistance and tailored performance have also been significant contributors to the rapid rise in composite materials application.

Composite structures with multi-layered configurations are typically used in solid rocket motors (SRMs) in the aerospace field. Fiber reinforced composite structures with rubber insulation layer adhesively bonded is known to be one such advanced material for rocket motor application. Adhesive liner, an integral part of an SRM, is used to bond the propellant to the rubber insulator covering the inner surface of the rocket motor case. Integrity of these adhesively bonded multi-layered composite structures is important to serve the intended purpose i.e., reliable performance of the rocket motor. In addition to the unavoidable variations in the processing parameters of multi-layered composite structures, other processes such as transportation and handling including the subsequent storage and usage may also introduce different types of defects in the structures. Long duration storage and usage generally results in ageing and degradation, which can give rise to the generation of interfacial defects such as de-bonds, delamination, airgaps etc. and defects within constituent materials like cracks, tears, voids, porosity etc. Composite structures can fail catastrophically due to weakening of strength in presence of above defects. There could be economical and strategic loss due to the catastrophe. Therefore, the detection and characterization of such type of defects is very essential to avoid catastrophic failure. The aim of this study is to evaluate the defect detection capability of low field nuclear magnetic resonance (NMR) and to estimate the defect parameters like precise depth and size by depth profiling non-destructively.

For the present study, glass fiber reinforced polymer (GFRP) flat and cylindrical samples were fabricated by filament winding process. Composite surface was prepared, followed by application of primer and rubber solution. Then rubber lining was carried out and vulcanized. Then solid propellant in slurry form was cast on GFRP-rubber lined flat and cylindrical structure. To retain rubber insulation to propellant bond intact, a carbon black based adhesive liner compatible to both rubber insulation and propellant was applied before propellant casting.

Experiments were conducted on both flat and cylindrical samples using single-sided low field NMR having magnetic field strength of 0.3T (12.88 MHz RF frequency) to detect and characterize planar defects within the constituent materials as well as bonded interfaces with a spatial resolution of 100 μm non-invasively. NMR results indicated distinct signal intensity values for different constituent materials. Results were compared with traditional non-destructive evaluation (NDE) techniques like acousto-ultrasonic testing and X-ray radiography and found that single-sided low field NMR is more sensitive. The present study revealed the applicability of single-sided low field NMR for onsite measurement of thickness and relaxation times of constituent materials of multi-layered composite structures. Overlapping/collinear defects at multiple interfaces were detected and characterized which is not possible by conventional ultrasonic testing and X-ray radiography. Depth profile study of flat and cylindrical structures indicated that the depth profiling is not affected by the shape of the sample for assessing the soundness of constituent materials and integrity of the bonded interfaces.

1. INTRODUCTION

1.1. Introduction

Composite materials must be regarded as a very different media from metals when considering which non-destructive evaluation (NDE) methods are appropriate. Generally, reinforced plastics have poor electric conductivity, low thermal conductivity, high acoustic attenuation and most importantly significant anisotropy of mechanical and physical properties. The life of a metal component is determined by the nucleation and growth of cracks or damage in the material. However, a fibre-reinforced composite is heterogeneous medium that can contain multiple defect geometries caused by improper cure, fibre misalignment, inclusions, poor reinforcement distribution, machining damage, fastener fretting and environmental degradation.

The application of composite materials in components and structures has evolved due to the need to reduce structural weight and improve performance. Other attributes of composite materials, such as corrosion resistance, excellent surface profiles, enhanced fatigue resistance

and tailored performance have also been significant contributors to the rapid rise in composite materials application. However, defects and damages still occur in composite materials and it is the assessment of defect and damage criticality and the subsequent repair requirements that currently challenging for users of composite materials. When composite materials components are damaged or defective in some way, the users need to determine the location, orientation, number, size, shape, depth, type and extent of the anomaly by suitable NDE techniques.

NDE is a method of examining an object (either a material or a component or a system) of any type, size or shape to determine the presence or absence of any discontinuities or flaws or to evaluate (to examine and judge carefully) other material characteristics without impairing its future usefulness. Evaluation is nothing but a review of the indications noticed to determine whether the object meets the specified acceptance criteria. NDE plays a very vital role not only in the quality control of the finished product but also during various stages of processing or manufacturing such as prior to manufacturing at raw materials stage and during manufacturing as a process control check. NDE is also used as a tool to monitor health or condition of various products during operation or usage to assess and predict the remaining life of the product while retaining its structural integrity. Table 1.1 describes the advantages and limitations of NDE over destructive testing. NDE enables optimum utilization of products or components without sacrificing or compromising safety. The use of advanced computers for data acquisition and processing and automation for reliable testing have largely improved the health monitoring of complex components, plants and machineries. The dependency on operators for routine testing is reduced and thus concentration can be more on the technological aspects. Finally, the end result is saving in cost, time and improvement in precision and reliability of the results obtained [1-3].

Table 1.1 Comparison of Non-destructive and Destructive Testing

Non-destructive Testing	Destructive Testing
Tests are conducted directly on the components. Hence, each and every component can be tested i. e. 100% inspection on actual components is possible.	Tests are not conducted directly on the components. Hence, sampling is required and correlation between the sample and component needs to be established.
Test piece does not get damaged.	Test piece gets damaged.

Many NDE methods can be applied on the same component. Hence, many or all the properties of interest can be measured.	A single test may measure only one or a few of the properties.
Repeated tests of a component over a period of time are possible.	Repeated tests of a component over a period of time can't readily be possible.
In-service testing is possible.	In-service testing is not possible.
Measurements are indirect and hence reliability is to be verified	Measurements are direct and reliable
Usually qualitative measurements. Measurements can also be done quantitatively.	Usually quantitative measurements.
Skilled judgement and experience are required for evaluation of indications.	Correlation of test measurements with material properties is direct.

NDE methods range from the simple to the intricate. Visual testing is the simplest of all. Surface discontinuities invisible to the normal human eye may be revealed by penetrant or magnetic methods. If discontinuities are beyond the surface level, NDE methods capable of examining the interior like ultrasonics or radiography may be required. The major NDE methods regularly used by the industries for various diagnostic applications are:

a) Visual testing (with or without optical aid)

b) Leak testing

c) Optical holography

d) Liquid penetrant testing (LPT)

e) Magnetic particle testing (MPT)

f) Eddy current testing (ECT)

g) Acoustic emission testing (AET)

h) Infrared thermography (IRT)

i) Ultrasonic testing (UT)

j) Radiographic testing (RT)

k) Real time radiography (RTR)

Most of the NDE methods work on a simple principle that a suitable beam of energy, which is capable of interacting with the discontinuity to be detected, is launched into the components under inspection. The emerging beam out of the component (either reflected, scattered or transmitted) is detected with a suitable detection system, processed and analyzed for its information content. The data thus collected is used to evaluate the soundness of the component for acceptance or rejection. The NDE methods may either be used singly or in conjunction with one another depending upon the kind of application. Generally, there will be some overlap between various methods, but they are complimentary to each other. All these will depend upon the type of flaw present and the shape and size of the components to be inspected. The role of NDE is always to guarantee with a level of confidence that defects having a size greater than the critical size for failure are absent from the component when it is used in service.

Due to the multitude of small inherent variations in the numerous parameters involved at each stage of manufacturing, possibility of ending up with a product containing some defects is difficult to rule out. This is the basic problem all over the world. Discontinuities or anomalies present, if any, might prove to be detrimental to the performance of the components. Therefore, a thorough NDE inspection becomes indispensable to assess the suitability of a product for the specific purpose for which it is made. Judicious application of NDE methods not only saves cost in the long run but also ensures a reliable and satisfactory performance of the components. The essential features, basic principles of the above NDE methods and their advantages and disadvantages are explained briefly in the following sections [4-6].

1.1.1. Visual Testing

Visual testing is probably the first and most widely used method in NDE industry, but last method to be formally acknowledged. History of NDE methods says that the visual testing has been in use since beginning of the civilization. It is simple, easy to apply, quickly carried out and usually low in cost. Even though a component is to be inspected using other NDE methods, a good visual test can reveal gross surface defects thus leading to an immediate rejection of the component and consequently saving much time and money, which would otherwise be spent on more complicated means of testing. It is often necessary to examine for the presence of finer

defects. For this purpose, visual methods have been developed to a very high degree of precision. With the advent of microprocessors and computers, visual testing can be carried out very reliably and with minimum cost. Image processing, pattern recognition and automatic acceptance/rejection choice are used when large number of components are to be inspected.

1.1.1.1 Basic Principle

The basic principle of visual testing is illumination of the component to be examined with light, usually in the visible range. The component is then inspected with naked eye or by magnifying devices and light sensitive devices. The equipment used for visual testing is very simple, but sufficient illumination is highly essential for better interpretation. The surface of the component to be inspected should be checked for cleanliness, presence of foreign materials, corrosion and damage. The region to be inspected should be adequately cleaned before inspection.

1.1.1.2 The Human Eye

The most valuable NDE tool is the human eye, which has excellent visual perception. The eye performs the function of a spectrum analyser that measures the wavelengths (400 to 760 nm) and intensity as well as determining the origin of light (sun or artificial source). The sensitivity of human eye varies for light with different wavelengths. Under ordinary conditions, the eye is most sensitive to yellow-green light, which has a wavelength of 5560 A^0. The human eye will give satisfactory vision over a wide range of conditions. For this reason, eye cannot be a good judge for distinguishing the differences in brightness or intensity, except under the most restricted conditions. For visual examination, adequate lighting i. e. about 800-1000 lux is of prime importance. The period of time during which a human inspector is permitted to work should be limited to not more than 2 hours on continuous basis to avoid errors due to decrease in visual reliability and discrimination due to tiredness or fatigue.

Visual testing of an object by an experienced inspector without optical aids can reveal the following information:

- The general condition of the object
- The presence or absence of oxide film or corrosive product on the surface of the object
- The presence or absence of cracks, orientation and position of cracks
- Surface porosity and other discontinuities
- Potential sources of mechanical weakness like misalignment, sharp notches, etc and

- The results of visual inspection may be of great assistance to other tests

Visual testing is also the primary inspection method for in-service inspections to detect surface defects. Most types of damage scorch, stain, dent, penetrate, abrade or chip the composite surface, making the damage visible. Once damage is detected, the affected area needs to be inspected closer using flashlights, magnifying glasses, mirrors, microscope, borescope (Figure 1.1), endoscope, flexiscope, telescope etc. These tools are used to magnify defects that otherwise might not be seen easily and to allow visual inspection of areas that are not readily accessible. Resin starvation, resin richness, wrinkles, ply bridging, discoloration (due to overheating, lightning strike, etc.), impact damage by any cause, foreign matter, blisters and de-bonds are some of the discrepancies that can be detected by visual inspection. Visual inspection cannot find internal flaws in the composite, such as delamination, de-bonds and matrix crazing. More sophisticated NDT techniques are needed to detect these types of defects to ensure the soundness of the product.

Fig. 1.1 Video Borescope (Source: Klein Tools)

1.1.2 Leak Testing

Leak testing method is used for checking fabricated components and systems of pressure vessels, vacuum devices, electronic components, nuclear reactors, pipelines, gas containers at pressures etc. Leak is a very small opening in the wall of an enclosure capable of allowing liquid or gas from one side of the wall to the other side under pressure or difference in concentration existing across the wall. Unit of measurement used for leak testing is cubic centimeter per second (Leak rate).

Different test methods are available based on the range of leak detection capability. These are broadly grouped as “fine leak methods” and “gross leak methods”. The leak detection range of fine leak methods is 10^{-7} to 10^{-11} cubic centimeter per second. It includes halogen diode sniffer, helium mass spectrometer and argon mass spectrometer etc. The leak detection range of gross leak methods is up to 10^{-4} cubic centimeter per second. It includes bubble tests, pressure rise or drop method, ultrasonic leak detectors and ammonia sensitized paper method etc. Leak test methods are used first to find whether the component is leaking or not (proving test) and then to pin point the location of leak (location test).

1.1.3 Optical Holography

Optical holography is the name given to the method of obtaining an accurate three-dimensional image of a given component for detection of surface strains or deformities. Basically, holography is an optical interferometric technique with high sensitivity to inner surface discontinuities like cracks, de-bonds, delamination, residual stresses, etc. As shown in Figure 1.2, light from a laser source (coherent light) is split into two beams; one beam called the object beam strikes the object surface and gets scattered. This scattered beam is made to interfere with the second part of the original beam and is called as reference beam. This interference pattern can be recorded on a photographic plate which is known as a hologram. If the object is loaded or stressed by suitable means and the hologram is re-exposed, the difference in the configurations arising due to loading produces fringes superimposed on the original object to give three-dimensional pictures.

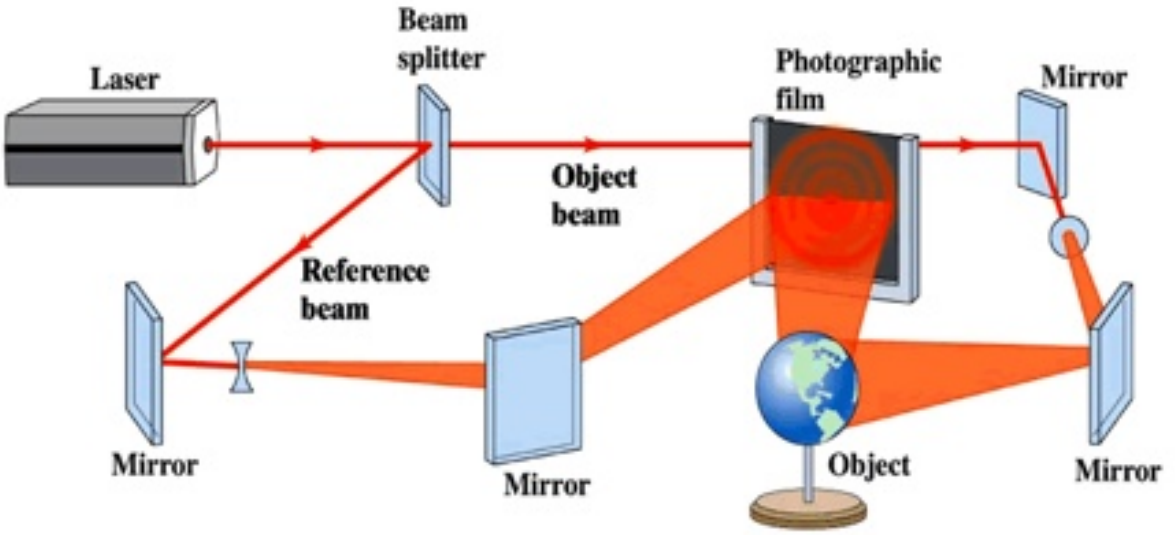

Fig. 1.2 Optical Holography setup (Source: Assignment Point)

Optical holography helps to study the surface condition of an object under stress conditions. Two holograms; one before stressing and the other after stressing are superimposed and viewed with lasers to reveal deformities due to stresses. Major applications of holography using pulsed lasers is for the inspection of laminar structure for non-bonding. The presence of defects such as voids, de-bonds, cracks in the object cause stress concentration in the defective regions and produce abrupt changes in displacements and surface fringe patterns which can be identified and characterized. Holography is used for the NDE of surfaces of highly complicated and precision components without the disadvantages of having to use a high-power microscope. In a simple operation, a hologram can provide a record of the image of an entire surface which can be readily compared with that of a standard defect free surface.

1.1.4 Liquid Penetrant Testing (LPT)

LPT inspection utilizes the natural accumulation of a fluid around a discontinuity to create a recognizable indication of a crack or other surface opening defect. Capillary action attracts the fluid to the discontinuity as compared to its surroundings. In order to locate the area of excess fluid (defect region), the background area must be of sufficient contrast thus leading to distinct detection of the defect on the surface as shown in Figure 1.3. To achieve good defect visibility, the liquid is always either be colored with a bright dye or fluorescent compound.

Fig. 1.3 Liquid penetrant testing of a product

1.1.4.1 Basic Principle

LPT depends mainly on the ability of liquid to wet the surface of a solid object or specimen and flow over that surface to form a continuous and reasonably uniform coating, thus penetrating into cavities that are open to the surface. The ability of a given liquid to flow over a surface and enter surface cavities mainly depends on the surface tension and capillary action. Viscosity, another factor, although has negligible effect on penetrating ability of liquid, affects the flowing ability of penetrant. Highly viscous liquids are not suitable as penetrants because of poor flowability over the surface of the component under inspection; consequently, more time is required to penetrate fine discontinuities or flaws.

Visible light or ultraviolet (UV) light is required for inspection of penetrant indications. Initially, the only detection method used was the unaided observation by the eye of the inspector under visible light. The characteristics of the human eye strongly affect the perception of brightness of an indication. The advantages of this in penetrant inspection is that, regions holding greater amounts of the fluorescent penetrant appear very bright.

1.1.4.2 Test Procedure

There are five essential steps (Figure 1.4) to be followed in this inspection:

A. Surface preparation – involves cleaning of the surface of the material to be inspected such that it is free of contaminants that might interfere with the penetrant performance;
B. Penetrant application – the liquid penetrant is applied to the surface of the part and sufficient “penetration time” is allowed for penetration into the possible surface defects;

C. Excess penetrant removal – after the sufficient dwell time, the excess penetrant is to be removed using a lint-free cloth;
D. Development – the above removal process permits the penetrant in the defects to remain and are made visible by the application of developer;
E. Observation and inspection – the test sensitivity depend upon the penetrating power of dye and the characteristics of defects and test materials. Accessibility and surface properties are the major limitations in this method.

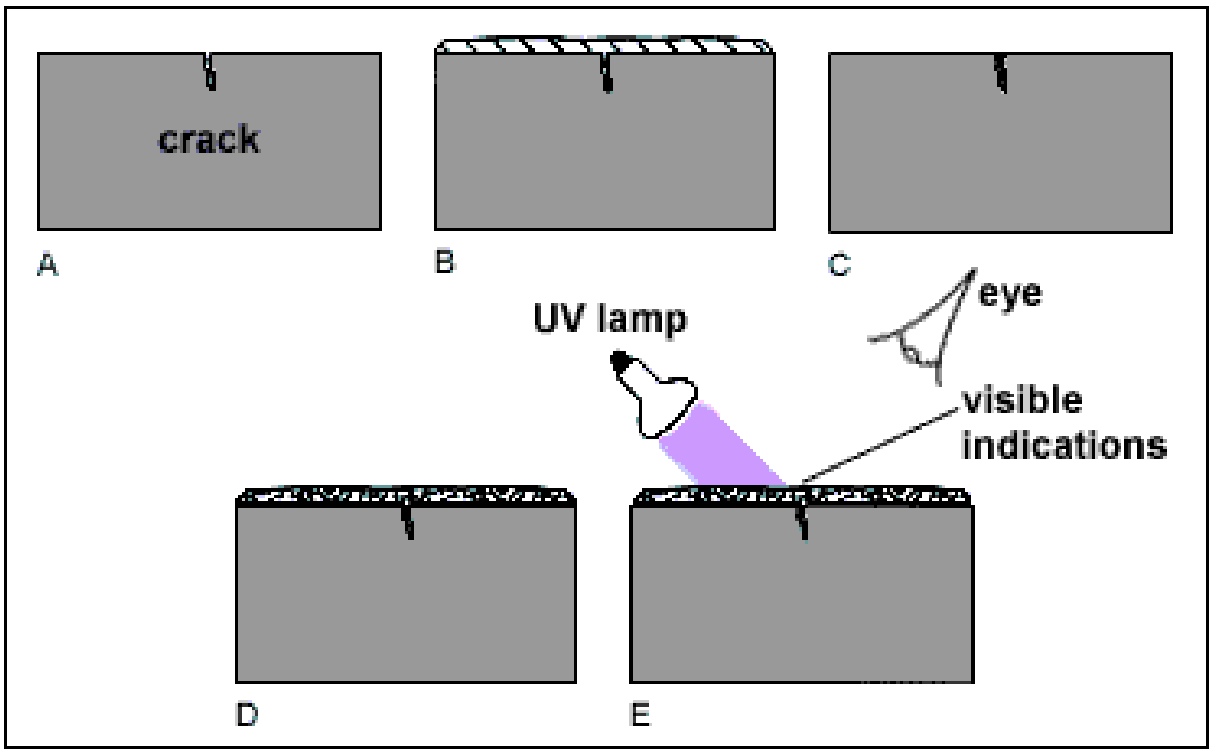

Fig. 1.4 Essential steps of LPT

1.1.4.3 Sensitivity

The sensitivity of LPT method can be defined as the ability of penetrant to reveal a particular type of discontinuity in a material. This is related to fine or wide discontinuities which are deep or shallow in nature. Factors affecting sensitivity are the ability of the penetrant to enter the discontinuity and removal of the penetrant from the surface of the component without its significant removal from the defect. In addition, the penetrant must have the ability to come out of the discontinuity, with the aid of a developer and to form an indication which is readily visible with good contrast with respect to the background.

1.1.4.4 Applications and Limitations

Liquid penetrant testing is mainly used to detect defects such as cracks, laps, seams, porosity etc. in products like pressure vessels, pipes, weld joints etc., which are open to the surface of the test component. LPT method is very reliable in the detection of fatigue cracks which occur during the service life of a material. This method has a significant advantage over other NDT methods, with the possible exception of MPT. This is because of the fact that a part can be tested over its complete surface in a relatively short time, irrespective of shape, size and orientation the defect. In the case of magnetic materials, MPT is preferred because it will also detect subsurface discontinuities, defects filled with oxide and defects covered by paint films. The LPT method has another limitation that it cannot be applied to porous materials.

1.1.5 Magnetic Particle Testing (MPT)

Magnetic particle testing is used for testing of materials (ferromagnetic materials) which can be easily magnetized. This method is capable of detecting flaws open to the surface and just below the surface. The MPT equipment (Figure 1.5) is cheap, robust and can be handled by semi-skilled person without requiring elaborate safety precautions as required for radiography.

1.1.5.1 Basic Principle

Magnets are classified as permanent or temporary. The latter type retains magnetic qualities only as long as a magnetizing force is being applied. Materials are usually classified into three categories: (a) diamagnetic – which are feebly repelled by a strong magnet, (b) paramagnetic – that can be magnetized but only weak and (c) ferromagnetic – those which can be strongly magnetized and are suitable for magnetic particle inspection.

When a test piece is magnetized, magnetic lines of force (magnetic flux) are predominantly inside the ferromagnetic material. The magnetic field introduced into the test piece is composed of magnetic lines of force. Wherever there is a discontinuity which interrupts the flow of magnetic lines of force, some of these lines must exit and re-enter the test piece. These points of exit and re-entry form opposite magnetic poles. When fine magnetic particles are sprinkled onto the test piece, these particles are attracted by these magnetic poles to create a visual indication approximating the size and shape of the discontinuity. It is the abrupt change in permeability that causes this particle build-up.

The magnetic particles can be applied in powder form or as liquid suspension (magnetic ink). Planar flaws such as cracks must be favorably oriented with respect to the direction of the magnetic field for better detectability. The color of the magnetic particles should be in good contrast to the color of the surface of the test piece for easy detection. For highest sensitivity, the flux density should be oriented 90^0 to the flaw. However, it is normally possible to detect discontinuities which lie up to about $\pm 45^0$ to the direction magnetic flux lines. It is important to note that, because of the better sensitivity, when the flaw is at 90^0 to the lines of force, the magnetic flux should be induced in several different directions when the possible flaw orientations are not known.

Fig. 1.5 Magnetic Particle Testing Equipment (Source: DCM Tech)

1.1.5.2 Test Procedure

The following steps are necessary to ensure satisfactory detection of flaws:

(a) Surface preparation of component to be inspected – involves degreasing, removal of loose dust and scale to prevent contamination of the magnetic ink, removal of paint locally of (in case of painted parts) to provide sufficient contact areas for current flow;
(b) Initial demagnetization – Removal of residual magnetism (achieved either during machining on magnetic chucks or handling in the vicinity of any magnetic field) to avoid false indications;
(c) Magnetization of the component – Application of suitable operating values of electrical parameters of AC or DC for optimum magnetization of the test piece.
(d) Application of magnetic particles – The particles used in wet method should be carefully and completely dispersed in a liquid bath of proper consistency and color and flash point. In case of dry method, care must be taken to ensure light and even distribution of magnetic powder so that particle movement towards the leakage field is smooth.
(e) Viewing – The red or black paste or powder indications are viewed under proper illumination. The level of illumination can be 500 lux at the surface. Good daylight is the best.
(f) Marking of indications – All relevant indications should be marked after allowing the ink to drain.
(g) Demagnetization – Demagnetization can only be accomplished totally when a material is heated to approximately 1033K. The basis of electrical demagnetization is the diminishing, reversing magnetizing force adequate to overcome the original field.
(h) Removal of ink from the component – Ink particles can be deleterious during later use of the component or assembly to other components. A paraffin oil wash or hand brush is normally sufficient for removal of the ink.

1.1.5.3 Sensitivity

MPT methods are sensitive to locate small and shallow surface cracks in ferromagnetic materials. In general, a surface discontinuity whose depth is at least five times its opening (width) at the surface will be detected. If the defects sought are usual cracks, comparatively low level of magnetic force will give sufficient build up.

1.1.5.4 Limitations

There are certain limitations for using MPT methods. It can detect only surface opening and subsurface defects in ferromagnetic materials. The operator must know that thin coatings of paint and other nonmagnetic surface layers such as plating adversely affect sensitivity. The magnetic field must be in a direction normal to the discontinuity for proper diagnosis. If required, same procedure needed to be repeated in more than one angle. Local heating and burning of components should be avoided. Complete demagnetization of the test piece is essential before further use.

1.1.6 Eddy Current Testing (ECT)

Eddy current testing is used for sorting materials, measurement and control of dimensions of tubes, sheets and rods, coating thickness and pre-service and in-service examination of heat exchanger tubes for detection of surface/sub-surface defects.

1.1.6.1 Basic Principle

In ECT, an alternating current (frequency 1kHz-2 MHz) is made to flow in a coil (also called probe) which, in turn, produces an alternating magnetic field around it. This coil when brought close to the electrically conducting surface of a metallic material to be inspected, induces an eddy current flow in the material due to electromagnetic induction (Figure 1.6). These eddy currents are generally parallel to the coil winding. The presence of any discontinuity or defect in the material disturbs the eddy current flow. These eddy currents, in turn, generate an alternating magnetic field (in opposite direction) which may be detected either as a voltage across a second coil or by the perturbation of the impedance of the original coil.

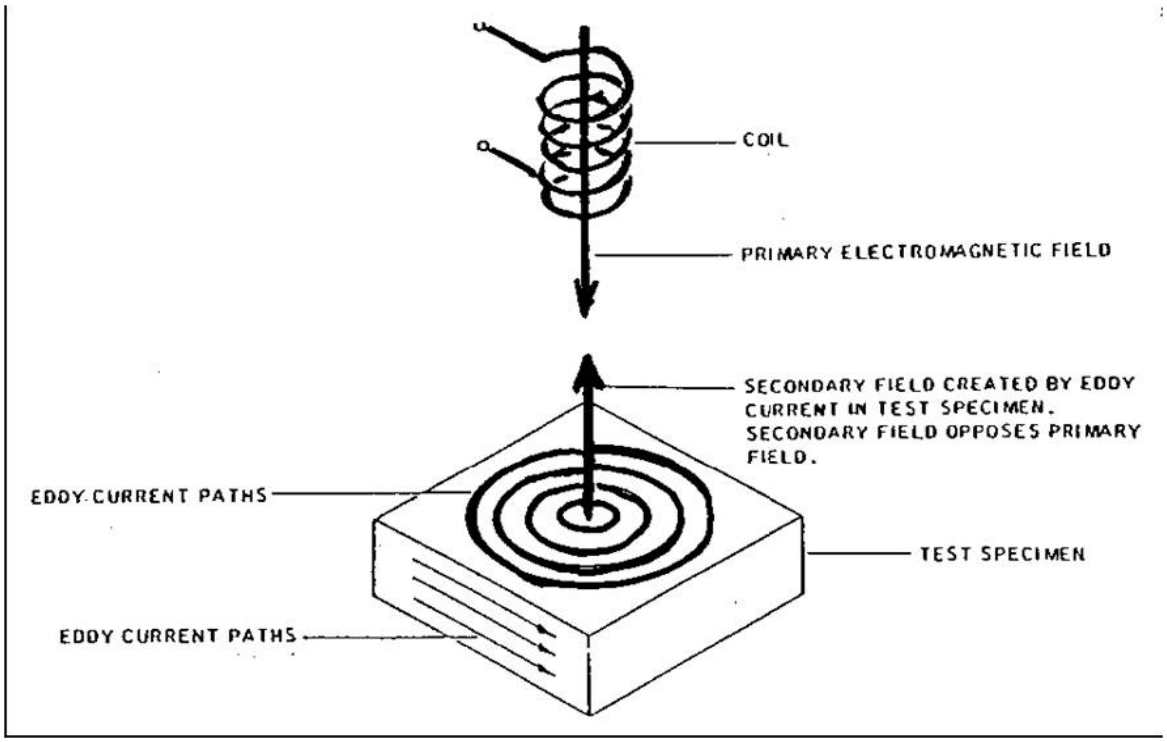

Fig. 1.6 Initial balance conditions of current and fields (Source: NDT Services)

The impedance change is affected, mainly, by electrical conductivity, magnetic permeability and geometry of the material, test frequency and the spacing between the coil and the material.

1.1.6.2 Limitations

Like other NDE methods, ECT has certain limitations. The major limitation of ECT is that only electrically conductive materials can be inspected. The EC signal is more closely related to volume of the material lost than to the wall thickness lost. Hence, evaluations should be made cautiously. For critical applications, results may need to be verified by an alternate technique. ECT equipment (Figure 1.7) is costly as compared to MPT equipment.

Fig. 1.7 Eddy Current Testing Equipment (Source: Huatec)

1.1.7 Acoustic Emission Testing (AET)

Acoustic emission technique is emerging as a powerful tool for NDE of plant components such as pressure vessels, pipes welds, etc. The dynamic nature of AE makes it a highly potential technique for monitoring the integrity of critical structures and components in various industries like nuclear and fossil fuel power plants, aerospace, chemical, petrochemical, transportation, manufacturing, fabrication, etc.

Acoustic emission testing method is superior to other NDE methods due to:

(a) Continuous monitoring,
(b) Inspection of complete volume of the component,
(c) Issue of advance warning and

(d) Detection and location of any crack initiation and propagation and system leaks

1.1.7.1 Basic Principle

AE inspection detects and analyses minute AE signals generated by growing discontinuities in material under a stimulus such as stress and temperature. Proper analysis of these signals can provide information concerning the detection and location of these discontinuities and the structural integrity.

If a material is loaded to a given stress level and then unloaded, usually no emission will be observed upon immediate reloading until the previous stress has been exceeded. This is known as Kaiser effect and is due to the fact that AE is closely related to plastic deformation and fracture.

1.1.7.2 Sensitivity

The acoustic emission testing is sensitive compared to the conventional NDE testing methods. The minimum detectable crack size for UT, RT and ECT methods is about 0.5 mm, if ideal conditions are met for each method whereas AET can detect crack growth of the order of 25 microns.

1.1.7.3 Applications

A broad classification of the applications include:

(a) Inspection during proof pressure testing and online monitoring of pressure vessels (Figure 1.8), pipelines and engineering structures
(b) Leakage detection and location
(c) Quality control during fabrication
(d) Investigating processes such as fatigue, stress corrosion and corrosion
(e) Monitoring underground pipelines
(f) Online weld monitoring

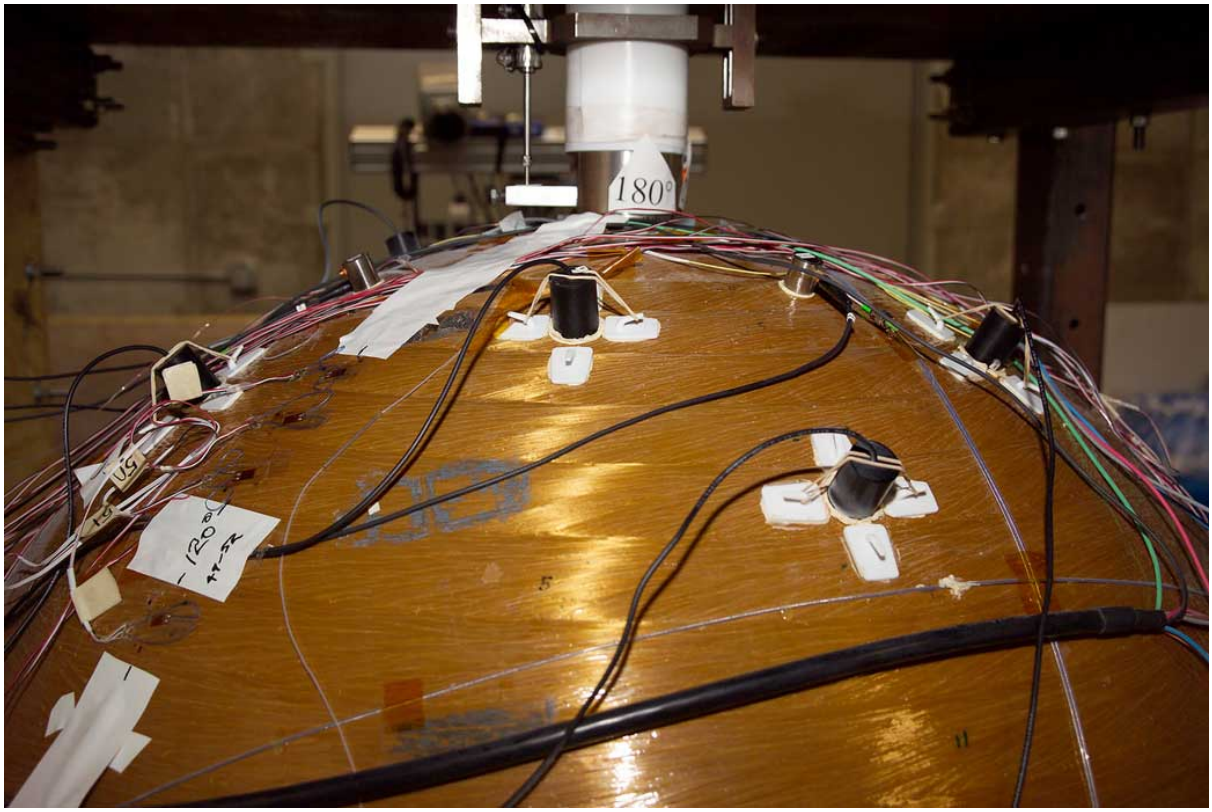

Fig. 1.8 Acoustic Emission Testing of a composite pressure vessel (Source: Grand Research Store)

1.1.8 Infrared Thermography (IRT)

All objects around us emit electromagnetic radiations at and above ambient temperatures. Infrared radiations (IR) are invisible to eye. Variation in the temperature of the surface of the object can be visualized from the thermal image of an object. This means that deviations from normal temperature can be detected from a distance. Day by day, IRT is being used in various fileds like sports, medical etc.

1.1.8.1 Basic Principle

NDE using IR is a unique method as it is non-intrusive and non-contact (can be used from a distance without contacting the test object). For NDE, the IR band width from 2 to 14 μm is being used. The properties of IR are similar to those of other electromagnetic radiations such as visible light. Infrared radiations travel in straight lines outward from the source. They can propagate in vacuum and in certain liquids, solids and gases. They can be optically focused and directed by lenses or mirrors or dispersed by prisms. IR can also be transmitted through certain

materials which are opaque to light. The intensity of the emitted spectrum is dependent upon the absolute temperature of the body. The basic factors affecting the thermal measurement include (a) emissivity, (b) surroundings and (c) atmosphere.

1.1.8.2 Techniques

IRT can be classified basically into two categories: (a) passive and (b) active. In passive technique, the natural heat distribution is measured over the surface of a hot structure. This is generally used in temperature monitoring. In an active technique (Figure 1.9), heating or cooling is induced or applied to the part or the complete surface and the movement and redistribution of temperature profile across the test surface is measured. The anomaly present in the object causes an abnormal behavior to the forward thermal wave which further causes a temperature rise at defective location over the object's surface. The temperature variation between anomaly region to sound surface region is used to discriminate them. The emitted objects thermal and temporal response is recorded using infrared imager and further stored in the computer.

Fig. 1.9 Infrared Thermography inspection system

1.1.9 Ultrasonic Testing (UT)

Ultrasonic Testing is the most versatile NDE method used in almost all major industries. UT is applicable to most materials, metallic or non-metallic. By this method, surface and internal discontinuities such as voids, cracks, foreign material inclusions and lack of bond can be accurately evaluated from one side. UT utilizes high frequency acoustic waves generated by piezoelectric transducers. Frequencies from 1 to 10 MHz are typically used, although lower or higher ranges are sometimes required for certain applications [7]. The resultant acoustic wavelengths in the test material (depend on the ultrasonic wave velocity) are of the order of one to ten millimeters. A highly directional sound beam is transmitted to the test piece through a suitable couplant, usually grease or oil like material. While various types of instrumentation and display modes are feasible, the most widely employed is the pulse-echo technique with A-scan mode (Figure 1.10).

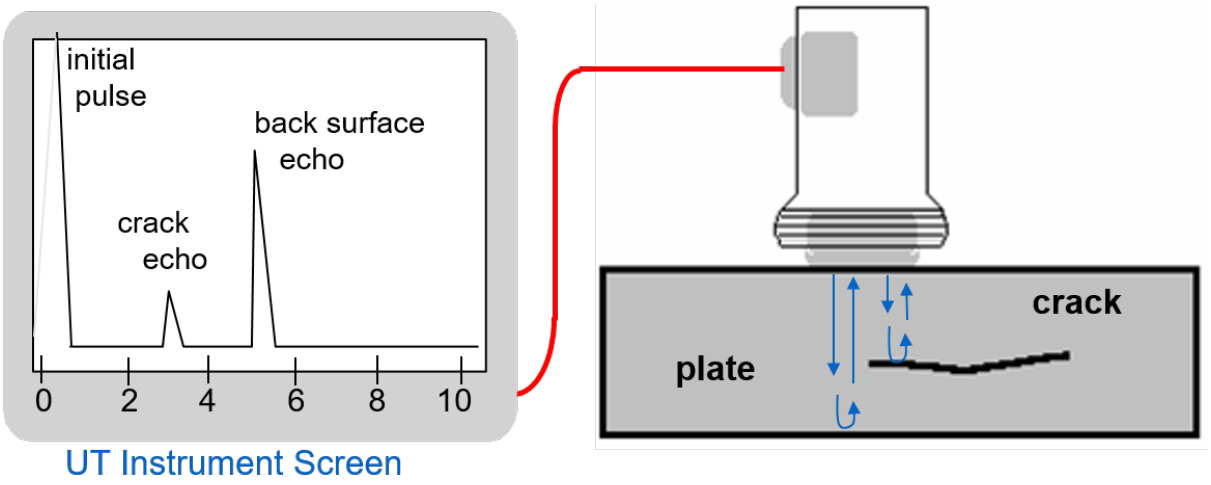

Fig. 1.10 Pulse Echo Technique (Source: Techshore Inspection Services)

Many a time, the conventional pulse-echo technique (PET) may not provide required test information. This may occur, when a flaw or other anomaly does not provide a suitable reflection surface or where the orientation or location of the flaw is not favorable for detection using single probe. In such cases, through transmission (TT) technique is used for defect characterization. In this method, two separate transducers are used on either side of the test piece; one as transmitter and the other as receiver as shown in Figure 1.11. Variation in intensity across the transmitted beam indicates the soundness of the test piece. Attenuation of the sound beam is indicative of coarse grain structure of the test piece. Scanning of the test piece using TT technique will result in the location of defects, flaws and inclusions in the plane parallel to the surface of the test piece. This is used for NDE of multi-layered and multi-component material as encountered in solid rocket motor case/insulation/liner/propellants, in composite structures and in large castings [8].

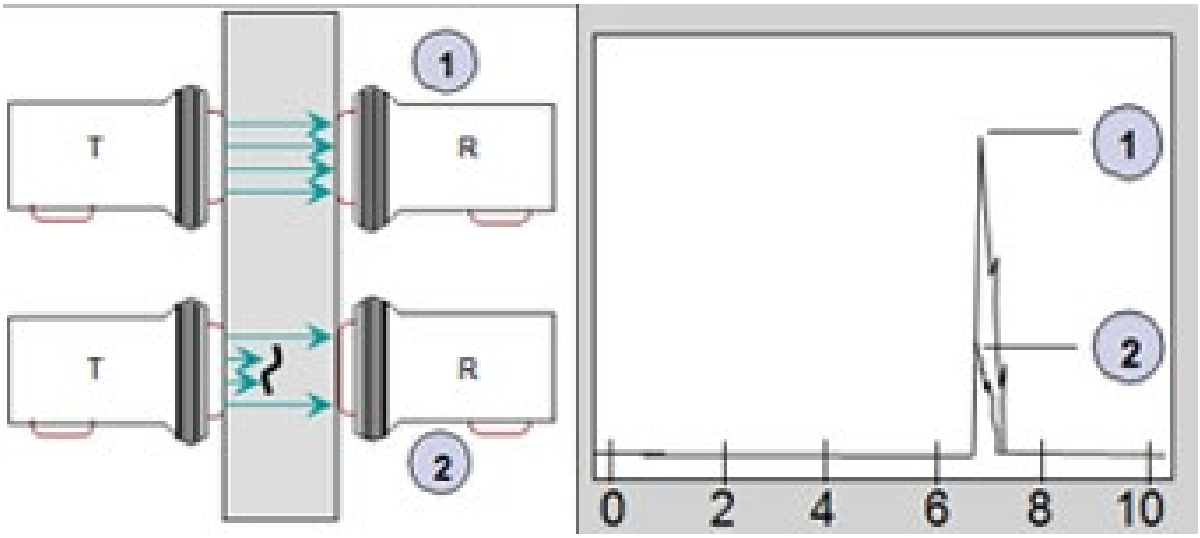

Fig. 1.11 Through Transmission Technique (Source: United Gamma NDT)

The main advantages of UT are:

(a) Testing from only one accessible surface is possible
(b) Structures with large section thickness can be tested
(c) Discontinuities deeper in the test piece can be detected because of high penetrating power of ultrasonic waves
(d) Detection of extremely small planar flaws is possible
(e) Instantaneous results lead to on spot decisions.
(f) Economical compared to other NDE methods
(g) Safe to operator as well as object to be inspected unlike radiography

The limitation of UT is that it depends on the operator skills to implement and interpret the results.

1.1.10 Radiographic Testing (RT)

Radiographic test is one of the most widely used NDE methods for the detection of internal defects such as porosity and voids. With proper orientation of the X-ray beam, planar defects can also be detected with radiography. It is also suitable for detecting changes in material composition, thickness measurements and locating unwanted or defective components hidden from view in an assembled part. No prior preparation of the specimen surface is necessary unlike other NDE methods. Radiographic test setup including the machineries and manipulators

are costly. Care should be taken while conducting the radiography test on the structures, to protect both the operator and public around the setup as radiation is hazardous.

Radiographic testing finds extensive use in the inspection and evaluation of composite materials. This method uses X-rays (0.001 Aº to 1 Aº) or gamma rays to penetrate the given component to reveal its internal condition. It is well known that when X-rays penetrate the component, they encounter three processes namely 1) absorption, 2) scattering and 3) transmission. Scattered X-rays are those that have deviated from the incident direction upon interaction with the material. Scattering and absorption lead to reduction in the intensity of the X-ray beam known as the attenuation. The transmitted beam exposes the recording medium such as film kept very close to the component. The attenuation of the X-ray beam depends on the density and the thickness of the component to be inspected. Higher density objects such as lead and steel for instance, offer more attenuation (less transmission) than lower density object solid propellant grain, rubber and composite materials. Therefore, for the same amount of radiation, a given film receives lesser radiation and gives comparatively lighter shade for the high-density material than for lower density material as shown in Figure 1.12. The exposed film is processed using suitable chemicals such as developer, acid stop bath and fixer and washed thoroughly in the flowing water and dried in an electric drier. The processed film is used for the interpretation of the component based on the optical density difference among various location. The film thus processed is called a radiograph, which is a permanent record of the image of the part being inspected. The degree of blackness of the shade on the radiograph is measured by a quantity called optical density. A good radiograph is said to have an optical density in the range of 2.0 to 4.0 H & D units in the interested region. The quality of a radiograph is assessed in terms of contrast sharpness and granularity [9].

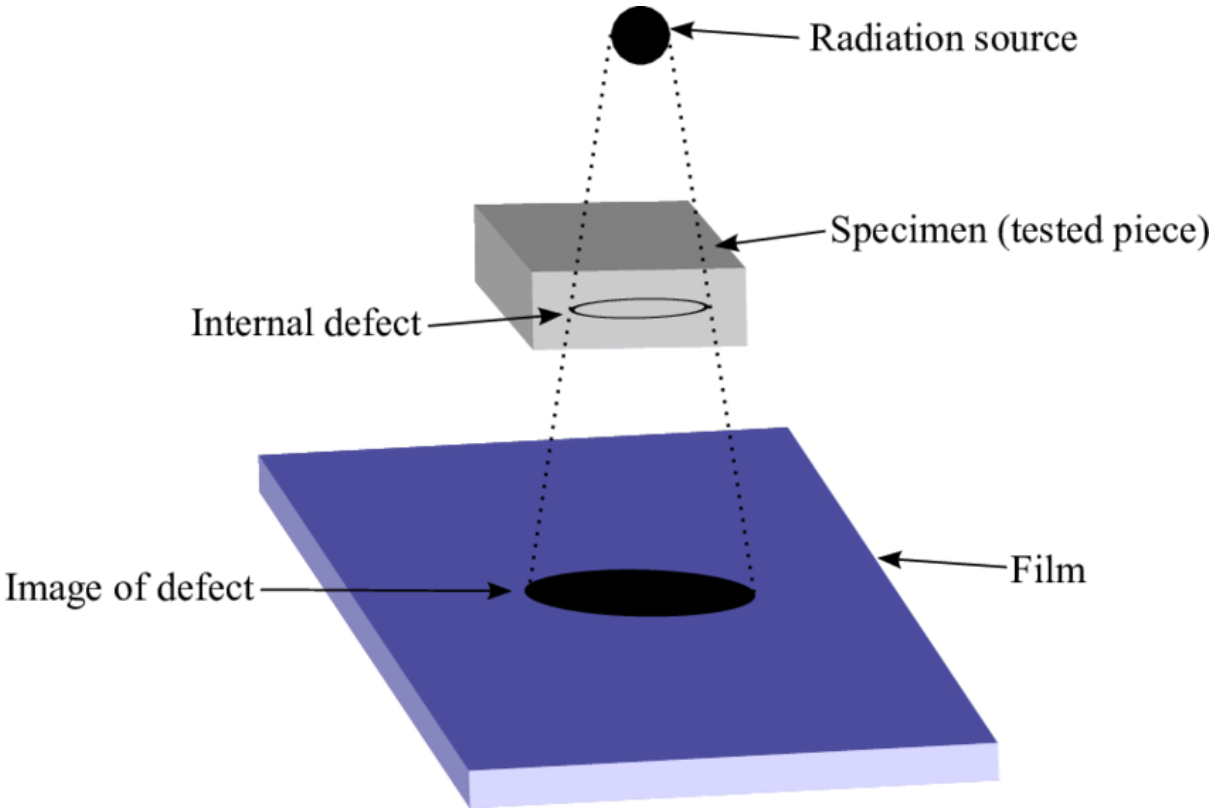

Fig. 1.12 Radiographic Testing (Source: ResearchGate)

An X-ray image is thus a result of differences in the attenuation of X-rays between different parts of an object. These attenuation differences arise because of interactions of X-rays with the object mainly in the form of photoelectric effect, Compton scattering and pair production. The above scattering processes dominate in low (up to 1 MeV), medium (1 – 10 MeV) and high (above 1.02 MeV) X-ray energy ranges respectively. The effect of these interactions is such that the resulting attenuation increases as a function of object thickness and its physical density. The minimum thickness change (which may be due to a defect) that can be detected using radiography depends on a number of parameters such as specific subject contrast, film contrast, total un-sharpness, viewing conditions etc. The attenuation of X-rays by a material obeys the basic absorption law as below:

$$I_x = I_o e^{-\mu x} \tag{1.1}$$

where,

I_o - measured intensity at the detector with no material in the beam

I_x - measured intensity at the detector with the material of thickness x in the beam

μ - linear attenuation coefficient of the material and is related to the Half-value layer (HVL) of the material by

$$\mu = \frac{0.693}{HVL} \tag{1.2}$$

To form an image on a film, exposure by a correct amount of radiation is required. For large thickness components, it is difficult to get the required amount of radiation to form a good image with low energy X-rays as its penetrating power and the intensity are very low. Therefore, to produce a good quality of radiograph, one has to select correct X-ray energy for the given application [10]. Accordingly low energy conventional X-ray tubes up to (450 kV) are utilized to inspect smaller to medium size components such as igniters, small nozzles, and fasteners etc. and high-energy X-ray machines such as linear accelerators (Linac) in the Million electron Volts (MeV) range up to 15 MeV for establishing the reliability of large size components such as large solid propellant rocket motors.

1.1.11 Real Time Radiography (RTR)

Real time radiography has emerged in the recent years as an alternative to film-based radiography in many spheres of industrial activity and thus eliminated the use of expensive X-ray films and also the associated manpower involvement for the cassette loading/unloading/positioning as well as the film processing. Three different types of fluorescent screen-based systems are most commonly used at present namely: (a) rare earth screens, (b) scintillator crystals, and (c) scintillating fiber optical systems. They are found to exhibit large differences in light conversion rate, contrast and spatial resolution and are employed depending upon the inspection requirements. The development of high resolution RTR systems involving charge coupling device (CCD) as well as photo diode arrays has led light sensitive linear arrays of pixel sizes down to the range of tens of microns.

1.1.11.1 Basic Principle

In RTR, the X-ray images are of electronic in nature. The fluorescent screen is exposed to the X-rays transmitted by a component under inspection and its light output is coupled to either a CCD camera or a photo-diode array. The corresponding electronic signals are then digitized using an analog to digital converter and the radiographic image is displayed on a high-resolution

monitor using a computer. As the image information is available in digital form, it is readily amenable for further processing to improve the overall image contrast using suitable image processing methods. The processed image is then subjected for interpretation and analysis.

1.1.11.2 Applications and Limitations

The multi-layered composite structures and SRMs to be inspected are to be either kept on a rotary table or a pair of roller stands for their radiographic coverage. Both tangential as well as normal grain coverage can be provided by suitably rotating the SRM or hoisting/lowering of the X-ray machine/RTR camera system simultaneously. As the X-ray images are instantly displayed on the monitor, 100% coverage of SRMs can be done in a time interval which may be unimaginable with film-based RT coverage. Also, as the motor is covered at all angles, it is expected to have a vast improvement in the detection probability of cracks in the propellant grain. Although the RTR has so many advantages in its applications to a variety of components, its applicability is yet to be established in the area of high energy radiography, particularly from the high-resolution point of view.

1.2 Organization of the Thesis

The current study deals with the non-destructive evaluation of multi-layered glass fiber reinforced polymer composites. Defects like air gap, de-bond between layers of the composite etc. were added to the material and the effectiveness of the NMR to detect these defects was studied. Similarly, the effect of the shape of the object to be tested was also reported by conducting the tests on composites with same defects, but the object shaped as flat and curved. The thesis is organized as follows:

Chapter 1 introduces the composite materials and the need to study their structural integrity without damaging it. The use of the non-destructive evaluation techniques in this endeavor and various techniques of NDE available are reported.

Chapter 2 deals with the current state of knowledge regarding the advantages and disadvantages of different NDE techniques and the need for the usage of newer technique like NMR along with the knowledge gaps regarding the usage of NMR as NDE method for multi-layered composites.

Chapter 3 depicts all the materials used and their manufacturing techniques, the experimentations utilized for the study along with the assumptions made and parameters that are utilized.

Chapter 4 shows the results obtained when NMR is used to detect the defects present in the flat composite sample. The results were then compared with those obtained from using other techniques like acousto-ultrasonic and X-ray radiography techniques.

Chapter 5 shows the results of NMR on the curved sample and comparison with the results of acousto-ultrasonic, microwave NDE, X-ray radiography and computed tomography methods.

Chapter 6 compares the NMR data of the flat and the curved samples showing the effect of the shape on the effectiveness of the NMR test.

Chapter 7 summarizes the results from the above tests

Chapter 8 Scope of the future extension of the research is presented.

2. Literature Review

Composite structures with multi-layered configurations are typically used in solid rocket motors in the aerospace field. Fiber reinforced composite structures with rubber insulation layer adhesively bonded is known to be one such advanced material for rocket motor application. Integrity of these adhesively bonded multi-layered composite structures is important to serve the intended purpose i.e., reliable performance of the rocket motor [11-15]. Composite structure can fail catastrophically due to weakening of strength in presence of defects such as de-bonds, airgaps etc. There could be economical and strategic loss due to the catastrophe. Therefore, in-service non-destructive evaluation (NDE) of these structures is indispensable to avoid the possible failures due to defects [16-19]. The purpose of NDE is to identify possible degradation of interfacial bond strength and give reliable report for taking preventive action. Out of many established NDE methods, ultrasonic testing and X-ray radiography (either film based or digital) are widely used for field applications [20-22]. However, both the techniques are useful

for detecting de-bonded surfaces with sufficiently large interlayer separation, but not suitable for early detection of degradation of adhesive bond in multi-layered composite structures due to which the structures undergo irreversible damage. The need for prognostic tool for detecting degradation of adhesive bond has been a requirement for industry. Specialized NDE techniques were of interest, one such technique is single sided low field nuclear magnetic resonance (NMR) [23-26].

2.1 NMR Theory

NMR can be defined as a physical phenomenon which is utilized to investigate molecular properties of matter by irradiating atomic nuclei in a magnetic field with electromagnetic radio waves [27]. All nuclei have an intrinsic nuclear spin. However, only nuclei with a non-zero spin quantum number can be probed with NMR, as only nuclei with non-zero spin quantum numbers will have a net nuclear spin angular momentum and magnetic moment when placed in an applied magnetic field, which is referred to as precession as shown in Figure 2.1. The nuclei precess at the precession or Larmor frequency ω, which is proportional to the strength B_0 of the applied magnetic field,

$$\omega = 2\pi f = 2\pi \frac{\Delta E}{h} = \gamma B_0 \tag{2.1}$$

where,

ω - Larmor or precession frequency in radians

f - frequency of precession in Hz

ΔE - energy difference or energy gap

h - Planck's constant

γ - gyromagnetic ratio of the nucleus of interest

B_0 - Strength of applied magnetic field

The most common nuclei that are probed using NMR are ^{1}H and ^{13}C, which both have a spin quantum number of ±1/2.

When nuclei are placed in an applied magnetic field, the spins will also align either parallel or antiparallel to the magnetic field [28-33]. The rearrangement of spins into parallel and

antiparallel populations creates an energy difference. This is in accordance to the Boltzmann distribution, as given below:

$$\frac{P_{antiparallel\ to\ B_0}}{P_{parrallel\ to\ B_0}} = e^{-\Delta E/kT} = exp\left(\frac{-\Delta E}{kT}\right) \tag{2.2}$$

where,

P - population or fraction of the particles in each state

k - Boltzmann constant

T - absolute temperature in Kelvin

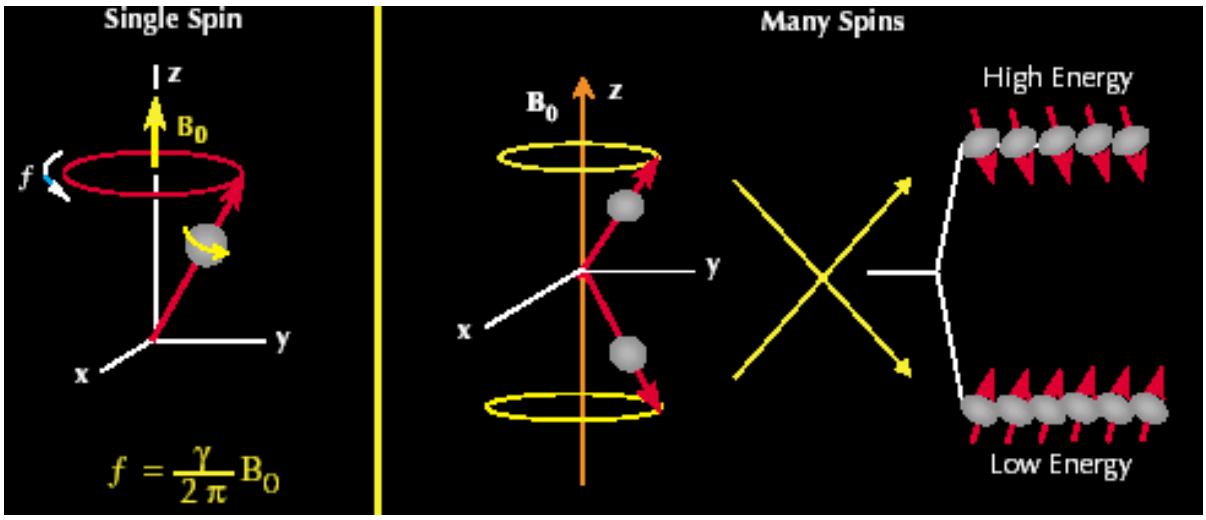

Fig. 2.1 Nuclei in magnetic fields

2.2 Single sided low field NMR Theory

Single sided low field NMR was developed as an alternative that overcomes some of the difficulties posed by conventional NMR instrumentation. The use of permanent magnets in single sided NMR results in a weaker inhomogeneous magnetic field. The inhomogeneities in the magnetic field eliminates the ability to elucidate the detailed structural information. However, parameters that can be obtained using conventional NMR can still be obtained using single sided NMR, for example transverse relaxation [34-36].

2.3 Transverse Relaxation

Transverse relaxation is a parameter that describes the amount of time it takes for nuclear spins in the transverse plane (x, y-plane) to dephase. On single sided NMR instruments, T_2 relaxation is measured using the Carr-Purcell-Meiboom-Gill (CPMG) pulse sequence as shown in Figure 2.2.

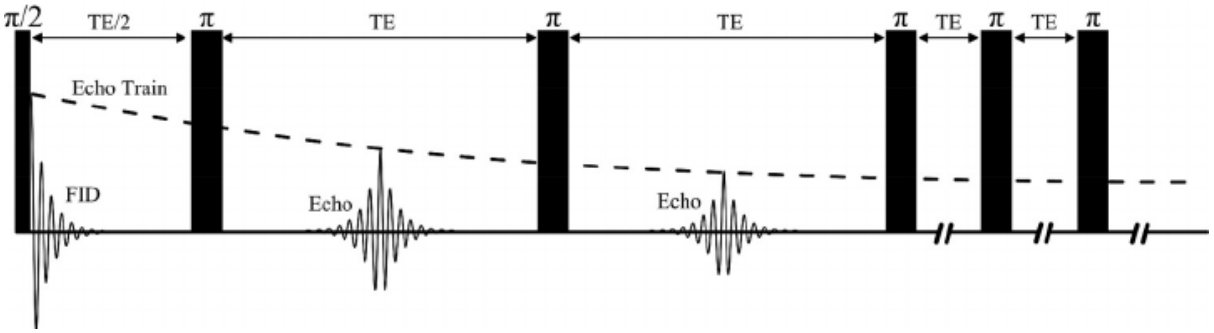

Fig. 2.2 Schematic of the CPMG pulse sequence

The smaller the T_2 relaxation time, the less molecular motion is present in the sample. In the context of polymers, a smaller T_2 relaxation time for a polymer corresponds to a sample that has less molecular motion [37-40]. The more that spin interacts with each other, the faster spin decoherence occurs. Physically, this translates into a more rigid polymer and shows evidence of greater crosslinking and residual dipolar coupling present in the sample. As the polymer network becomes more disrupted, there should be evidence of greater molecular motion and therefore larger corresponding T_2 relaxation times.

2.4 NDE Applications of Single sided low field NMR

Single sided low field NMR technique is a well-known analytical tool to study chemical nature of materials including rubber/elastomers as well as adhesively bonded composite structures [41-43]. The usability of single sided low field NMR for the non-destructive determination of the degree of cross-linking and curing as process monitoring was investigated by N Halmen et al [44, 45]. The results of the above study indicated the possibility of distinguishing the samples with different degrees of cross-linking. The homogeneity of samples and the curing kinetics of adhesives can also be monitored. The measurements show good agreement with reference tests (wet chemical analysis, differential scanning calorimetry (DSC), dielectric analysis). Furthermore, the influence of sample temperature on the characteristic relaxation times can be

observed. M Kelly et al [46] used single-sided NMR to non-destructively probe and spatially resolve the change in the characteristic transverse relaxation time of epoxies during curing on a substrate. Changes in physical properties of epoxy was monitored in real-time.

Non-destructive characterization of the crumb-rubber fraction in asphalt was demonstrated by carrying out a field study using NMR-MOUSE (mobile universal surface explorer). With the help of a laboratory calibration procedure employing dry-process pavement samples with known crumb-rubber fractions, the unknown crumb-rubber fraction of pavements can be estimated at room temperature [47 - 51]. The crumb-rubber fraction and its distribution are key factors determining the quality of pavements with rubber-modified asphalt.

The potential of magnetic resonance imaging (MRI) as a NDE technique has been successfully applied for detection, quantification, identification and discrimination of various liquid contaminants trapped inside the honeycomb core cells of aircraft-grade structural polymer composite sandwich panels. It has also been applied to define accurately the extent of crushed-core damage in liquid impregnated honeycomb cells [52 - 54]. The potential of multi-slice MRI is studied for in-vitro NDE of defective and damaged FRP specimens emerged in water-based saline solution simulating biofluids. The orientation, positioning, shape and particularly the size of planar defects are evaluated accurately [55 - 58].

NMR Mouse has been shown to be a very useful technique to study the form and content of water in polymer composites. Composites using activated carbon fibers with phenolic resin have complex water absorption behavior. Measurement of transverse relaxation times has given an insight into the form in which water was held within the carbon fiber/phenolic sample. Transverse relaxation curves showed water to be primarily in two states in the resin, corresponding to “bound” and “mobile” molecules [59, 60].

NMR techniques are effectively used as NDT tools for the characterization of the ageing state of prepreg materials. Beside the sensitive measurement of the crosslink density, there is a potential to separate also the influence of moisture content as a further parameter contributing to the ageing process. The advantage of the NMR technique compared to other techniques such as dielectric measurement or DSC, is that there is no influence of the sample volume and geometry. Furthermore, NMR needs no time-consuming sample preparation techniques (lamination and curing) and the measurement can be performed easily and quickly [61].

Research contributions to NMR by Peter Blümler is discussed here. To study the dynamic changes in the plant structures and functions, a technique which combine the magnetic resonance imaging (MRI) and positron emission tomography (PET) was used and three contrasting root and stem systems were studied for their structural changes. This technique of co-registration of MRI and PET opens a way to study the structural changes during the operation [62, 63]. To make NMR machine mobile, changing the magnet type to Halbach-type permanent magnet ring [64] was proposed, and the study of various porous media was reported [65-68].

Blümich B et al [69] studied the applications of profile NMR-MOUSE in porous-media. Relaxation measurements were found to be the better way to quantify moisture content in gray concrete. CPMG amplitude obtained from the sensitive slice of the profile NMR-MOUSE is found to be a good measure of moisture content in mortar bases of wall paintings. Relaxation time distribution was able to characterize the type of mortar. Experiments were conducted to study diesel particulate filters built from an array of porous ceramic walls. At full water saturation, the porosity and the pore-size distribution, as well as their spatial variations can be determined as a non-destructive alternative to mercury intrusion porosimetry.

Oliveira-Silva et al [70] developed a benchtop single-sided NMR system, with well-logging tool characteristics, to estimate the quality of oil and reservoir productivity before starting of actual production. The developed system was used in self-diffusion, T_1-T_2 and D-T_2 measurements of standard liquids and rock cores, demonstrating its functionality. Although this NMR equipment was originally built for applications in petroleum science and engineering, it found uses in many other areas, such as industry, agriculture and medicine.

Recent work on profile NMR of cylindrical samples [71, 72] have paved way for many applications in industry. Single sided low field NMR uses permanent magnets for generating DC magnetic field (B_0) for magnetizing the polymer materials. It generates magnetic field outside the magnets unlike high field NMR systems wherein magnetic field is generated within the core. In case of single sided low field NMR, B_0 is superimposed by an AC magnetic field (B_1) for creating a slice of sensitive volume which is moved inside the materials using a precise stepper motor (HP lift) system. The main advantages of single sided low field NMR include

- single sided inspection, hence access to both sides of sample material is not required

- non-contact method
- non-invasive, wide application for testing and evaluation of composite structures
- no couplant or other intermediate materials are not required unlike ultrasonics
- non-ionizing radiation, safe to operate unlike X-ray radiography
- portable, hence can be taken to field/shop floor for testing with battery backup
- both qualitative and quantitative assessment of defective and non-defective regions is possible with distinguishable material signatures.

Out of many NDE methods, only few of the techniques have potential applications for bond quality inspection of cylindrical composite structures where access of structure for inspection is available only from outside. Among these are single-sided low field NMR, Acousto-ultrasonic inspection and X-ray radiography. X-ray radiography is a very useful NDE method because it allows a view into the interior part of the structure. This inspection method is accomplished by passing X-rays through the part or assembly being inspected while recording the absorption of the rays onto a film sensitive to X-rays [73-76]. As the method records changes in total density through its thickness, it is an effective method for detecting flaws parallel to X-ray beam direction. X-ray radiography has limited applications for onsite inspection due to radiation hazard and limitations of electronics.

Acousto-ultrasonic scanning (AUS) system uses low frequency stress waves generated using piezoelectric transducer and compares the stress wave energy transmitted through the composite structure for evaluating the adhesive bond [77-80]. Low frequency Acousto-ultrasonic technique is a contact single sided pitch-catch technique in which two probes are used, one for transmission and other for reception of stress waves. As reported earlier, AUS uses tone burst excitation at single frequency for inspecting composite structures in pitch-catch mode (both transmitter Tx and receiver Rx are on the same side of the composite structure, but the receiver Rx is some distance away from the transmitter) as shown below in Figure 2.3.

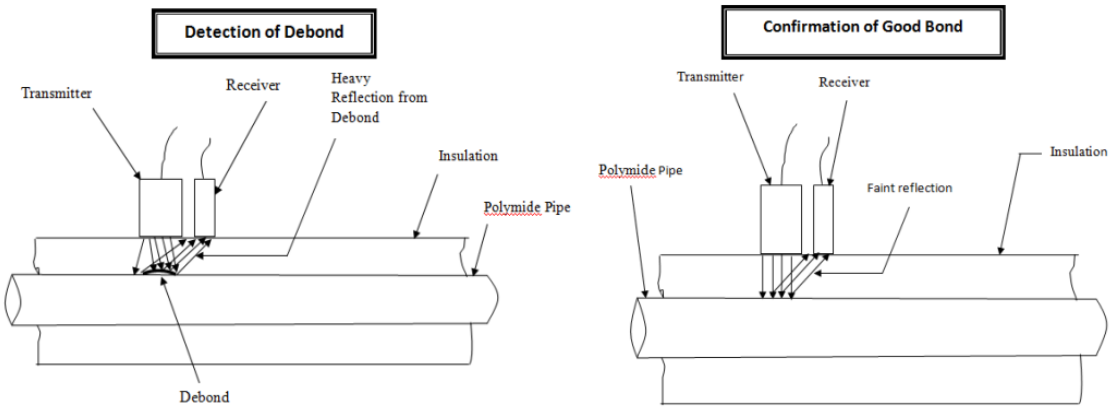

Fig. 2.3 AUS of insulated pipe (a) with defect and (b) without defect

Acousto-ultrasonic signals received at the receiver transducer resemble acoustic emission burst-type waves that decay exponentially [81-86]. The advantages of AUS over the conventional NDE techniques are detailed below:

- Inspection of thick multi-layered composite structures
- Testing of bonded interfaces
- No requirement of couplant during inspection
- Inspection from one side of the structure
- Inspection from one side possible
- Contact or non-contact mode of inspection possible
- Portable and economical inspection setup

2.5 Objectives

In addition to the unavoidable variations in the processing parameters of multi-layered composite structures, other processes such as transportation and handling including the subsequent storage and usage may also introduce different types of defects in the structures. Long duration storage and usage generally results in ageing and degradation, which can give rise to the generation of interfacial defects such as de-bonds, delamination etc. and defects within constituent materials like cracks, tears, voids, porosity etc. The detection and characterization of such type of defects is very essential to avoid catastrophic failure. The

present work focuses to enhance the defect detection capability of low field NMR and to estimate the defect parameters like precise depth and size by depth profiling. The main objectives of the work are

- To assess the soundness of rubber, adhesive liner and propellant in multi-layered GFRP composite structures.
- To assess the integrity of multi-layered GFRP composite structures (GFRP-rubber interface and rubber-adhesive liner-propellant interfaces).
- To evaluate the thickness and transverse relaxation times of constituent materials i. e. rubber, adhesive liner, propellant and airgap at the interfaces.
- To detect and characterize collinear defects in multi-layered GFRP composite structures.
- To study the effects of curvature on depth profile NMR data.

3. Materials and Methods

This chapter briefly describes the details of sample preparation, single sided low field NMR system and experimental setup developed for non-destructive evaluation (NDE) of multi-layered composite structures and data acquisition procedure.

3.1. Preparation of Flat GFRP Composite Samples

GFRP composite laminates (2nos. of size 300mmX200mm each as shown in Figure 3.1) of 4mm thick were fabricated using filament winding process on flat metallic mould using hoop winding process. The fabrication process involves winding glass filaments under tension over the rotating flat mandrel. The mandrel rotates around the spindle while a delivery eye on a carriage traverses horizontally in line with the axis of the rotating mandrel, laying down fibers in the desired hoop winding pattern. The glass filaments are impregnated in a bath with epoxy resin as they are wound on to the mandrel. Once the mandrel is completely covered to the

desired thickness, the component is sent for curing in an oven. After the component is cured, the mandrel is removed by cutting from the template using lathe machine.

Rubber (co-polymer of acrylonitrile and polybutadiene) of 2 mm thickness is used as insulation in each laminate as shown in Figure 3.2. Rubber based adhesive is used for bonding GFRP flat laminate with rubber insulation. In one of the samples, an air-gap or de-bond is implanted between laminate and rubber for the present studies. This sample is called the 'programmed de-bond sample' as shown in Figure 3.3. After the initial set of experiments, the rubber surface is abraded and then cleaned by Tri-Chloro-Ethylene (TCE) to remove oily and greasy substances from the surface and dried in an oven at 105^0C for 5 hours to evaporate the solvent and moisture. Thin layer of adhesive liner is applied by using spray gun. This GFRP-rubber-adhesive liner sample was further bonded with propellant as shown in Figure 3.4 – 3.6. The sample has now got representative layers of GFRP composite, rubber-based adhesive, rubber insulation, adhesive liner and propellant for the single sided low field NMR studies.

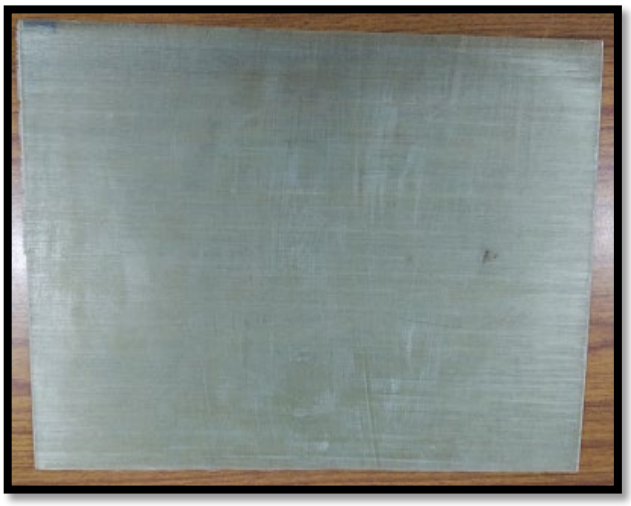

Fig. 3.1 GFRP laminate

Fig. 3.2 GFRP-rubber laminate

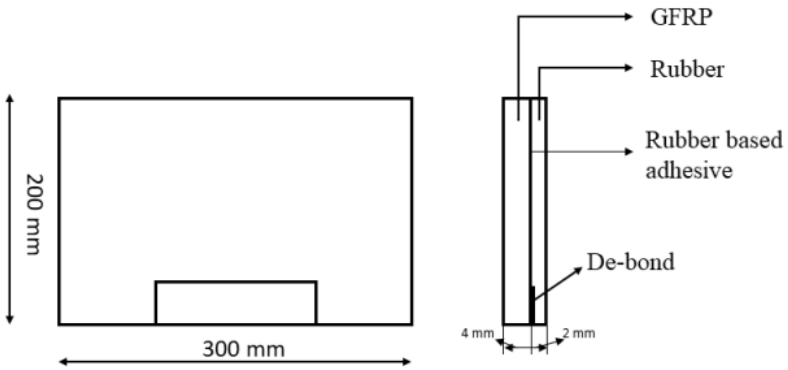

Fig. 3.3 Programmed de-bond sample

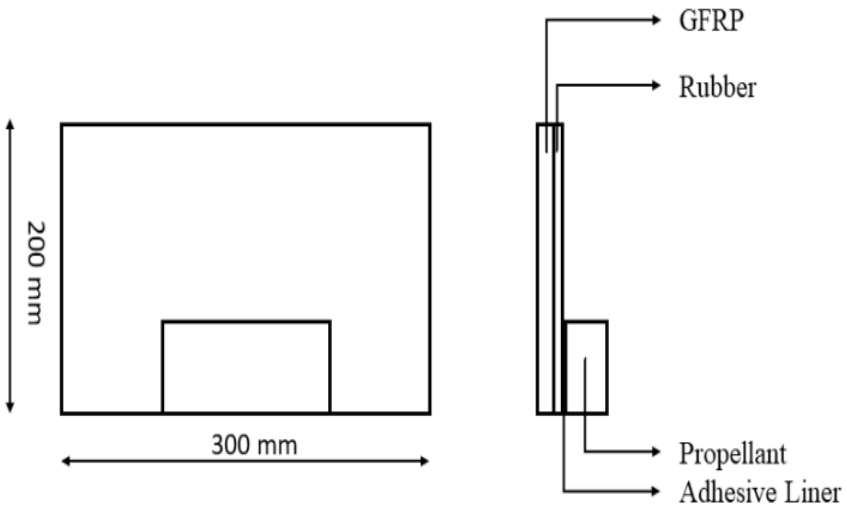

Fig. 3.4 GFRP-rubber-liner-propellant sample

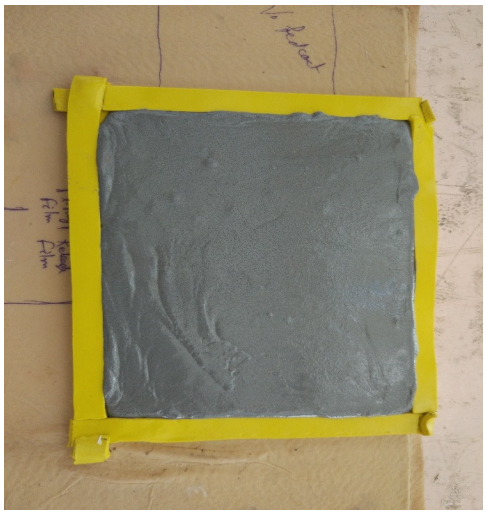

Fig. 3.5 Propellant cast over laminate

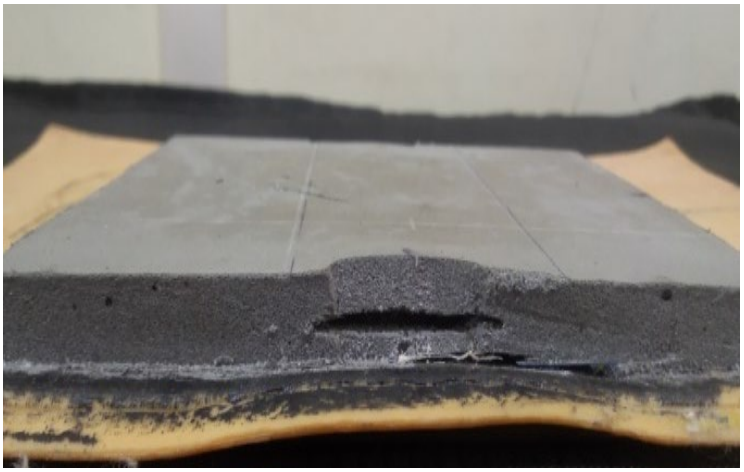

Fig. 3.6 Flat sample with colinear defects

In the second GFRP-rubber laminate sample (called the ‘varied thickness sample’), rubber surface is further coated with adhesive liner material with varying thickness starting with 200 microns to 600 microns as shown in Figure 3.7 and 3.8 (zone 1 to zone 4). Conventionally it is difficult to measure liner thickness; however, the increasing thickness is achieved by increasing number of coats for each instance. Adhesive liner thickness of zone 2 and zone 3 is in the order of 300 and 450 microns respectively.

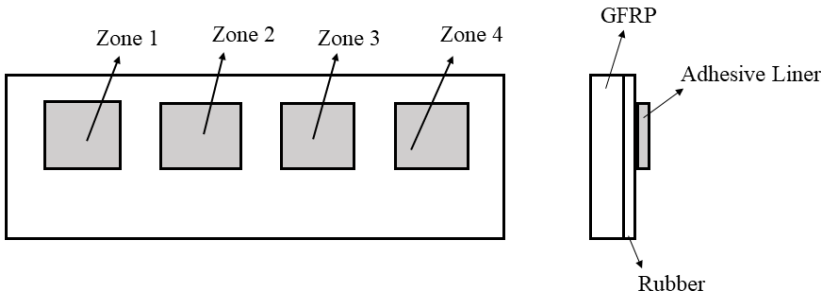

Fig. 3.7 Schematic of flat GFRP-rubber-adhesive liner varied thickness sample

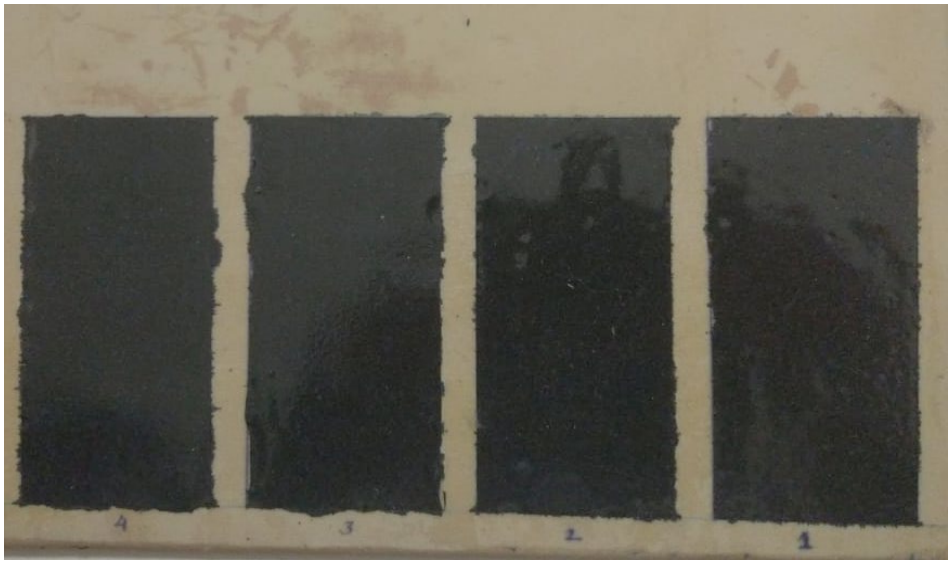

Fig. 3.8 Image of flat GFRP-rubber-adhesive liner varied thickness sample

3.2. Preparation of Multi-layered Cylindrical Samples

Composite cylindrical test samples for the current studies were fabricated by filament winding process and cured by oven curing method. Glass fibres were passed through epoxy resin bath before they were wrapped around a rotating metallic cylindrical mandrel. After required number of layers, the composite wrapped mandrel is cured in an oven under a prescribed curing cycle. Various stages of fabrication involved in realization of cylindrical samples are described below.

3.2.1. Material Identification

Composite materials are made by macroscopic homogeneous combination of two or more materials. The composite made here is a fiber reinforced polymer matrix material. The fiber used here is glass fiber in long roving form (E-glass roving, Type-30 i. e. SE1200-735TEX) and polymer used here is epoxy resin which is a thermoset polymer (Epofine 1555 + Finehard 5200). The matrix is epoxy resin system consists of epoxy resin and hardener in liquid form during processing and subsequently cured at elevated temperature to form rigid thermoset polymer which retains the shape of the tool after curing. The specifications, chemical composition and physical properties of E-glass roving are given in Table 3.1, 3.2 and 3.3 respectively.

Table 3.1 Specifications of E-glass roving (Owens Corning make)

Sl. No.	Parameter	Values
1	Tex; g/km	735±10 (nominal)
2	Roving width; mm	2.5±0.2
3	Density; g/cc	2.5-2.59

Table 3.2 Chemical composition of E-glass roving

Sl. No.	Chemical Constituents	Composition (Weight %)
1	SiO_2	52-56
2	B_2O_3	4-6
3	Al_2O_3	12-15
4	CaO	21-23
5	MgO	0.4-4
6	TiO_2	0.2-0.5
7	Na_2O	0-1
8	K_2O	Trace
9	Fe_2O_3	0.2-0.4
10	F_2	0.2-0.7

Table 3.3 Physical properties of E-glass roving

Sl. No.	Physical Properties	Values

1	Co-efficient of linear thermal expansion; $10^{-4}/^0C$	4.9-6
2	Specific Heat; Cal/g/^{0}C	0.192
3	Dielectric Constant at room temperature and 1MHz	5.86-6.6
4	Dielectric Strength; kV/cm	103
5	Volume Resistivity at room temperature; $\log_{10}(\Omega$ cm)	22.7-28.6
6	Refractive Index (Bulk)	1.547
7	Weight loss at 10% H_2SO_4 (24Hrs) in %	41

The specifications of epoxy resin and hardener are given in Table 3.4 and 3.5 respectively.

Table 3.4 Specifications of epoxy resin

Sl. No.	Parameter	Values
1	Grade	Epofine 1555
2	Colour	Pale yellow, Clear liquid
3	Specific Gravity	1.1-1.2
4	Viscosity at 25^{0}C; cP	14000-18000
5	Epoxy content, Eq/Kg	4.8-5.5
6	Volatile content; weight %	0.75 maximum
7	Shelf life	2years from the date of manufacture

Table 3.5 Specifications of epoxy hardener

Sl. No.	Physical Properties	Values
1	Grade	Finehard 5200
2	Colour	Clear brown liquid
3	Specific Gravity	1.0-1.1
4	Viscosity at 25^0C; cP	140-200
5	Shelf life	3years from the date of manufacture

3.2.2 Mandrel Preparation

This is the first step for making a composite product by filament winding. The tool used in this process to get the composite product is called mandrel. The shape of the mandrel corresponds to inner shape of the product. Here, it is a cylinder with 220mm diameter which is ID of the shell. Various materials can be used to make mandrels like steel, polyurethane (PU) foam, styrofoam, wood, Plaster of Paris (PoP) and even composites also. The type of material to be used depends on whether the curing is at room temperature or at elevated temperatures, number of products to be made from the tool, ease of fabrication of tool, weight of the tool etc. Here, in the present study, PoP tool is used. The PoP tool is easy to fabricate, economical and particularly suitable if only few numbers of products are to be made. The tool is made by casting PoP over a steel pipe or rod which will be used to hold the mandrel between centres on the Filament winding machine or Lathe machine.

PoP (Dentico Grade) is mixed with water in a ratio of 2:1 to make a paste like consistency. This paste is then applied over the pipe or rod and kept in a dry place for 24 to 48 hours to set as shown in Figure 3.9. After the PoP is set, it is machined to required shape (Figure 3.10) on a Lathe machine by turning operation. Once the required shape is achieved, the mandrel is covered with a release film which prevents adhesion of the cured resin to PoP mandrel and makes the removal of the product easy. The release film is a Teflon coated polyester or glass fiber woven cloth. The mandrel is ready for winding.

Fig. 3.9 Mandrel (PoP cast over a steel rod)

Fig. 3.10 Machined mandrel

3.2.3 Resin Mixing

The matrix used here is a thermosetting type epoxy resin system. The resin system consists of epoxy resin Epofine 1555 and an elevated temperature curing hardener Finehard 5200. Both resin and hardener in liquid form are mixed in a ratio of 100 parts of resin to 27 parts of hardener. The epoxy resin is a highly viscous liquid (10000 cPs) and hardener is a low viscosity liquid (50 cPs). For proper wetting of the fibers, the mix viscosity has to be maintained at 250 to 300 cPs. The mixing is done thoroughly in heated vessel preferably with motorized stirrer. The heating is done at 40^0C to 50^0C to achieve the desired mix viscosity. Once the proper mixing is done, the resin is poured into the resin bath of the filament winding machine.

3.2.4 Filament Winding

Filament winding process is widely used to make cylindrical and axisymmetric shaped composite products. Here, in the present study, a CNC Filament winding machine is used. It is

similar to a lathe machine in construction with head stock, tail stock on a bed, but instead of tool post, it has a fiber delivery head through which fibers are wound over the mandrel. The fiber delivery head is on another bed called carriage bed and can travel axially along the length of the mandrel. The carriage has a creel stand for mounting glass fiber spools 10 to 12 in number and has a provision for adjusting the tension of the fiber for winding. The carriage also houses the heated resin bath containing resin system through which fibers pass for wetting/impregnation before being wound over the mandrel.

For winding, the prepared mandrel is placed between centres on the machine. The fibers are pulled through the resin bath and out of the delivery head. The delivery head is maintained at an offset distance from the mandrel. The mandrel is rotated and the fiber bundle through the delivery head which now forms a band after wetting, is wound from one end to the other end of the rotating mandrel forming one layer. The fiber band is wound such that no gap is observed between adjacent bands as shown in Figure 3.11. The tension in fibers is adjusted for proper consolidation of layers and to maintain proper resin content in the composite. The feed of the delivery head is controlled by CNC with respect to mandrel rotation to maintain thickness and band spacing of the layer. Subsequent layers are wound to achieve desired thickness of product. Once the winding is finished, the fiber bundle is cut. The resin bath is cleaned and extra resin is put into bin. The mandrel is rotated and excess resin is squeezed using rubber squeezers and the resin is allowed to set while rotating.

Fig. 3.11 Filament winding

Fig. 3.12 Wound mandrel in curing oven

3.2.5 Curing Process

After winding, the wound mandrel is put in a hot air circulating oven as shown in Figure 3.12. The oven has provision to control the temperature, heating rate and holding time as per curing schedule. These parameters depend on the type and amount of resin system in the composite and also to some extent on the type and weight of mandrel. After the curing is over, the oven is switched off and mandrel is cooled to room temperature slowly. The following cure cycle (Figure 3.13) was used for the samples used in the present study.

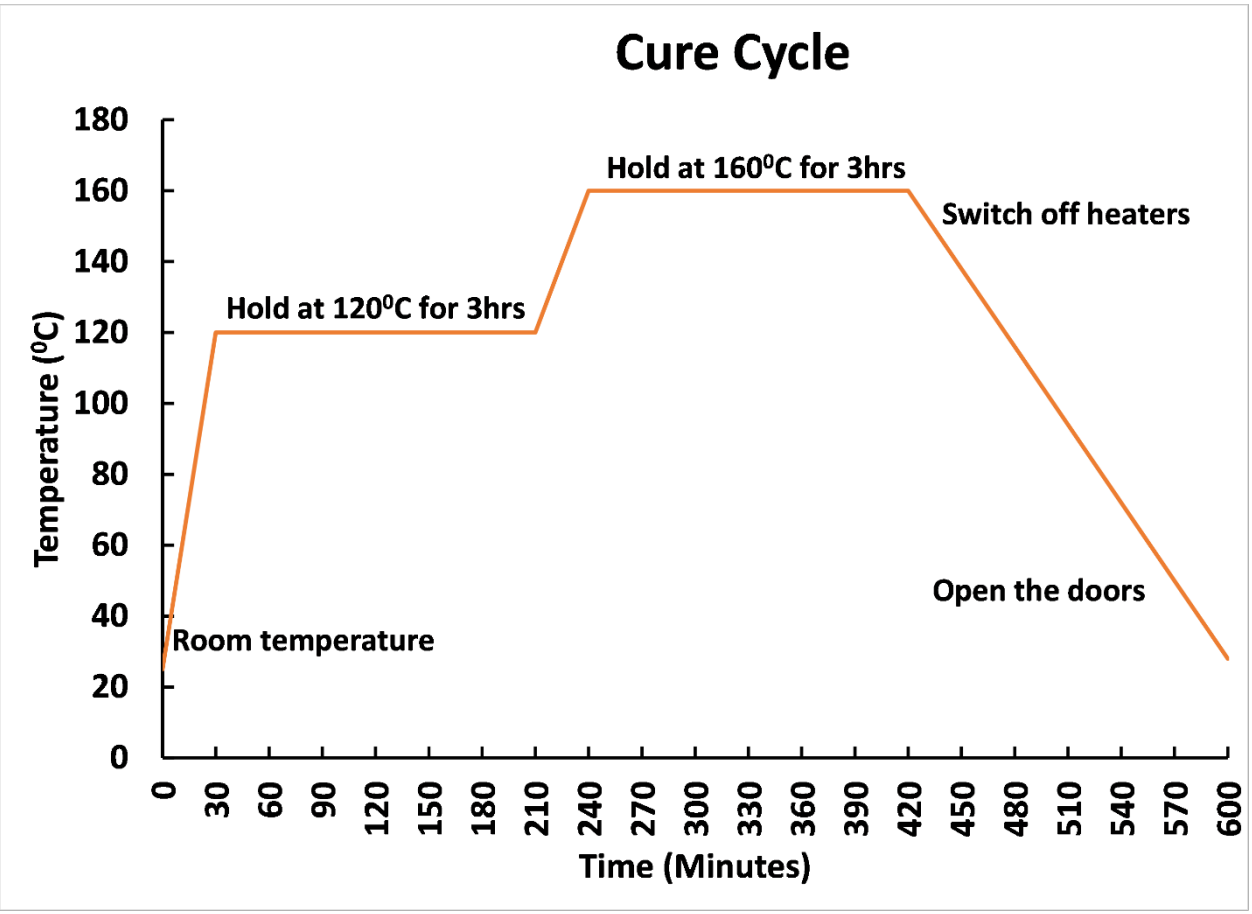

Fig. 3.13 Curing Cycle for GFRP samples

3.2.6 Extraction of Component

After the mandrel is cooled to room temperature, the composite cylindrical shell is trimmed or parted to dimensions using a parting tool preferably carbide tipped tool on a lathe machine. Later, it is extracted from the mandrel by chipping of the PoP by chiseling. The release film is removed and composite shell is cleaned. The pipe or rod over which the PoP was cast is cleaned and can be used for recasting of next product.

Cured glass epoxy composite cylinders (220mm diameter, 5mm thick and 250mm long) realized from the process described above were later adhesively bonded with rubber liner material (2 layers of 2 mm thick rubber material). Two cylindrical GFRP composite structures were fabricated viz. (i) GFRP cylinder-1 with adhesively bonded rubber (with defects) coated with carbon black based adhesive liner and hydroxyl-terminated polybutadiene (HTPB) based composite solid propellant for defect characterization (ii) GFRP cylinder-2 with adhesively

bonded rubber insulation (without defect) coated with carbon black based adhesive liner of increased thicknesses (four zones) to explore the possibility of using single sided low field NMR system as a quality control tool.

3.3 Single sided low field NMR NDE

3.3.1 Experimental Setup

Single sided low field NMR system is based on the principle of inside-out NMR, where the sample is outside the magnet. These systems are provided with stepper motor for precise lifting of magnets to magnetize the region of interest inside the sample. For the present studies, we have used commercially available proton solid state NMR system (Model PM 25, Make: Magritek) with 12.88 MHz RF frequency. The profile NMR-MOUSE (PM 25) is a portable open NMR sensor equipped with a permanent magnet (B_o equivalent to 0.3T) geometry that generates a highly uniform gradient perpendicular to the scanning surface outside the magnets. Figure 3.14 shows the low field NMR experimental setup used for the present work and Figure 3.15 shows its schematic arrangement. A flat sensitive volume is excited and detected by a surface RF coil (frequency 12.88 MHz) placed on top of the magnet at a position that defines the maximum penetration depth into the sample. By repositioning the sensitive slice across the object, this scanner produces 1D profiles of the sample with a spatial resolution of 100 μm. Carr-Purcell-Meiboom-Gill (CPMG) pulse sequences were used for determining the T_2 relaxation times. The present study reports results from the experiments performed with CPMG pulse sequence at pre-defined position programmed using Prospa software. The sensor excites a sensitive volume at a fixed distance from the magnet surface as per the program. By mechanically moving the sensor, the sensitive volume is stepped through the sample and the CPMG sequence is then applied at each position with an echo-time of 60 μs. Then, signal from each position is plotted as amplitude versus depth plot to generate depth profile of the sample. The main setting and experimental parameters used for the present work are given in Table 3.6.

Table 3.6 Main setting and experimental parameters of low field profile NMR system (PM 25)

Parameter	Value	Parameter	Value
Measuring frequency	12.88 MHz	Sensitive volume (lateral size)	40 x 40 mm^2

Number of Echoes	8	Resolution	100 µm
Number of Scans	256	Gradient strength	256 KHz/mm
Repetition time	400 ms	Pulse length	17.5 μs
Step Size	100 µm	Phase	210^0

Fig. 3.14 Single sided low field NMR system (A: Spectrometer, B: MOUSE with HP lift)

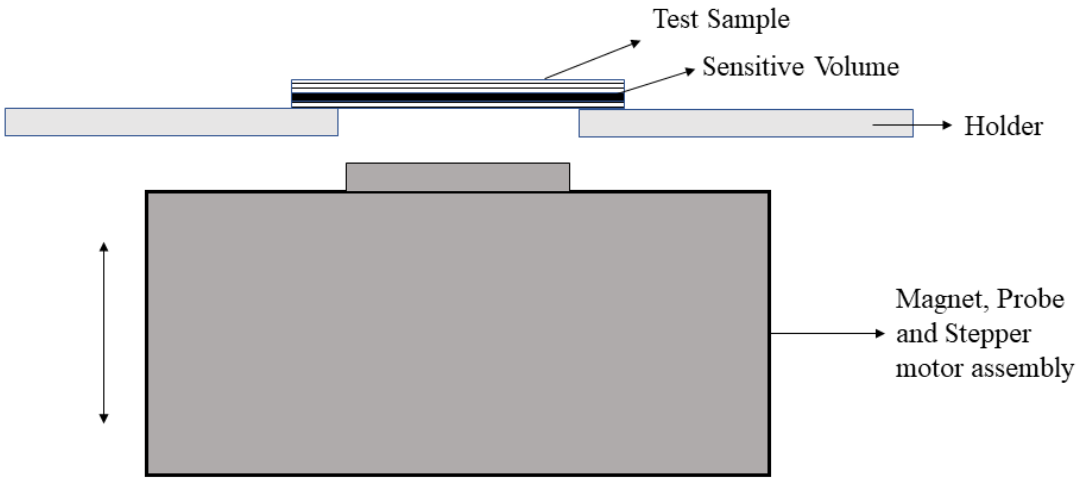

Fig. 3.15 Schematic diagram of testing arrangement

3.3.2 Experimentation and Data Processing

All NMR measurements were carried out using the PM25 sensor, a single sided NMR magnet with a field strength of about 0.3 T and gradient strength of 256 KHz/mm, connected to a Kea^2 spectrometer. Both the PM25 and the Kea^2 spectrometer are produced by Magritek. The sensitive volume of the magnet, which is directly above the radio frequency coil, can measure sample areas up to 40mm x 40mm. The maximum depth within a sample that the sensitive volume can probe is 26mm. By placing additional spacers on top of the gradient system, the maximum penetration depth can be adjusted to achieve the best sensitivity for each task. While adding spacers decreases the maximum penetration depth, the amount of signal that can be detected by the magnet increases. Adding in the spacers also shortens the pulse length and minimum echo times that can be used during CPMG experiments. The magnet is also attached to mechanized high precision (HP) lift that can move the magnet up or down by 30 or more μm increments. The lift allows the user to optimize the magnet's position to ensure that the region of the specimen with the greatest signal density is probed. The magnet, spectrometer and HP lift are all connected to a computer that runs software called Prospa, which is also produced by Magritek. In Prospa, the signal output generated by experiments is recorded.

All T_2 measurements were performed on the PM25 sensor by CPMG experiments for the 90^0 and 180^0 pulses. A total of 256 acquisition scans were used. All single sided data was plotted and fitted to a bi - exponential decay curve of the form:

$$S(t) = A_{short}\, e^{-t/T_{2short}} + A_{long}\, e^{-t/T_{2long}}$$

where,

S - signal intensity

t - time in seconds

T_{2short} and T_{2long} are the unique T_2 values observed. A_{short} and A_{long} are the signal intensities attributed to T_{2short} and T_{2long} respectively.

3.4 Acousto-Ultrasonic Scanning (AUS)

AUS is a non-destructive testing technique for evaluating materials and structures with multi-layered configurations. The name AUS is based on the fact that principles of acoustic emission

and ultrasonics are combined in this technique. Unlike conventional ultrasonics, AUS is not concerned with the detection and characterization of individual flaws. Instead, it is concerned with the assessment of the collective effects of various subcritical flaws and microstructural irregularities in composites which in turn govern mechanical properties and durability of multi-layered composite structures.

The experimental setup for low frequency AUS for interrogating the interfaces of the multi-layered composite structures consists of tone burst excitation pulser and broadband receiver system (frequency range of 10 KHz to 20 MHz) along with pre-amplifier electronics and low frequency ultrasonic probes. The entire electronics and back-up power supply is housed in safety certified composite enclosure. The system is portable for inspection at the shop floor. The test signals were captured in A-scan mode for further analysis. In A-scan mode, amplitude versus time of flight of tone burst excitation received using broadband receiver is captured. Two cycles of sinusoidal burst of 75 KHz frequency is used for testing. One probe for excitation and other probe for receiving were used in pitch catch mode. In multi-layered composite structures, the presence or absence of de-bond at the interface of rubber and GFRP composite is tested from same side by two test probes (Tx and Rx) across the test surface at a distance of 100mm from each other. Wherever the interface is bonded with adhesive; it is observed to transmit ultrasonic wave to the receiver probe with some attenuation due to loss of energy during transmission. The AUS system used for the present study is shown in Figure 3.16.

Fig. 3.16 Acousto-Ultrasonic System

3.5 Microwave NDE (MWNDE)

Microwave NDE is a latest NDE technique. Microwave NDE is used to study the components with dielectric properties [87-92]. Microwave NDE operates in the frequency range 1 GHz-40 GHz of the electromagnetic spectrum. The advantages of Microwave NDE when compared with the traditional NDE techniques are listed below:

- It is suitable of dielectric materials
- Couplant is not required for the inspection of components (Dry method).
- Probe can be used either for near field or far field inspection.
- Inspection is possible from single side or from both sides.
- Testing can be done in both contact and non-contact modes.
- Economical inspection setup

Microwave NDE uses electromagnetic waves for interrogating the materials. The changes in dielectric property affect the reflected wave amplitude and phase. Figure 3.17 shows microwave NDE setup used for the present studies. The microwave NDE setup consists of a vector network analyser (VNA), coaxial cable and open-ended rectangular waveguide (OEWG) probe. The bond quality between the composite cylinder and the rubber insulation is inspected by measuring the scattering parameters and reflection characteristics of the structure. Inspection is performed from rubber side. From the scattering parameters, amplitude and phase are computed. Bonded region and de-bonded region show variations in both amplitude and phase.

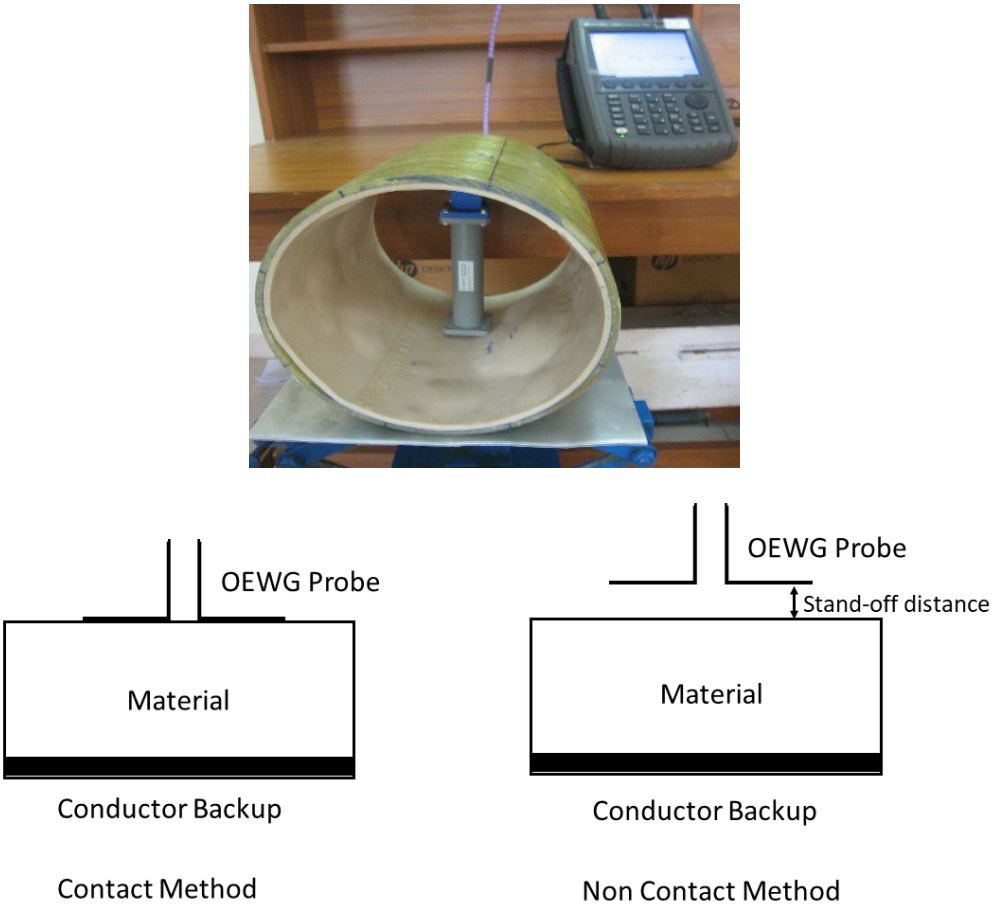

Fig. 3.17 (a) Microwave NDE inspection system (b) Schematic of NDE inspection

3.6 X-ray Radiography

Radiographic evaluation of multi-layered composite structures is particularly complicated as compared to other engineering components because of the nature of design configuration and the wide variety of materials that go into their manufacturing and manifests in low subject contrast when radiographed. The radiographic contrast can be improved up to certain extent by proper choice of radiation energy as well as the selection and optimization of suitable techniques.

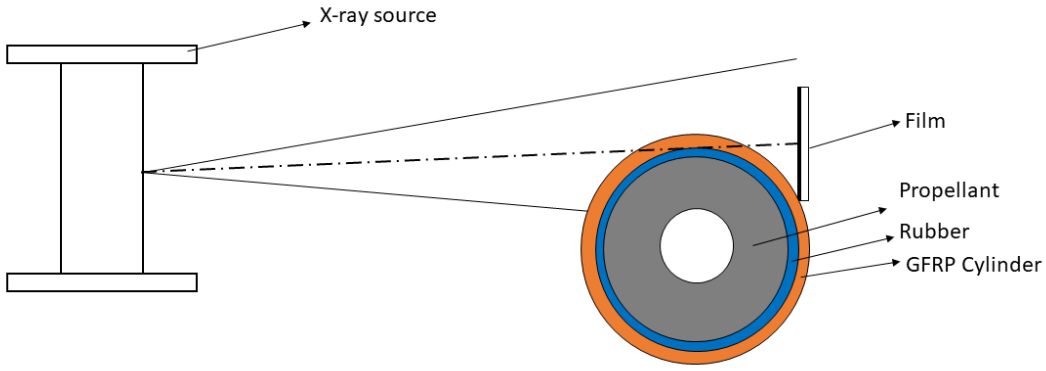

Fig. 3.18 Schematic of tangential radiography

Tangential radiography technique is used to reveal de-bonds at GFRP-rubber interface and rubber-propellant interface. To achieve this, X-rays are directed tangential to the above interfaces and emerging radiation is recorded on a film as given in Figure 3.18. The X-ray path lengths for exposure calculations are obtained using simple geometrical considerations as well as the half value layer (HVL) values of the different types of materials involved in the interface. The films are exposed to X-radiation in rigid metal cassettes for better film screen contact. The films exposed to X-rays are more sensitive to pressure marks and process variables. Hence, properly controlled manual film processing is practiced in the present study at standard conditions of 20^0C temperature, 5minutes development, 1minute in acid stop bath, 10minutes in fixer and 30minutes in water bath. Evaluation of radiographs is however a challenging task because of the thickness variation and wide variety of materials involved at the interface and their effect on the resulting image quality. A commercially available 450kV and 4mA X-ray source (Comet make) and Carestream Industrial X-ray films (MX 125 equivalent to fine grain film D4) are used for the current studies.

3.7 Computed Tomography

Computed tomography (CT) is a technique capable of overcoming many limitations of conventional NDE methods namely: 1) visualization of precise location, orientation and size of defects such as cracks in propellant grain and outer composite cylinder and interfacial defects such as de-bonds and delamination. In addition, CT provides the 3D imaging of the internal structure of the component.

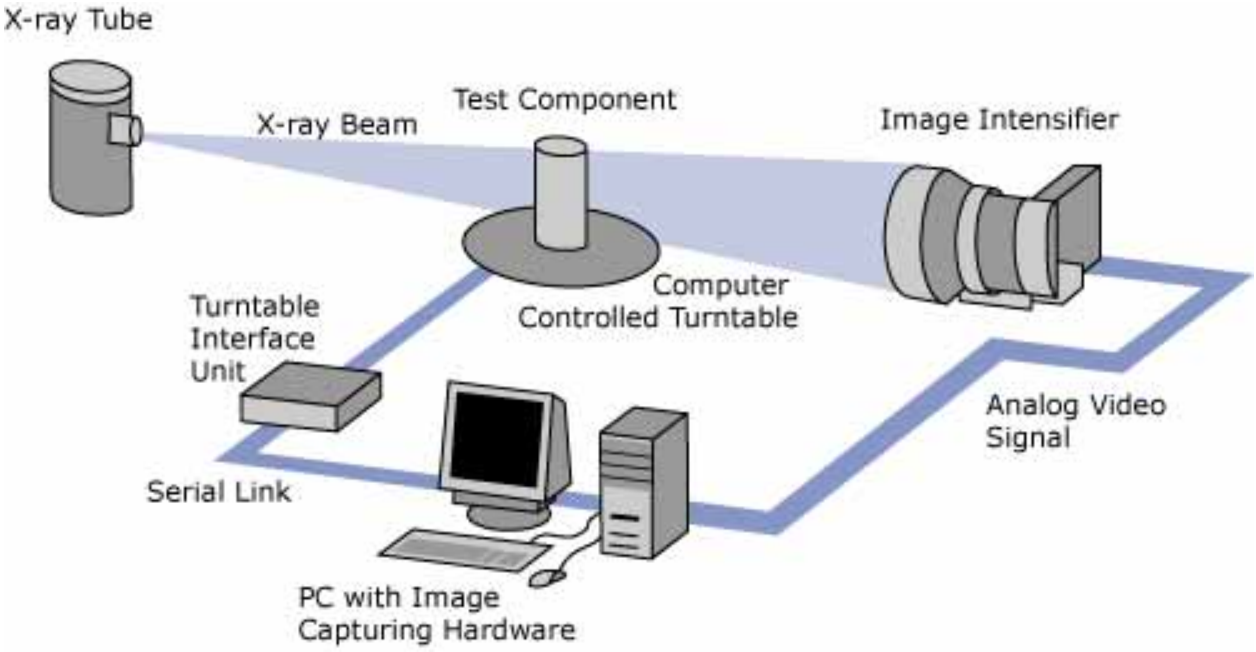

Fig. 3.19 Schematic of Computed Tomography setup

CT provides an image of a cross-section of thin slice of a component under inspection. As with X-ray radiography, CT provides imagery based on the varying attenuation of X-rays simultaneously, a tomographic system exposes only thin cross-sectional slice of the component at a time [93-96]. In CT, the X-ray energy transmitted by the component is measured by a single or array of detectors aligned on the other side of the component as shown in Figure 3.19. The component is then rotated 180^0 in small increments and the corresponding X-ray energy measurements are taken at each angle. These measurements are then used in a suitable reconstruction algorithm to generate the desired cross-sectional image. The CT system used for the present study consists of an X-ray tube (150kV and 0.5mA source), sensitive detector array, high precision mechanical manipulators and high-speed computer for handling huge data.

4. NMR Depth Profile Studies on Flat Sample

In the current chapter, three NDT techniques, NMR, AUS and X-ray radiography are utilized to detect the defects made in a multi-layered, glass fibre reinforced polymer (GFRP) based composite laminate. The responses from the three techniques are compared and presented in the chapter. Adhesively bonded interfaces of GFRP-rubber and rubber-propellant were investigated for planar interfacial defects with a spatial resolution of 100 microns. Single-sided low field NMR having magnetic field strength of 0.3 T (12.88 MHz RF frequency) has been used for non-invasive inspection of planar defects in GFRP based multi-layered composite structure. Investigation revealed applicability of single-sided low field NMR for onsite field applications. Results were compared with other conventional established techniques viz. acousto-ultrasonic and X-ray radiography. It is observed that the single-sided low field NMR is an excellent NDE tool to study adhesive bond and the defects such as de-bond, variations in thickness and degradation.

4.1. Depth profiling of Rubber Sheet

The experimental results obtained from depth profile NMR studies of rubber sample are shown in Figure 4.1. The thickness of the rubber sheet is 2.2 mm and can be verified by the NMR data shown. Experiments were performed using optimized experimental parameters i. e. pulse length of 10 μs and repetition time of 400ms. The number of scans for these experiments was fixed at 256. The experiments were performed at 100 microns spatial resolution with a step size of 100 microns. CPMG pulse sequences were used for detection. With the use of profile application macro of PROSPA, a CPMG Fast sequence is executed and this controls the position of PM25 MOUSE to scan the profiles. The sensor excites a sensitive volume at a fixed distance from the magnet surface. By mechanically moving the sensor, the sensitive volume is stepped through the sample and the CPMG sequence is then applied to each spatial position. In the software program, it is possible to add different parts of the CPMG train (contrast 1, 2 and 3) to introduce different T_2 weighted data into the intensity of the signal.

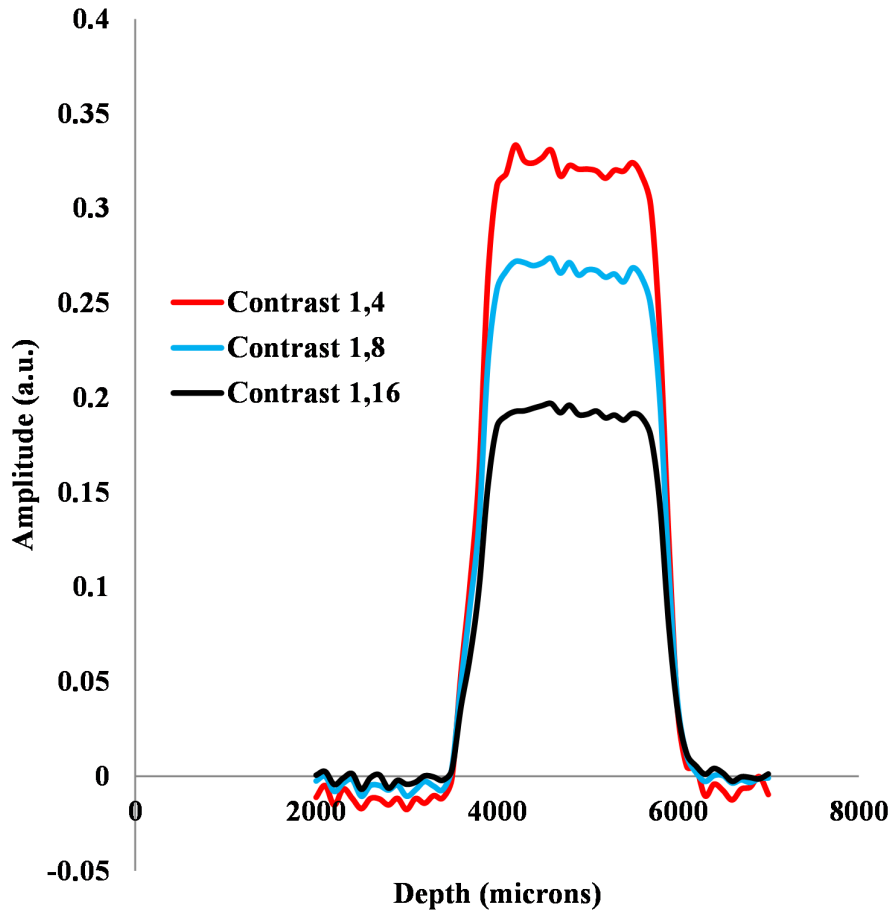

Fig. 4.1 Profile NMR data of rubber sheet.

Three different contrasts (contrast 1, 2 and 3) are echo sums of first 4 echoes, first 8 echoes and first 16 echoes as a function of depth. It indicates the proton density of the material and variations in the T_2 values. The values of echo amplitude fall to zero when the sensitivity volume of the probe is taken beyond the sample indicating clearly absence of protons. As the probe is moved across the sample, the response of protons to the magnetic field within the sensitive volume is seen from their sensor output values. Any value of amplitude greater than zero is indicative of presence of protons, hence relaxation in presence of external magnetic stimuli (CPMGFast RF pulses). The response function clearly falls to zero in the absence of protons indicating that at that particular depth the sensitive volume is out of rubber material, hence the rubber outer boundary. The values of thickness of the rubber material at the measurement zone can be estimated. In this case, the value of rubber sheet is observed to be 2200±100 microns. This is fairly accurate as was confirmed from physical measurements. However, measurements using NMR profile system is of similar accuracy, but non-contact

measurement. In order to understand the chemical nature of the rubber, T_2 relaxation measurements were done using CPMG pulse sequences.

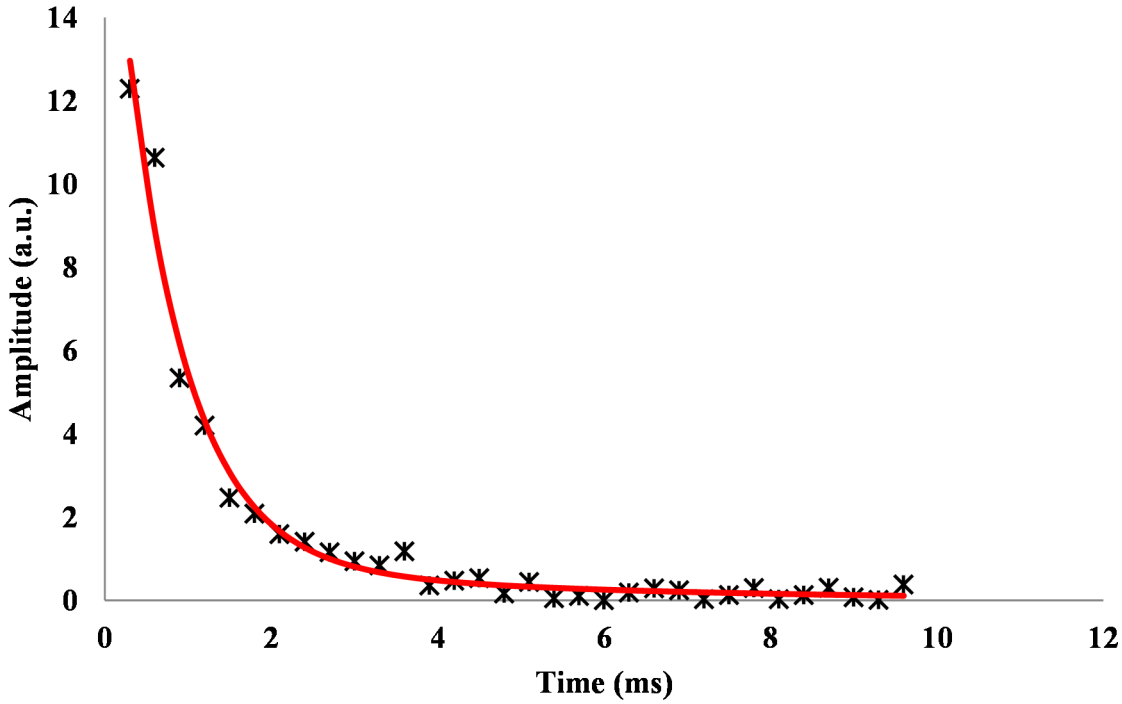

Fig. 4.2 Free induction decay (FID) curve of rubber (Bi-exponential fit)

Figure 4.2 shows peak amplitude values as a function of time indicating the bi-exponential decay pattern of the peaks with time. The decay data is then fit to bi-exponential function. The resulting two amplitude values are attributed to spin-spin relaxation times namely T_2 effective short and T_2 effective long associated with molecular mobilities. T_2 effective short value (0.7ms) is related to polymerized rubber with cross linked side chains, whereas T_2 effective long value (1.9ms) is attributed to polymer with free side chains and ends. The relative amplitudes of T_2 effective values can be attributed to fraction of polymer with cross-linked chains and free polymers. It may be used as an estimate for observing chemical changes in the polymer materials.

4.2. Depth profiling of GFRP – Rubber flat sample

The image of tangential X-ray radiography film of the composite sample tested using X-ray radiation is shown in Figure 4.3. Radiography film clearly shows the separation of rubber from composite due to non-application of the adhesive at that region. This confirms the presence of

air gap for proving the NDE capability of low field NMR system. Confirmation from radiography technique is essential for establishing the test procedure using low field NMR system. Further confirmation of presence or absence of air gap or de-bond in the multi-layered composite has been done using AUS.

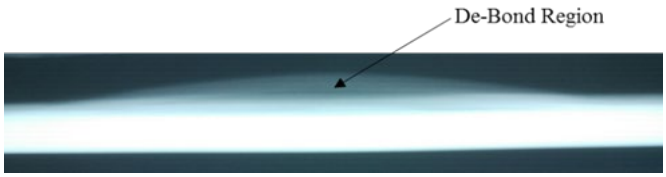

Fig. 4.3 X-ray image of GFRP-rubber sample with de-bond

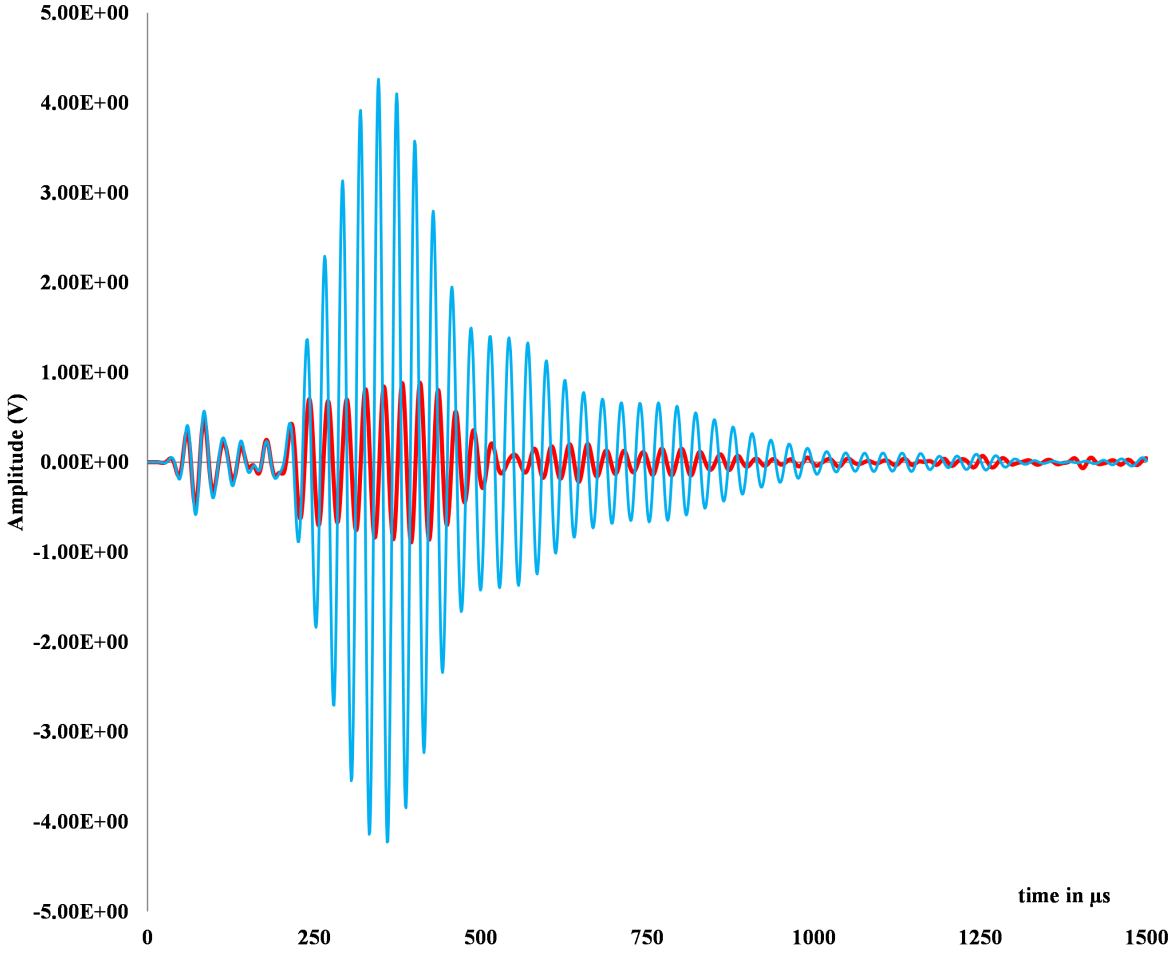

Fig. 4.4 AUS data of GFRP-rubber de-bond

The transmitted stress wave energy as received at the receiver as a function of time is shown in Figure 4.4. Red color waveform indicates the transmitted waveform as received by the receiver

over a bonded region. Inspection was further performed over the region indicated as de-bond (air gap) in the X-ray radiography method. It is observed that more stress wave energy is received at the receiver probe due to the reflection back at the de-bond region (lower absorption energy due to poor transmission at the de-bond region). AUS data further confirms the presence of de-bond in the inspected region as indicated by X-ray radiography data.

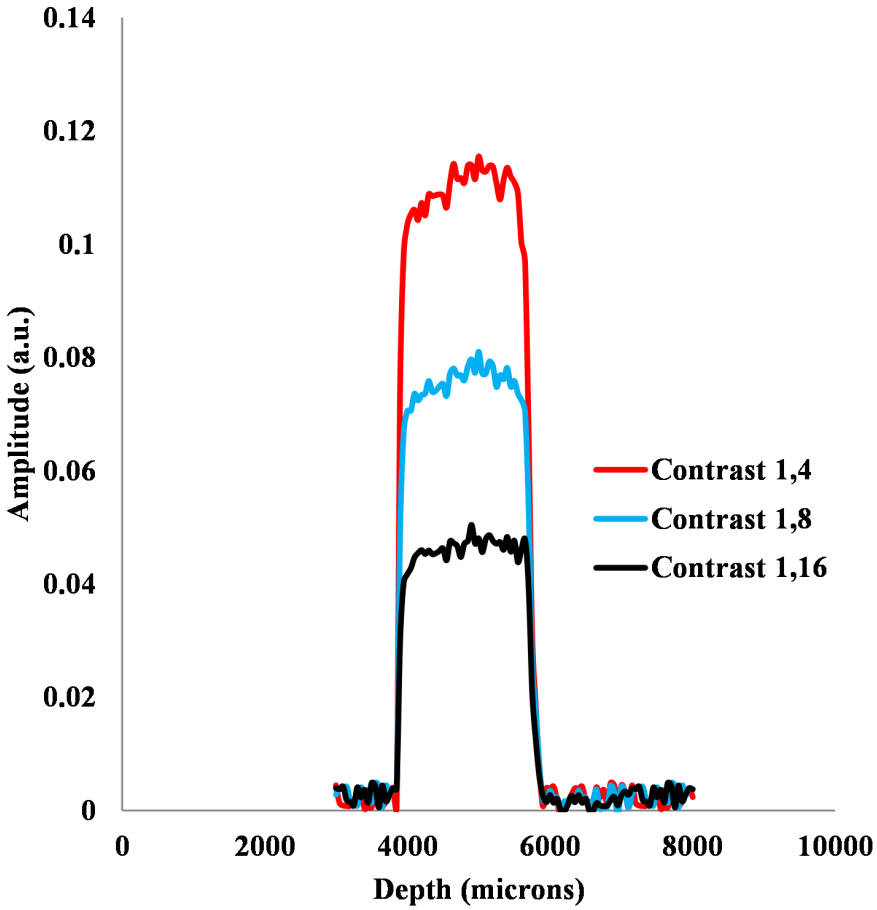

Fig. 4.5 Profile NMR data of GFRP-rubber bonded region

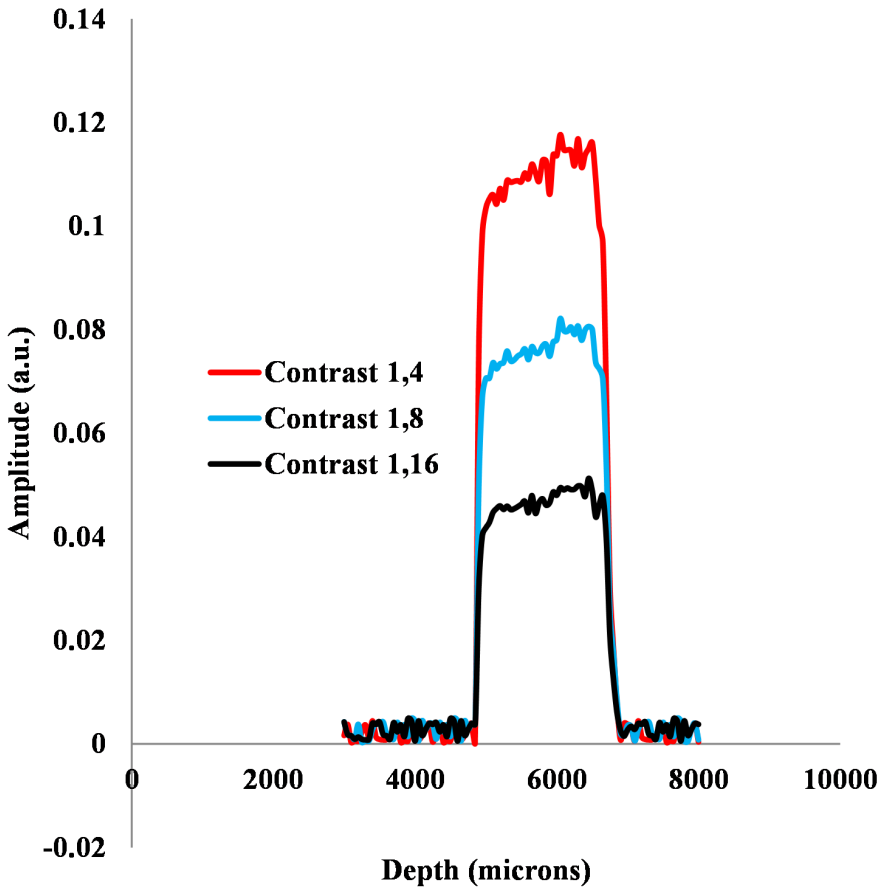

Fig. 4.6 Profile NMR data of GFRP-rubber de-bonded region

Depth profiling of good region was carried out using optimized test parameters for the test sample and the profile NMR data is shown in Figure 4.5. The sample thickness was calculated to be 6 mm due to adhesive bonding of 2 mm thick rubber layer to 4 mm thick GFRP composite laminate. As described previously, there is no appreciable signal from composite sample due to low proton density as well as absence of free protons for appreciable magnetization during low frequency AC magnetic field application. Hence, during initial 4 mm of the GFRP composite laminate, no signal is observed as seen above 0 to 4000 microns values being close to zero. However, when rubber sample is encountered, there is an appreciable signal variation as seen from 3800 microns to 5900 microns. This also indicates that rubber molecules were present from 3800 to 5900 microns, thus a thickness of 2100 microns can be ascertained to the rubber layer. The presence of rubber is clearly visible with observation of interface boundary (start of rubber layer and end of it). From the data, the thickness of rubber is accurately calculated non-destructively within an accuracy of ±100 microns. The depth profile data of the same sample

from Figure 4.6 was used to identify the de-bonded region (confirmed the presence of de-bond/air gap using X-ray radiography and AUS). The experimental data shows rise in amplitude at 4800 microns depth and fall in amplitude at 6900 microns. This indicates the presence of rubber with thickness of 2100 microns. The shift in initial value of rubber at depth of 3800 microns to 4800 microns indicates presence of air gap at that region. Since air has no proton density, no signal at air gap region is observed. It may be noted that air gap in the test sample in the tested zone has already been confirmed from X-ray radiography and AUS data. Thus, depth profile NMR is able to identify presence or absence of air gap qualitatively as well as quantitatively in the inspected region. It is clearly observed that the rubber evolution has started at 4800 microns instead of 3800 microns observed in non-defective region. The shift in rubber start signal is indicative of presence of air gap (1000 microns) in the tested region. The data is much clearer in indicating the shift in signal as well as the shifted value. The flatness in the data of rubber indicates homogeneity of the rubber material within its thickness. The amplitude value is also proportional to proton density and T_2 relaxation time.

4.3. Depth profiling of Adhesive Liner (Varied Thickness)

The depth profile data (Figure 4.7) of GFRP-rubber multi-layered composite with adhesive liner at zone 1 and the signal amplitude is shown as a function of depth in microns. It is observed that the depth profile data has distinct signatures for each of the materials. A sharp peak at 5500 microns depth is indicative of the adhesive liner sample. Rubber layer is identified between 3700 microns and 5350 microns. The signal strength of adhesive liner is much higher as compared to rubber owing to its higher proton density. The thickness of adhesive layer can be estimated from the profile data. In this case, the start of adhesive layer is observed to be at 5350 microns and ends at 5600 microns, indicating an overall thickness of adhesive layer to be 250 microns. Thus, from the profile NMR studies, it is possible to estimate adhesive material both qualitatively as well as quantitatively.

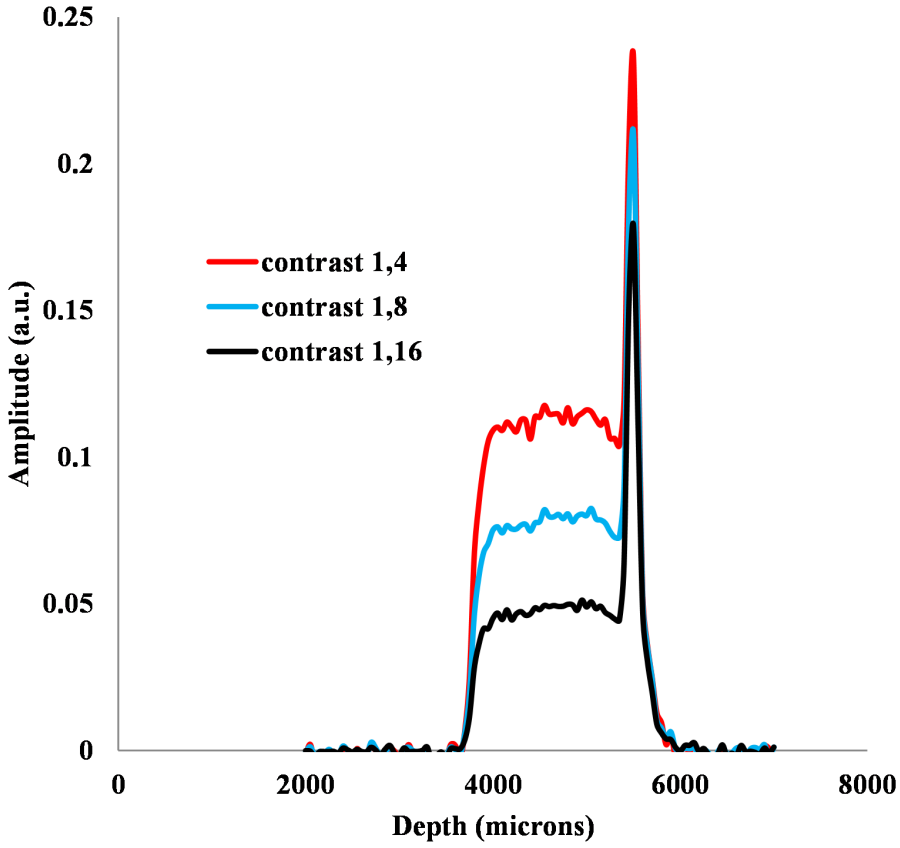

Fig. 4.7 Profile NMR data of adhesive liner zone 1

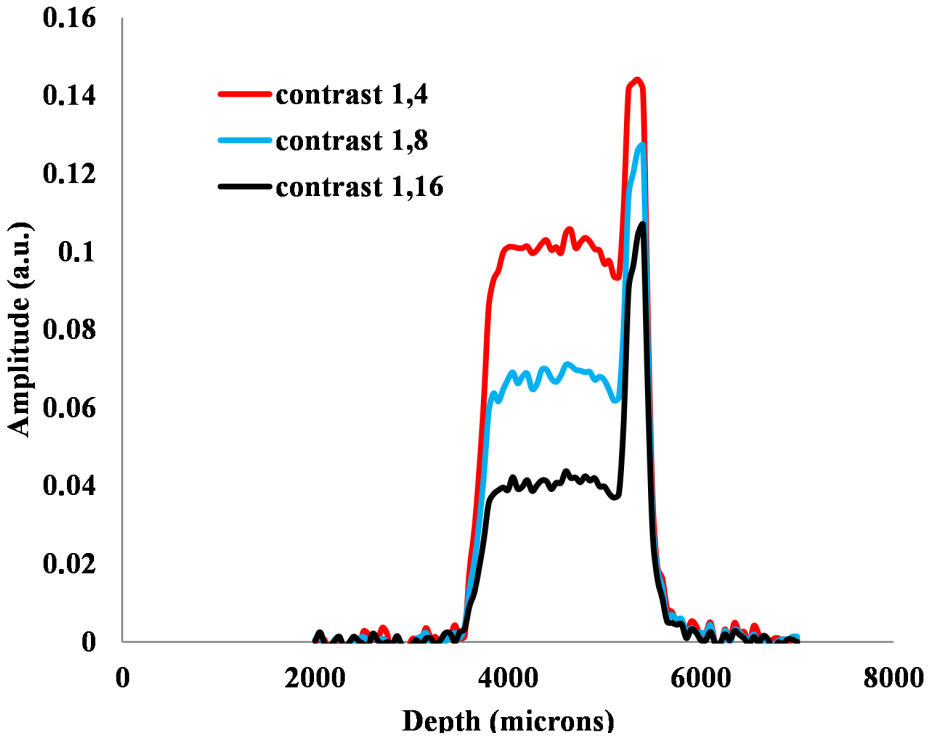

Fig. 4.8 Profile NMR data of adhesive liner zone 2

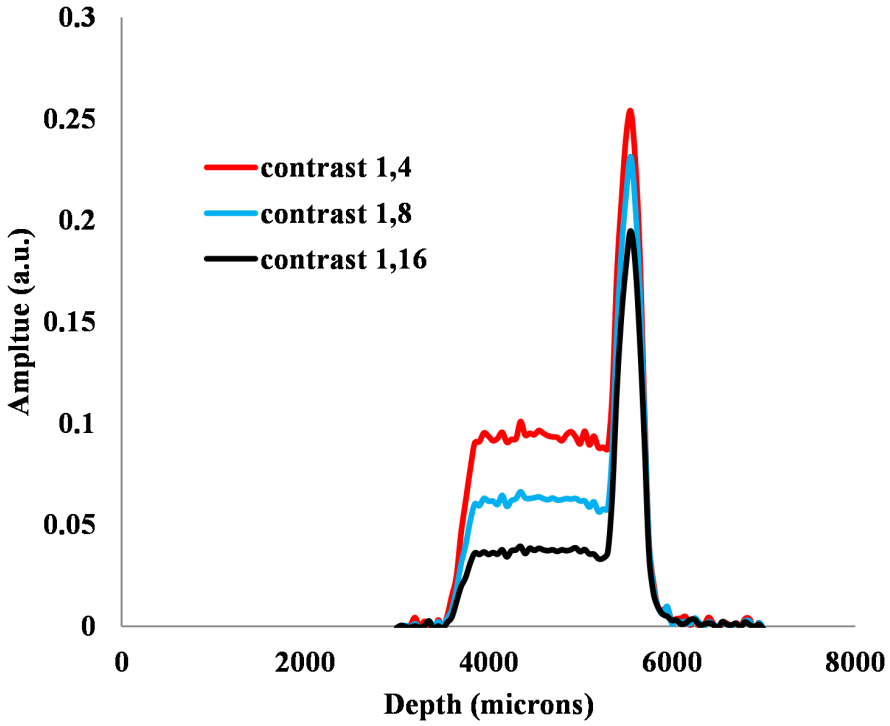

Fig. 4.9 Profile NMR data of adhesive liner zone 3

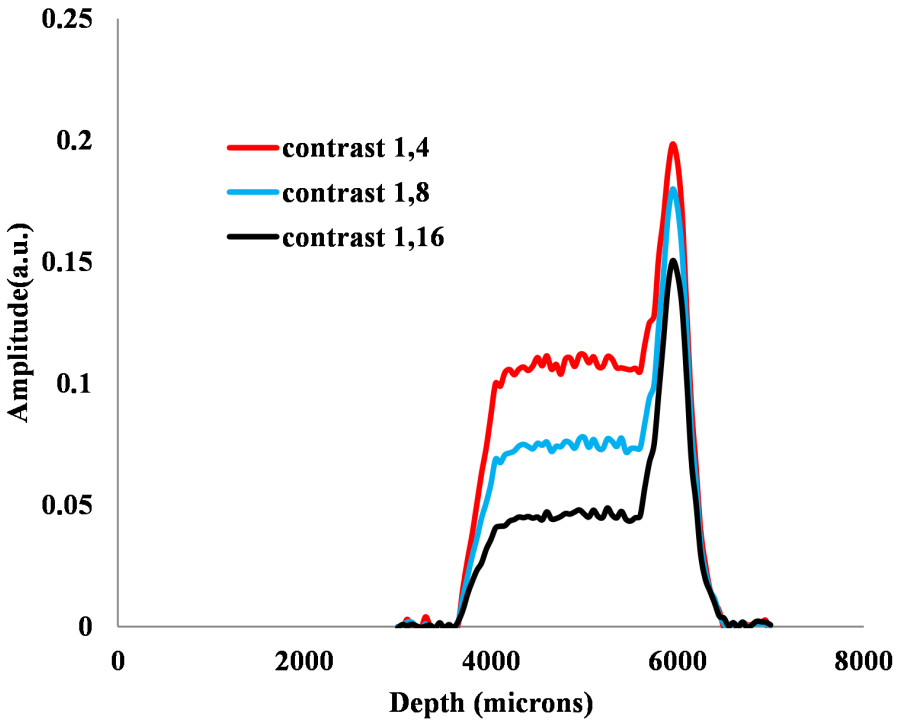

Fig. 4.10 Profile NMR data of adhesive liner zone 4

The depth profile data of sample at liner zone 2 and zone 3 are depicted in Figure 4.8 and Figure 4.9 respectively. It is observed that amplitude value increased from zero at a depth of 3600 microns indicating presence of protons of rubber layer. However, within rubber layer, the amplitude values showed flat response over the thickness indicating homogenous nature of the rubber. However, as the profile sensitive volume reached liner zone the amplitude value increased to higher amplitude than rubber sample indicating higher proton density of liner molecules. The rise in amplitude at 5150 microns and drop at 5500 microns is attributed to liner material. In this case, the liner thickness is estimated to be 350 microns for zone 2. Liner is observed to have higher amplitude than rubber with distinct peak indicating that the liner has finite thickness. Liner for zone 3 is observed to start at 5300 microns and end at 5750 microns, indicating clearly absence of material beyond its thickness. In this case, the liner thickness is estimated to be 450 microns for zone 3.

The depth profile data of liner zone 4 (Figure 4.10) is observed with different thickness coated on rubber substrate. The thickness value of liner is found to be 550 microns. All the liner zones have shown consistent signal amplitude in that zone and are much higher than rubber samples.

All the liner samples have finite thickness values, which were estimated from their depth profile data. Table 4.1 below shows thickness of liner material on rubber substrate.

Table 4. 1 Measurement of adhesive liner thickness by NMR

ZONE	THICKNESS (microns)
1	250
2	350
3	450
4	550

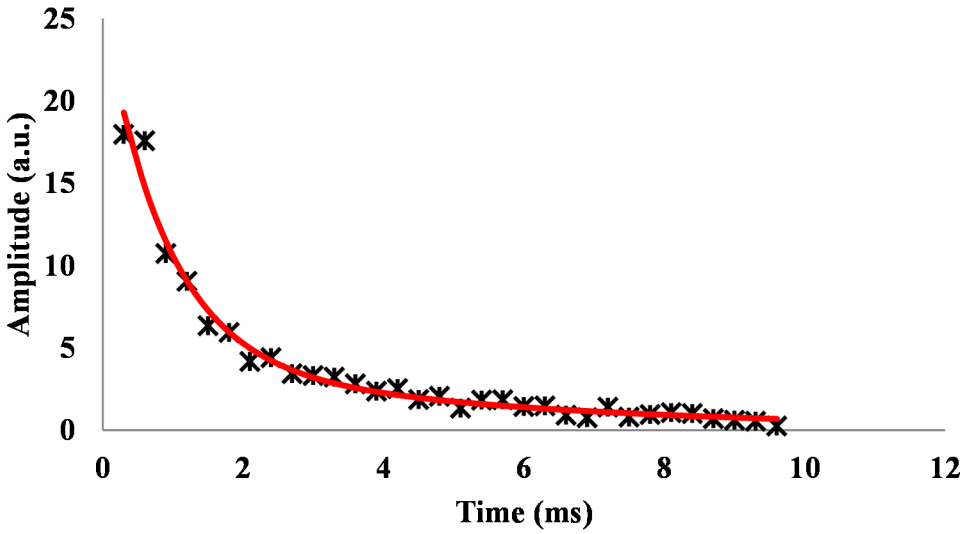

Fig. 4.11 FID data of adhesive liner (Bi-exponential fit)

The chemical nature of the elastomeric materials including rubber can be studied using single sided NMR relaxometry. For the present study, as described above, rubber has been used as substrate for coating thin adhesive liner layer. Initially, rubber has been studied using single sided low field NMR system to ascertain the system capabilities as well as to study rubber for

its chemical nature. The test sample of GFRP composite and rubber bonded has been studied for the spin-spin relaxation using low field NMR. Figure 4.11 shown above is the free induction decay curve of the sample. Each elastomeric material has characteristic curve which when fitted to bi-exponential curve fitting represents the contributions of short and long relaxation times. In this case, the experimental curve is bi-exponentially curve fitted to obtain bi-exponential fit coefficients representing T_2 short and T_2 long. T_2 short (0.9 ms) corresponds to solid component of the polymer, which is already cross-linked, and T_2 long (5.2 ms) corresponds to contribution from sample having un-polymerized, un-cross linked monomer sample.

4.4. Depth profiling of GFRP-Rubber-Liner-Propellant flat sample

Figure 4.12 shows the image of X-ray radiograph of test sample taken tangentially. Radiograph shows all layers intact and no separation of layers or defects at the interface were observed. Test sample was subjected to acousto-ultrasonic inspection at the zones tested by radiography using AUS. AUS inspection revealed abnormal signals indicating de-bond between GFRP and rubber interface as well as be-bond between rubber and propellant.

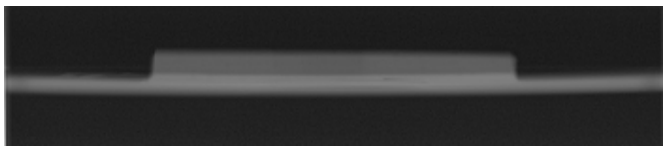

Fig. 4.12 X-ray image of GFRP-Rubber-Liner-Propellant sample

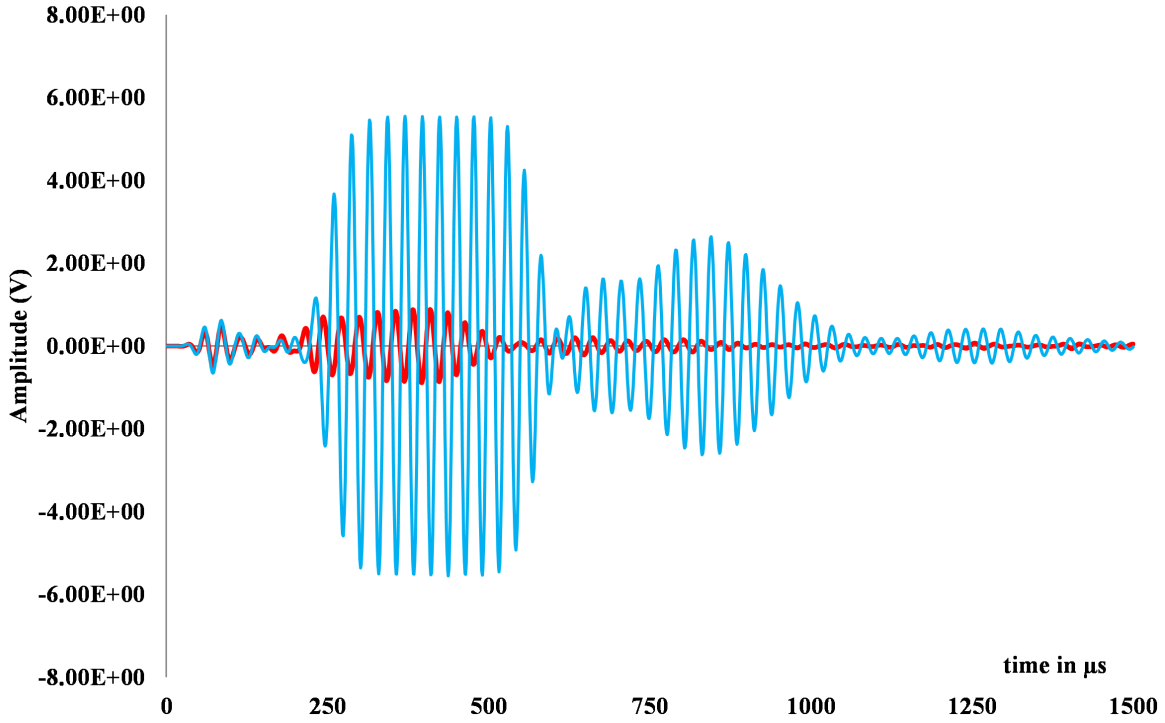

Fig. 4.13 AUS data of GFRP-Rubber de-bond and Rubber-Propellant de-bond

AUS data shown in Figure 4.13 has revealed presence of de-bonds at two interfaces namely (i) GFRP-rubber (250-550 µs) and (ii) rubber-propellant (600-1000 µs). These defects were not observed in tangential radiography; this may be due to poor sensitivity of the technique for such type of defects.

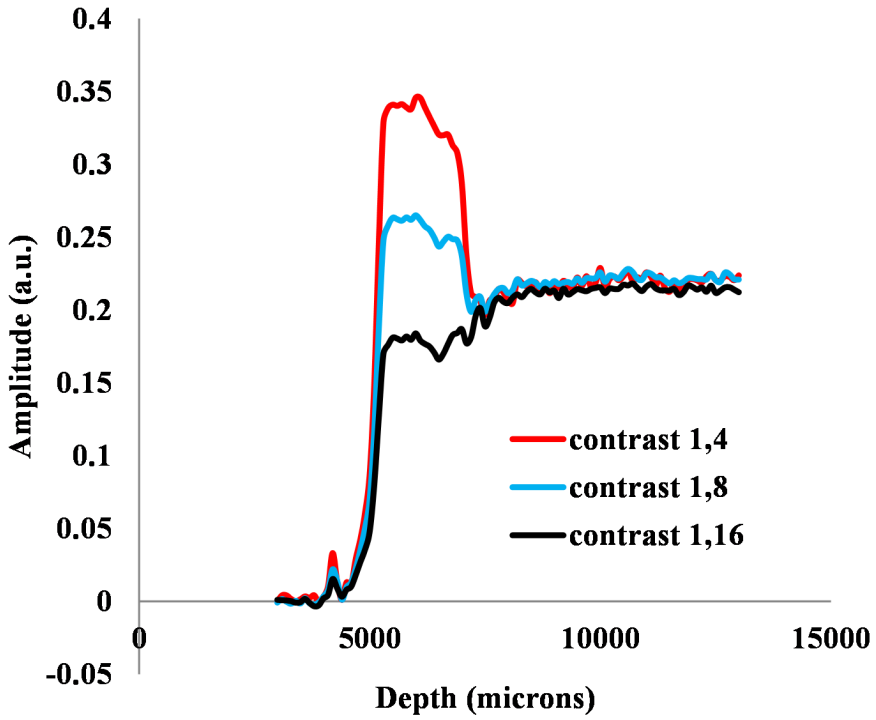

Fig. 4.14 Profile NMR data of GFRP-Rubber-Propellant (without Liner) region

The low frequency single sided NMR depth profile of the sample (GFRP-Rubber-Propellant) without liner material shows that rubber material has higher proton density as compared to propellant. The signal amplitude of rubber is much higher than propellant signal value. From the Figure 4.14, it is also observed that rubber thickness is about 2100 microns and the interface of rubber-propellant is distinct with clear hint of dip in the signal value at the transition point.

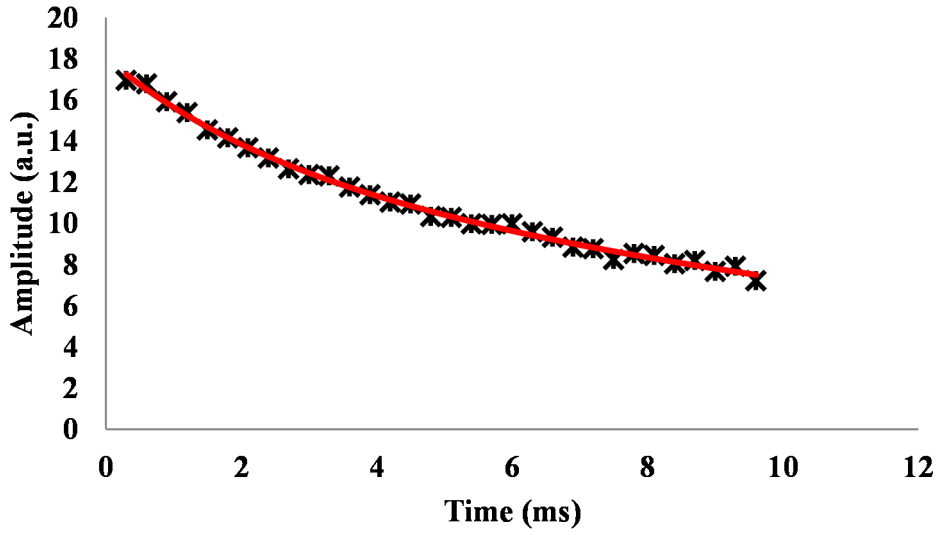

Fig. 4.15 Free induction decay (FID) data of Propellant (Bi-exponential fit)

Figure 4.15 shows signal amplitude of propellant as a function of acquisition time in depth profile experiment at a depth of 10mm which corresponds to propellant layer. Spin-spin relaxation times of propellant were evaluated for the sample using low field NMR procedures described earlier. From the experimental data, T_2 values of propellant were observed to be 11.4 ms and 12.4 ms corresponding to T_2 short and T_2 long components.

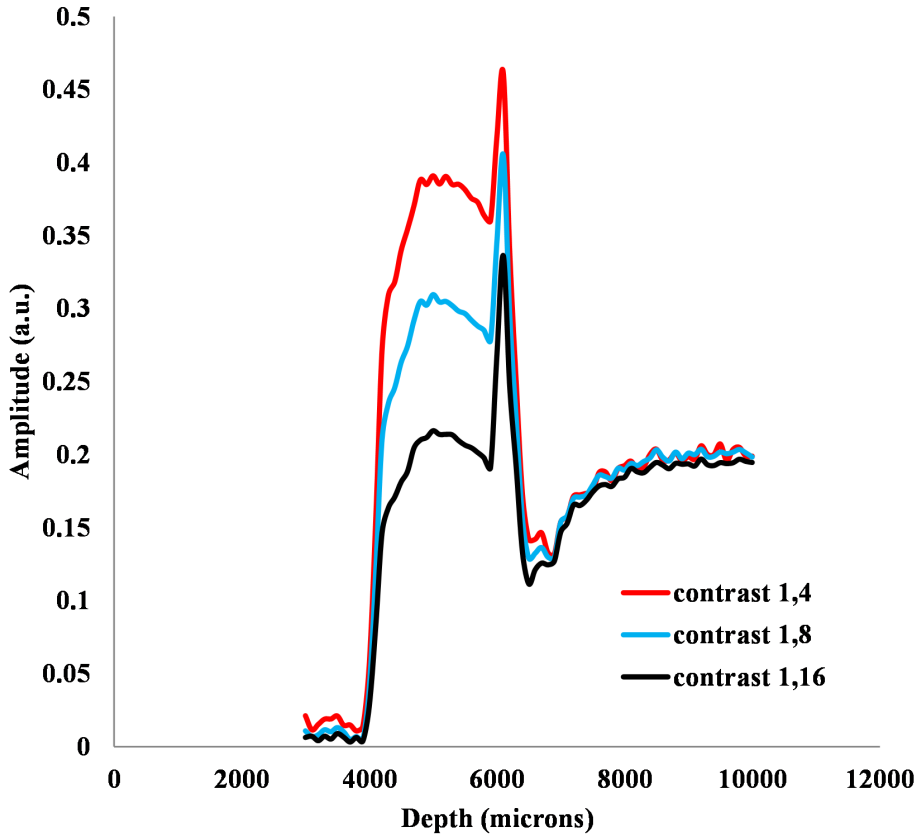

Fig. 4.16 Profile NMR data of GFRP-Rubber-Liner-Propellant (de-bond between liner and propellant) region

Another region of test sample with GFRP-Rubber-liner-propellant all bonded as per procedure has been tested using single sided low field NMR. Test sample was prepared with de-bond between liner and propellant. Due to no chemical adhesion between liner and propellant, it is expected that absence of material / protons at the interface may show in NMR depth profile. The depth profile of test sample shown in Figure 4.16 showed three distinct features. Initially, rubber sample response is seen between 3900 and 6000 microns followed by a sharp peak that of adhesive liner coated on rubber. From about 6400 microns to 7000 microns depth, there is sharp fall in signal, which is attributed to absence of any material / protons. This sharp dip is associated with absence of chemical bond and air gap indicating de-bond between liner and propellant at that interface. Later, flat propellant signal is observed beyond the de-bond. Thus, NMR accurately detected de-bond at the interface of the sample.

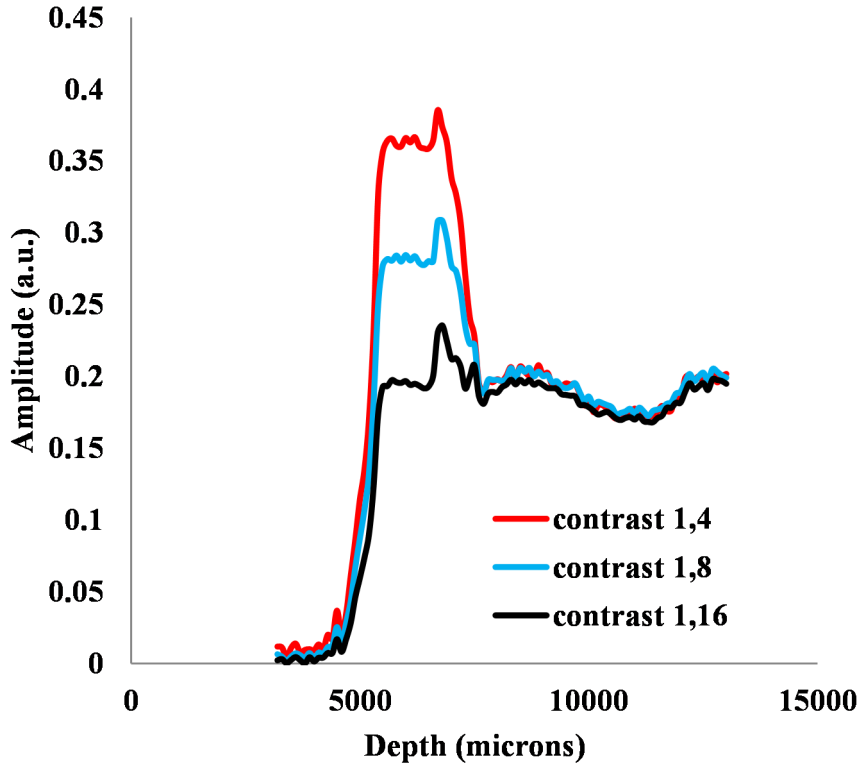

Fig. 4.17 Profile NMR data of GFRP-Rubber-Liner-Propellant (Propellant gap) region

One more region of test sample having defect within propellant in addition to defects at other two interfaces was subjected to NMR depth profile experiment. Figure 4.17 shows depth profile of test sample captured using single sided low field NMR. From the experimental results, it is observed that signals of rubber, liner and their interfaces were distinct. However, beyond the liner, propellant signal with reduced signal value is observed. It is also observed that the propellant sample data is not flat for entire width / depth of the sample. There were dips in signal at some points indicating the separation of material within propellant. This also indicated presence of defect within the propellant sample at that depth. The experimental data also shows observation of collinear defects present at various interfaces of the sample. Defect at GFRP-rubber interface is observed from the shift of depth profile curve due to de-bond at the GFRP-rubber interface. Similarly, a dip in the depth profile data at 7600 microns is indicative of air gap between adhesive liner-propellant interface. Defect at this interface is observed in spite of presence of another defect at GFRP-rubber interface. Depth profile also shows dip in the signal amplitude in the region between 9600 to 12000 microns which is indicative of presence of defect within the propellant material. The observation of presence of three defects which are

collinear at various interfaces of (i) GFRP-rubber, (ii) adhesive liner-propellant and (iii) within propellant material makes single sided low field NMR very useful for practical applications. Such an observation of collinear defects is not possible with conventional established NDE techniques such as ultrasonics and X-ray radiography.

4.5. Summary

The results from the low field NMR experiments were reported and are compared with the results from the traditional non-destructive evaluation techniques like AUS and X-ray radiography. The conclusions from the study are summarized as follows:

Single sided low field NMR studies were observed to be useful for studying bond quality of adhesively bonded surfaces of rubber-GFRP composite. It is observed that using single sided low field NMR technique, not only rubber layer thickness, but also the quality of the adhesive bond between rubber-GFRP composite can be studied. Quantitative measurement of adhesive liner thickness has been recorded. The type of defects viz. rubber thickness variation, air gap at the interfaces were detected and characterized with accuracies ranging from 50 microns to 200 microns. Similarly, de-bond between propellant and adhesive liner was detected. Results from single sided low field NMR studies have been validated by other conventional established NDT techniques such as X-ray radiography and acousto-ultrasonic methods. Results show that single sided low field NMR is a superior NDE technique compared to the existing techniques like X-ray radiography and acousto-ultrasonic methods for defect detection in multi-layered bonded structures.

5. NMR Depth Profile Studies of Cylindrical Structure

The present chapter deals with the application of NDE techniques to identify the defects in the glass fibre polymer based composite structures that are in cylindrical shape. NMR technique is used to identify the defects that are intentionally placed and the results obtained are compared with the results from the traditional NDE techniques like AUS and X-ray radiography.

5.1. Cylindrical GFRP Composite Structure

GFRP composite cylinder of 220 mm diameter has been studied. The cylindrical GFRP composite structures used in the present study with details are shown in Figure 5.1 and Figure 5.2. Two cylindrical GFRP composite structures were fabricated viz. (i) GFRP cylinder-1 with adhesively bonded rubber insulation (without defect) (ii) similar GFRP cylinder-2 with adhesively bonded rubber and other elastomeric materials (with defects).

Fig. 5.1 Cylindrical GFRP composite sample with rubber lining

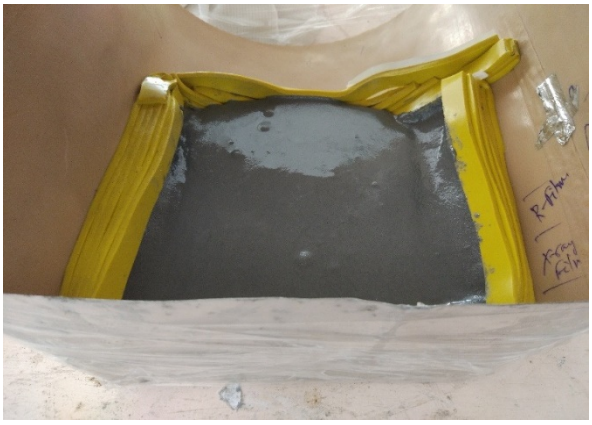

Fig. 5.2 Cylindrical GFRP composite sample with propellant adhesively bonded to rubber

5.2. Study of GFRP-rubber interface de-bond

GFRP cylinders were tested by keeping test sample over the search coil assembly on the insulation base provided with open slot as shown in Figure 5.3 and 5.4. The search coil assembly along with DC magnets can be moved with an aid of stepper motor arrangement designed for the profile NMR studies.

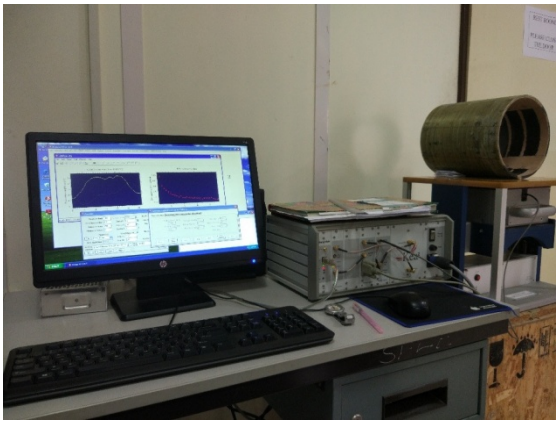

Fig. 5.3 Profile NMR arrangement for studies on cylindrical composite structures

Fig. 5.4 Stepper motor assembly for performing profile NMR experiments

GFRP cylindrical composite sample with only rubber lining was initially tested with X-ray radiography by taking tangential shots of the sample at various locations. It was observed that there was separation of rubber insulation with composite base layer indicating de-bond at those locations. Figure 5.5 and 5.6 shows tangential X-ray radiographs of composite cylindrical sample with de-bonded rubber layers at locations Y2 and P2 respectively. It is also observed that there were de-bonds between internal layers of rubber.

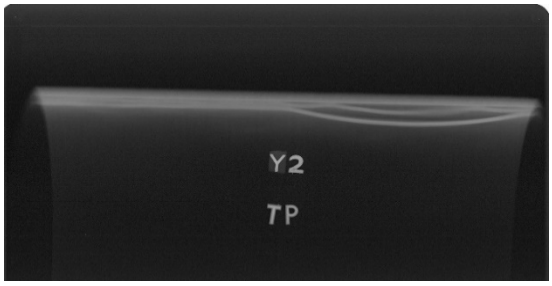

Fig. 5.5 Tangential X-ray radiograph of cylindrical sample at location Y2

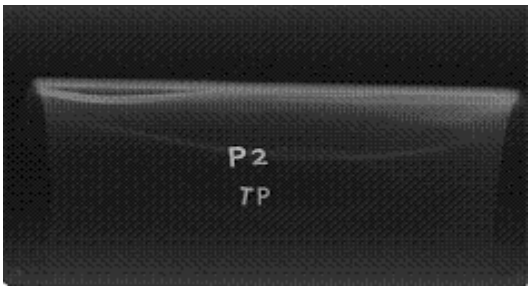

Fig. 5.6 Tangential X-ray radiograph of cylindrical sample at location P2

It may be noted that the test sample was fabricated with implanted defects to establish and validate low field NMR as an onsite NDE tool for composite structures. From the X-ray images, it is observed that there is finite air-gap between GFRP composite and rubber. It was further confirmed from acousto-ultrasonic system (AUS) data as shown in Figure 5.7. AUS data shows shift in wave pattern towards left (origin) due to presence of air-gap. The increase in amplitude of AUS data on defective region is due to reflection of acoustic energy from the defect towards the receiver. Figure 5.8 shows the AUS data collected over defective region Y2 where X-ray radiography indicated defect at GFRP-rubber interface as well as de-bond between rubber interlayers. It is observed that higher amplitude of AUS signal is received due to additional reflections from defect zone towards receiver. The second bunch of peaks in AUS is indicative of inter-layer separation within rubber.

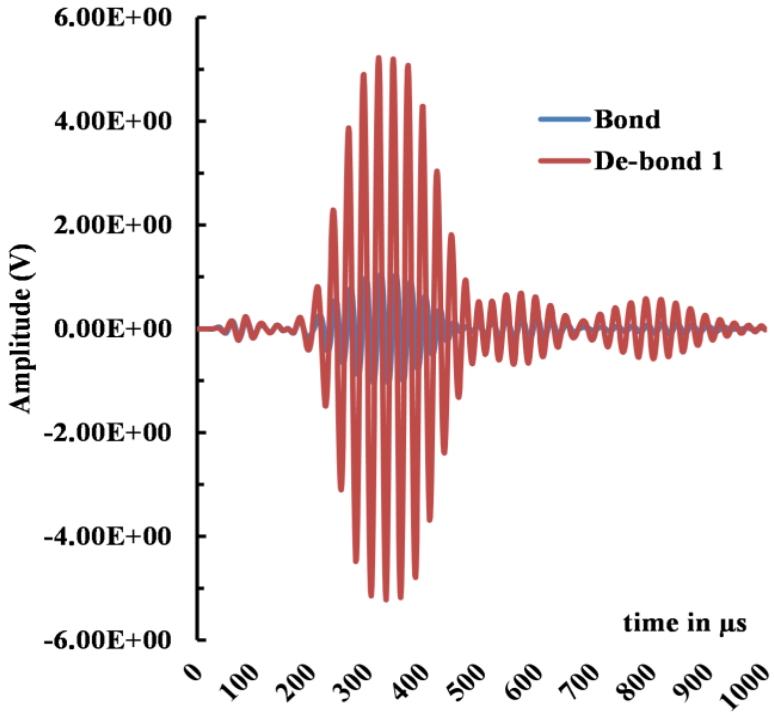

Fig. 5.7 Amplitude versus time plot of AUS data of de-bond region of cylinder. De-bond at GFRP–rubber interface is taken after recording non-defect region of the cylinder.

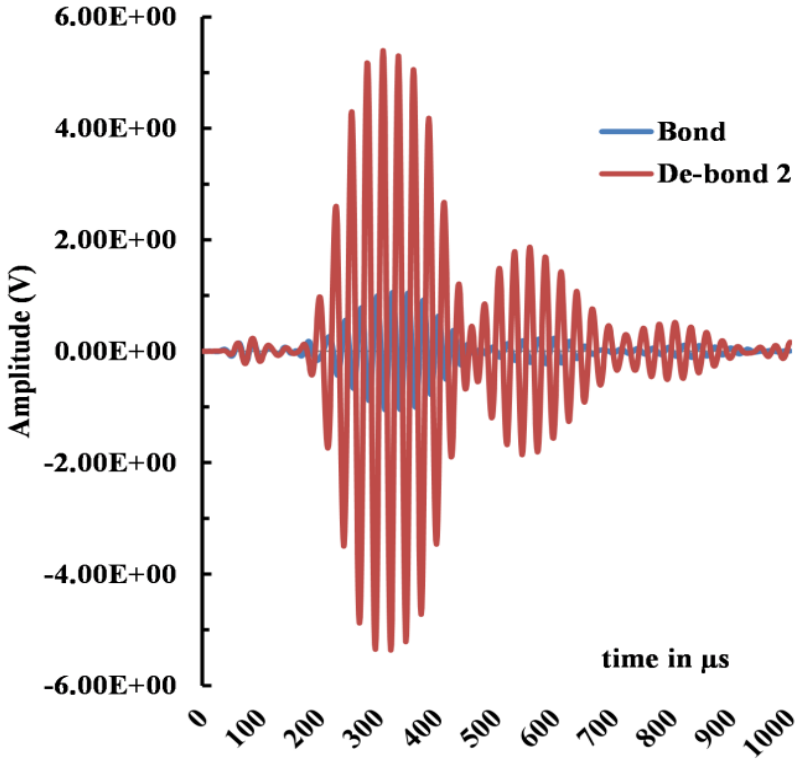

Fig. 5.8 AUS data of GFRP Cylinder with de-bond within rubber interlayers.

Profile NMR data on the inspected zones P2 and Y2 was obtained to establish the profile NMR sensitivity. On the selected zones, depth profile is performed with optimized parameters. Figure 5.9 shows profile NMR data collected over non-defect zone. Amplitude versus depth profile of the GFRP cylinder showed characteristic NMR amplitude of rubber. Thickness of rubber is observed to be 4mm from the peak amplitude data and corresponding X-axis intercepts. Wherever rubber proton molecules are present, the corresponding response to NMR magnetization was observed in the data. It was further observed that the baseline amplitude falls to zero beyond rubber region. Since GFRP proton density being lower than proton density of rubber molecules, the response of GFRP material is low and it is close to baseline.

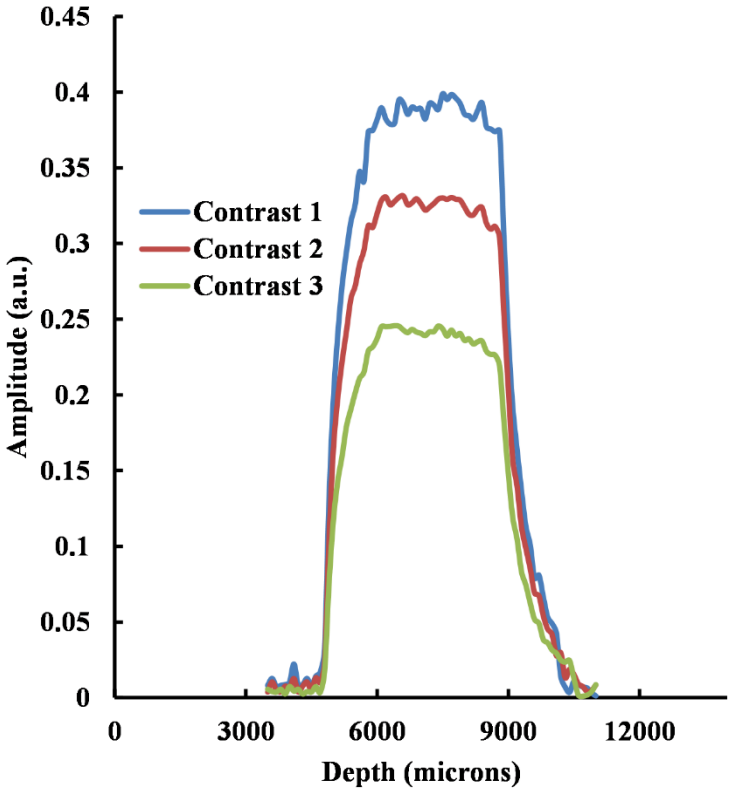

Fig. 5.9 Profile NMR data of GFRP cylinder with 4 mm rubber lining captured from GFRP side

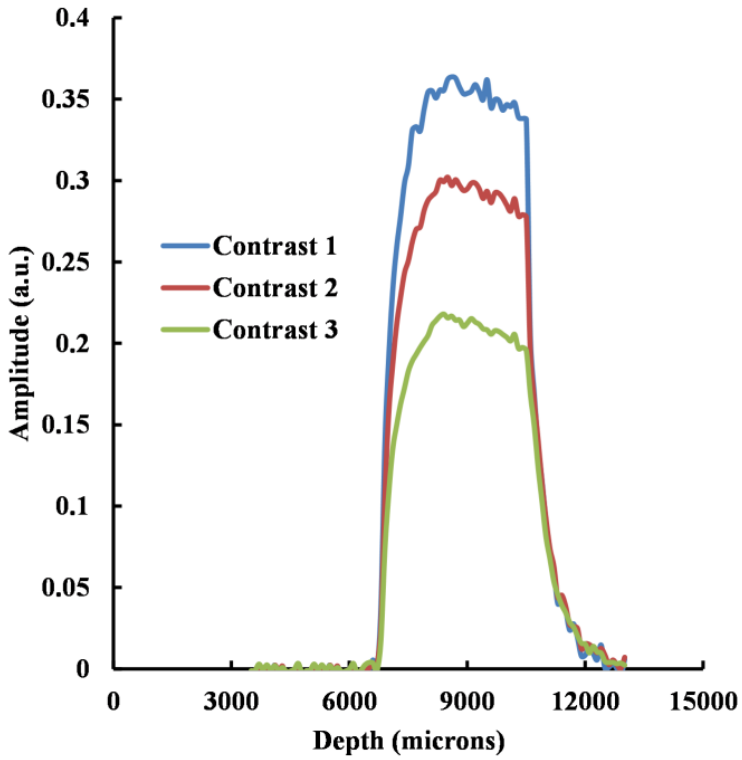

Fig. 5.10 Profile NMR data of GFRP cylinder with de-bonded rubber-composite interface captured from GFRP side

Figure 5.10 shows profile NMR data of cylindrical sample over defect region P2 where de-bond between GFRP-rubber interface was observed in X-ray tangential radiography as shown in Figure 5.6. Profile NMR shows shift in the onset of peak at 6800 microns as compared to 4800 microns for the same sample as seen in the Figure 5.9. This shift in the onset of peak for all the three contrasts of amplitude versus depth plot is attributed to presence of air-gap between GFRP composite and rubber layers. The presence of de-bond was earlier confirmed from X-ray tangential radiography. The shift in onset of peak in the depth profile NMR due to air-gap and signal due to protons present in the rubber molecules establishes the use of depth profile as an NDE tool for detecting de-bond in the multilayer samples.

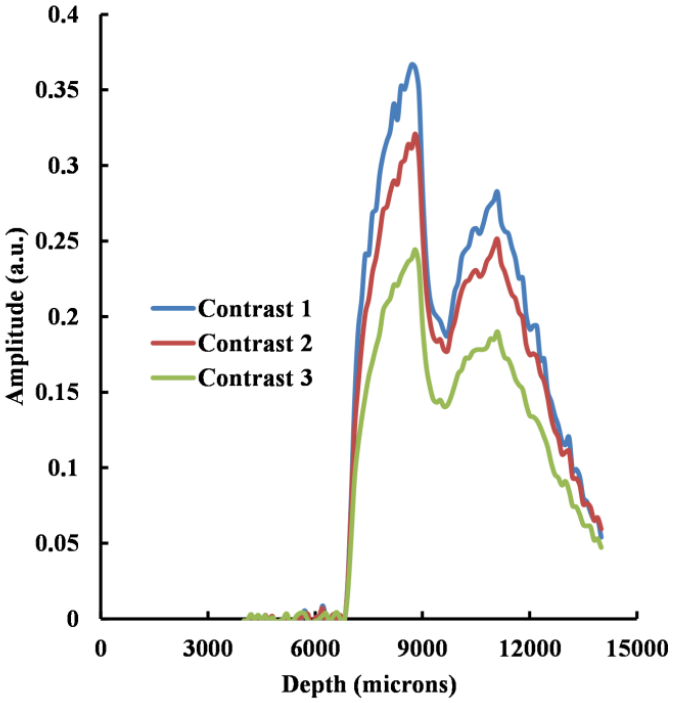

Fig. 5.11 Profile NMR data of GFRP cylinder with de-bond within rubber layers

Figure 5.11 shown above is profile NMR data of GFRP cylinder collected at region Y2. Tangential X-ray radiography of the region is shown in Figure 5.5. Radiography clearly shows interlayer separation of rubber. This is further confirmed from AUS data as shown in Figure 5.8, whereas rubber-composite interface is also de-bonded. The NMR profile data of region Y2 shows shift in rubber amplitude due to air-gap separation between the GFRP and rubber. Earlier in the Figure 5.9 the corresponding peaks of rubber were observed from 4800 value which is now shifted to 6800 indicating an air-gap of about 2000 microns. Further NMR profile data shows split in peak values of rubber indicating separation within rubber layers. Separation of rubber layers was also observed in AUS data.

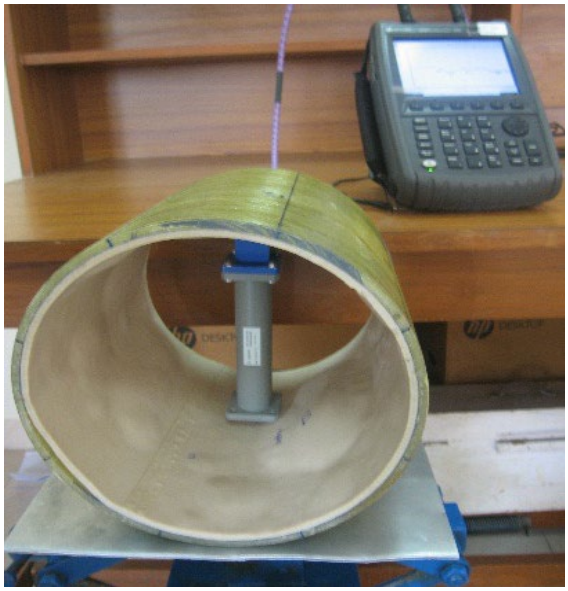

Fig. 5.12 Microwave NDE inspection system for composite structures using single sided open ended wave guide method.

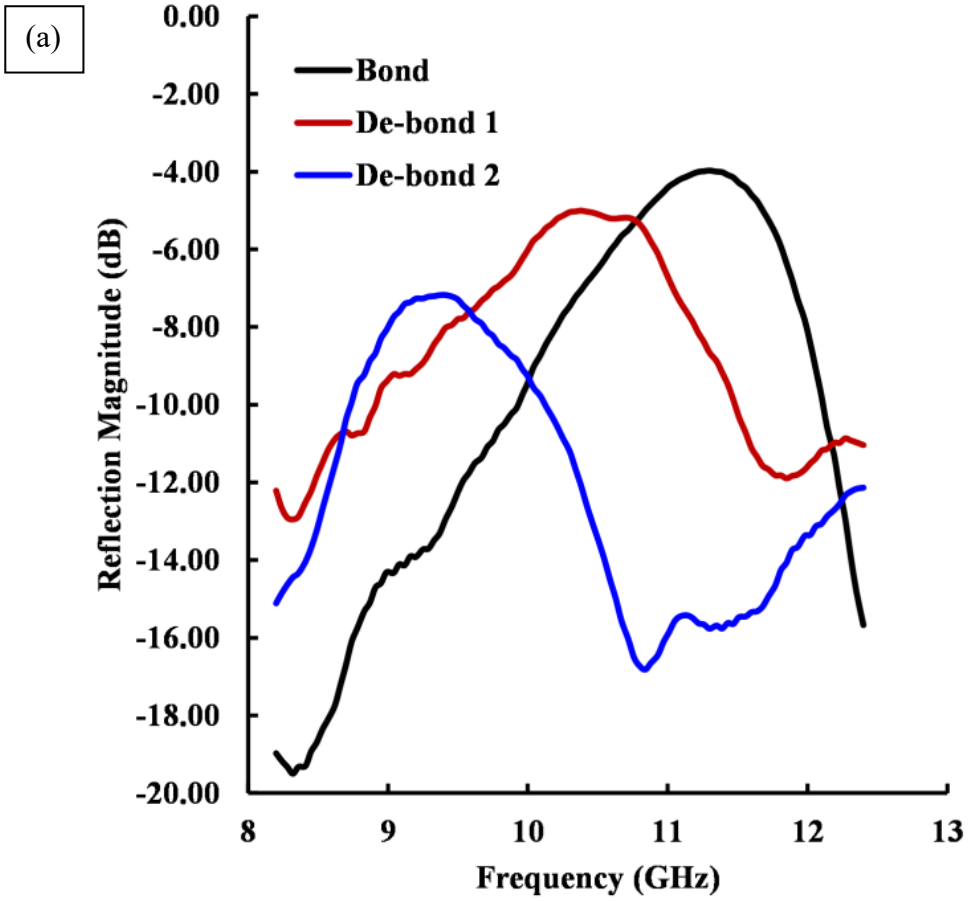

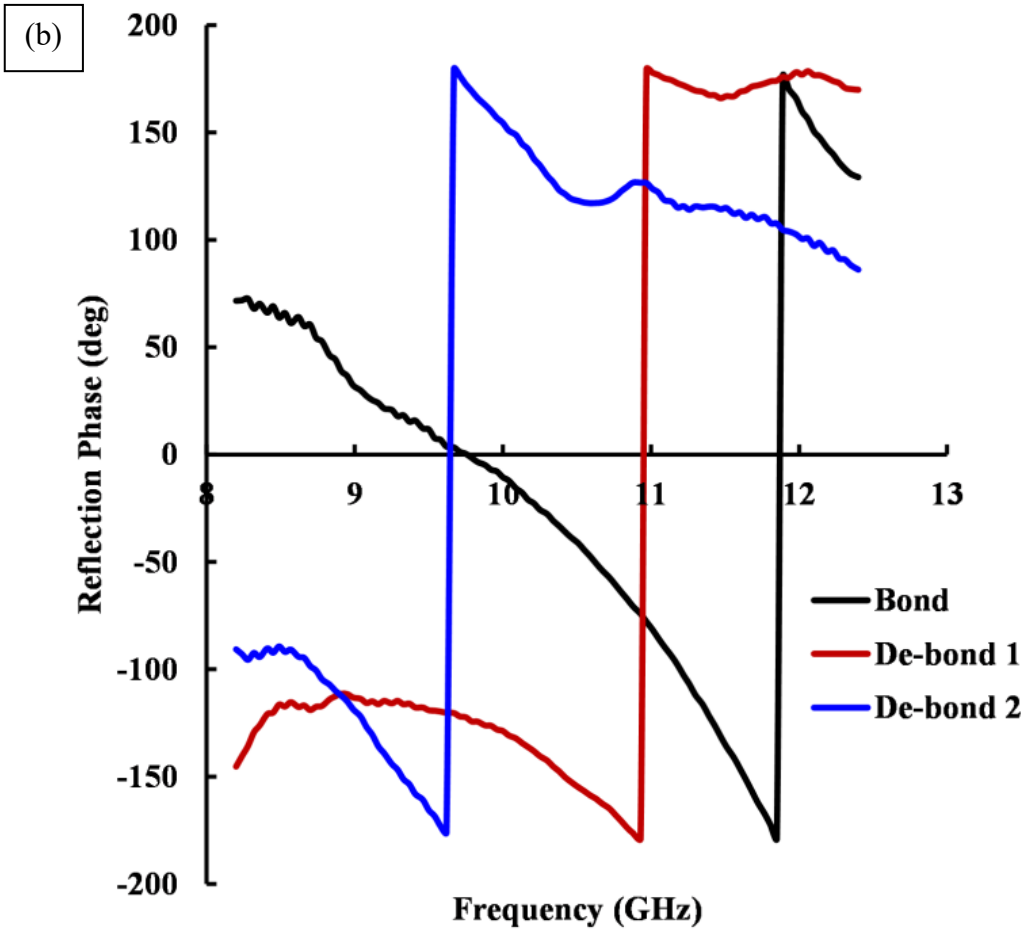

Fig. 5.13 (a) and (b) Microwave NDE data collected over defect and non-defect regions. De-bonded regions 1 and 2 show shift from signal captured over non-defect region shown in black colour.

Presence of defects and their intensity was further confirmed using Microwave dielectric NDE technique. Figure 5.12 shows microwave NDE setup used for the present studies. Microwave NDE uses electromagnetic waves for interrogating the materials. The changes in dielectric property affect the reflected wave amplitude and phase [97-100]. Peak of signal from defect region is observed to shift to lower frequencies as shown in Figure 5.13. Larger is the de-bond; higher is the shift in the signal towards lower frequency. Similarly reflected phase of the signal from defect region is observed to shift to lower frequency. Clear and distinct shift of the signal peak from non-defect signal peak is observed. Phase is observed to be more sensitive as compared to signal amplitude. Microwave NDE further confirms the observations made from low field NMR.

5.3 Adhesive liner thickness measurement

Composite GFRP cylinders with rubber bonded to the inside surface are further coated with adhesive liner material of finite thickness for bonding other elastomeric materials. However, obtaining desired adhesive liner thickness for bonding is a difficult task. For quality control and design, it is important to monitor the thickness of adhesive liner before bonding with other elastomeric materials. Since the adhesive liner material is in semi liquid sate, doing an accurate thickness measurement is not possible by conventional methods.

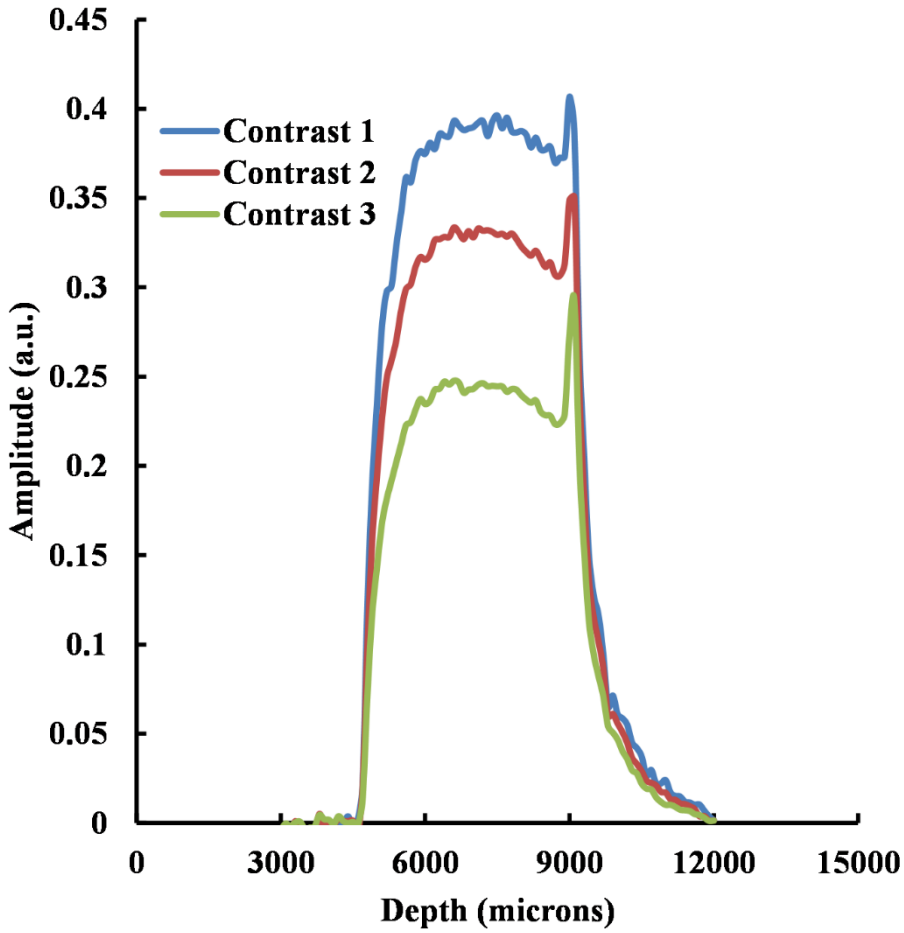

Fig. 5.14 Depth profile of GFRP-rubber cylinder coated with adhesive liner over the rubber surface at zone A

In the present study, on the inside surface of composite-rubber cylinder, adhesive liner material is coated with different thickness to explore the possibility of using single sided NMR as a NDE tool for quality control. Figure 5.14 shows profile NMR data of GFRP-rubber cylinder with

adhesive liner coating. From the depth profile data, it is observed that the thickness of adhesive liner is about 200 microns at zone A. Figure 5.15 depicts profile NMR data of GFRP-rubber cylinder with adhesive liner coating at zone B. From the data, it is observed that adhesive liner is about 400 microns. Similarly, GFRP-rubber cylinder is coated with several layers of adhesive liner material with increasing number of coats.

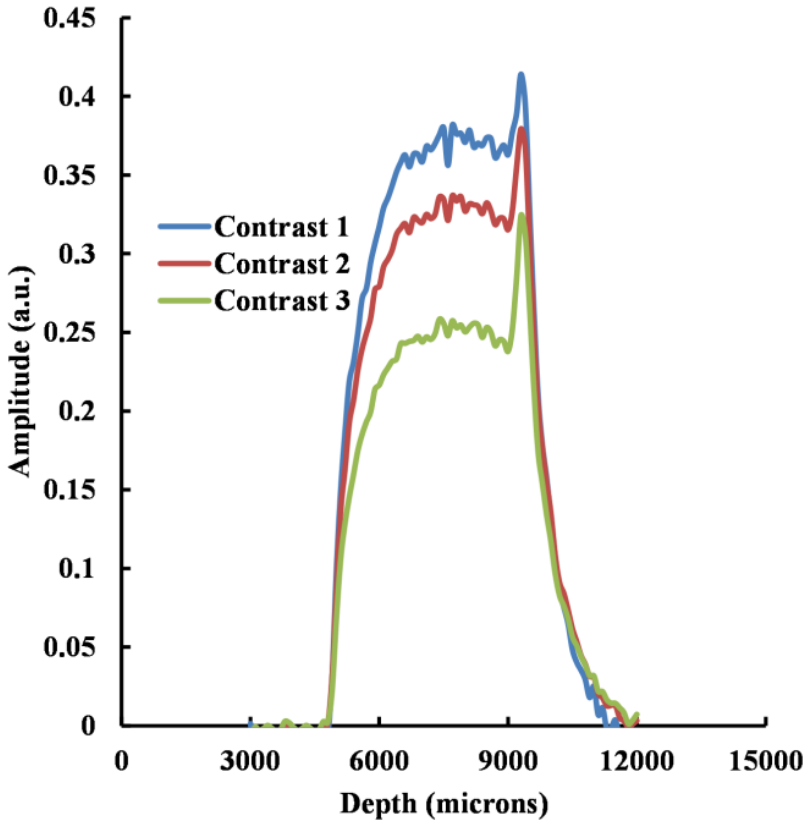

Fig. 5.15 Depth profile of GFRP-rubber cylinder coated with adhesive liner over the rubber surface at zone B

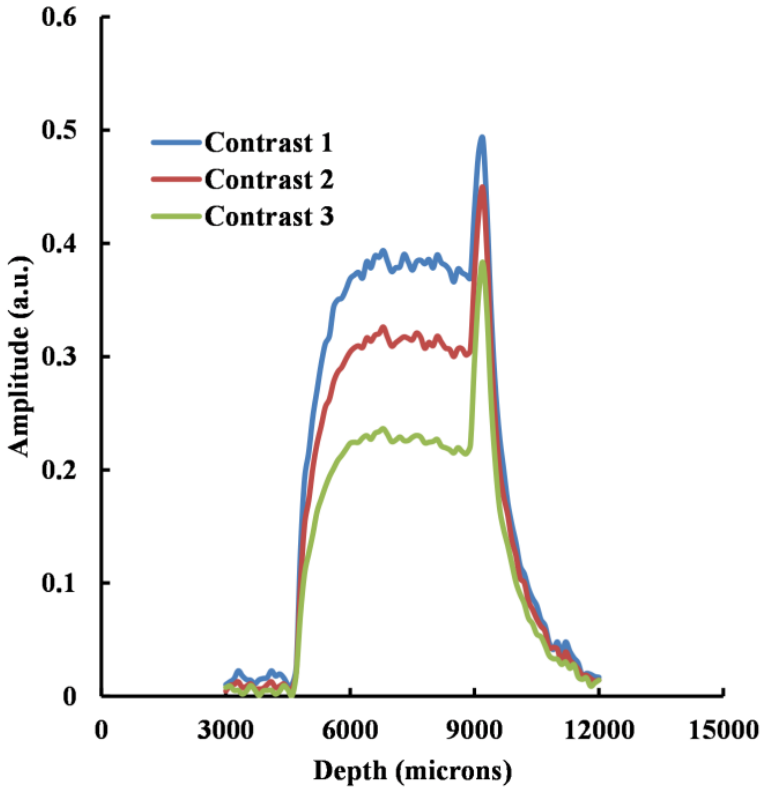

Fig. 5.16 Depth profile of GFRP-rubber cylinder coated with adhesive liner over the rubber surface at Zone C

Figure 5.16 shows depth profile data of GFRP cylinder coated with number of layers of adhesive liner material at zone C. Profile shows broadening of adhesive liner peak width with increasing number of coats. Broadening of adhesive liner peak indicates increasing thickness of adhesive liner due to increased number of coatings. From the profile NMR data, adhesive liner thickness is calculated to be about 600 microns at zone C. Figure 5.17 shows depth profile NMR data of cylinder with increasing liner thickness at zone D and adhesive liner thickness from profile NMR is estimated to be 800 microns.

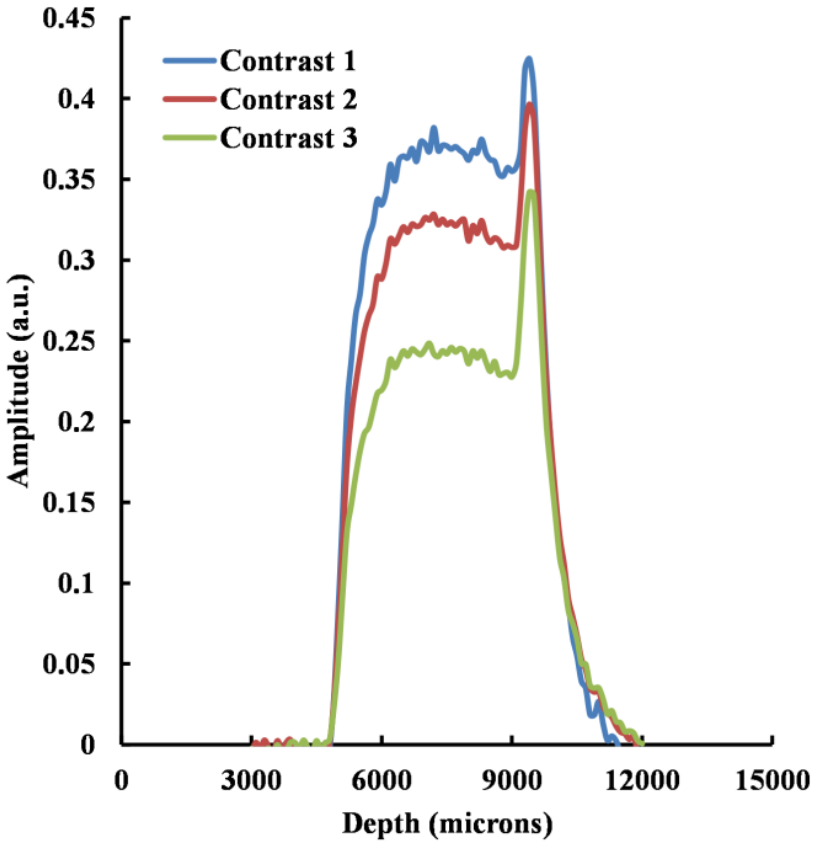

Fig. 5.17 Depth profile of GFRP-rubber cylinder coated with adhesive liner over the rubber surface at zone D

5.4 Studies on collinear defects at multiple interfaces

GFRP composite cylinder with multiple interfaces as described earlier has been subjected to X-ray radiography to ascertain the presence of implanted defects. Tangential radiographs were captured using 300 kV and 4mA X-ray source with 1minute exposure. Captured images were later digitized using film digitizer. Figure 5.18 (a) and (b) shows X-ray radiographs of GFRP cylinder with composite solid propellant. Higher density materials absorb more radiation and are seen as fairer objects in negative radiography film. Darker regions are lower density materials. Air-gap appears as dark line.

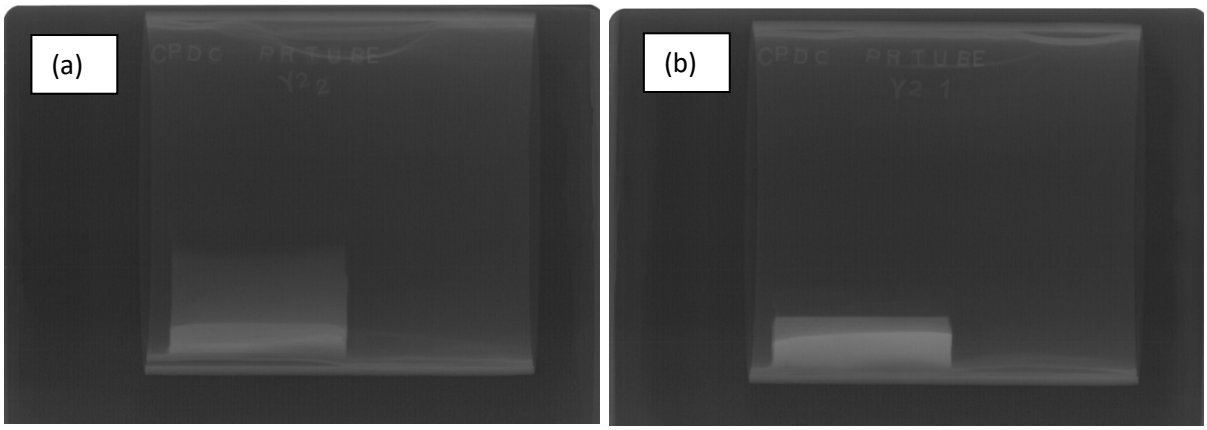

Fig. 5.18 (a) and (b) X-ray radiographs of composite cylinder with propellant cast over the rubber layer with adhesive liner.

X-ray radiography of composite cylinder is not able to distinguish planar defects at GFRP-rubber and rubber-propellant interfaces. It may be noted that the density of propellant (1.7 g/cc), rubber (1.2 g/cc) and GFRP composite (2.0 g/cc) are very close; hence it is very difficult to distinguish the planar defects located at the interfaces. In order to gain more insights, X-ray CT imaging was explored.

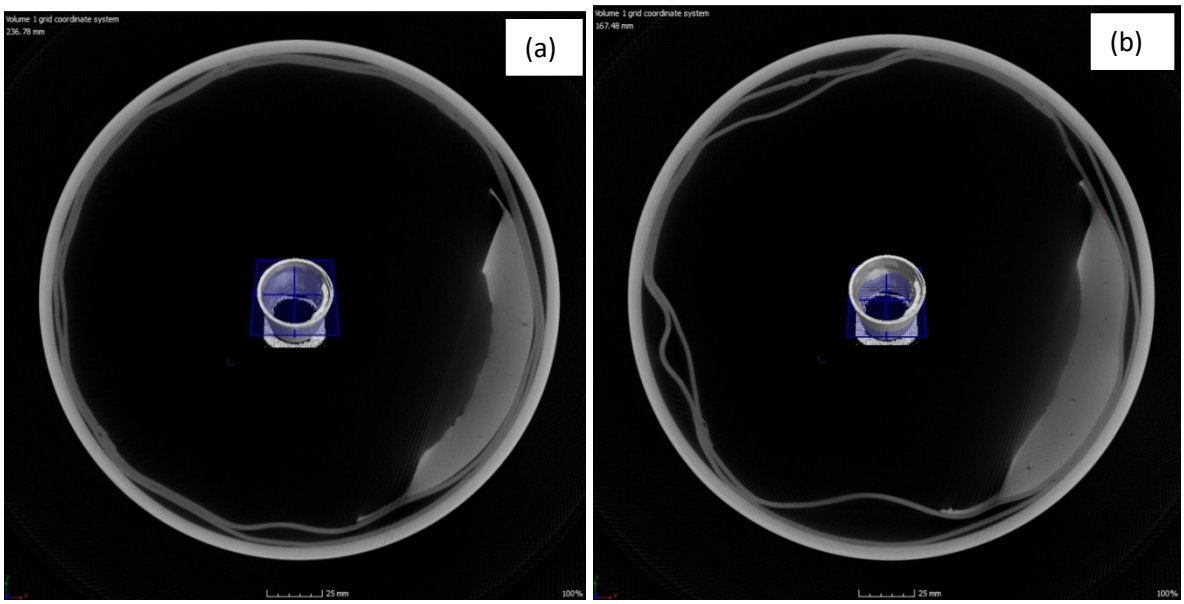

Fig. 5.19 (a) and (b) X-ray CT images of composite cylinder with propellant cast over the rubber layer with adhesive liner.

X-ray CT was performed on the composite cylindrical structure at 150 kV and 0.5 mA experimental parameters at 1^0 exposures. Figure 5.19 (a) and (b) shows CT scan images of the test structure. CT scan image shows multiple layers of the composite structure with constituents having different density. CT scan image also reveals the presence of implanted defects (air-gaps) as dark lines because of low density of air. It is also observed that there are multiple defects present at various interfaces of the structure indicating collinear nature of the defects. Since presence of multiple materials and interfaces within the composite structure has been ascertained, further testing was done using low field (12.88 MHz) NMR system. Figure 5.20 shows depth profile NMR data of cylindrical structure captured at no adhesive liner region as marked on the cylinder. Since, profile data was taken from GFRP composite side, initial data corresponding to the thickness of GFRP composite did not show appreciable signal values and remained closer to zero. The profile data of cylindrical sample initially shows peak corresponding to rubber layer (from depth 7000 microns to 12000 microns) followed by signature corresponding to propellant (12000 microns to 14000 microns). Data was not taken further as signature from thick propellant was sufficient to understand the nature of material. Profile data (peak amplitude at a particular location versus depth) shows a characteristic dip in the data within rubber layers, indicating presence of de-bond within rubber layers. The total thickness (starting from 7000 microns to 12000 microns) at which rubber signature was observed, corresponds to rubber layer and embedded air gap i.e., rubber thickness of 4000 microns and 1000 microns of air gap as seen in the experimental data. Thus, the quantification of air gap within rubber layers was possible.

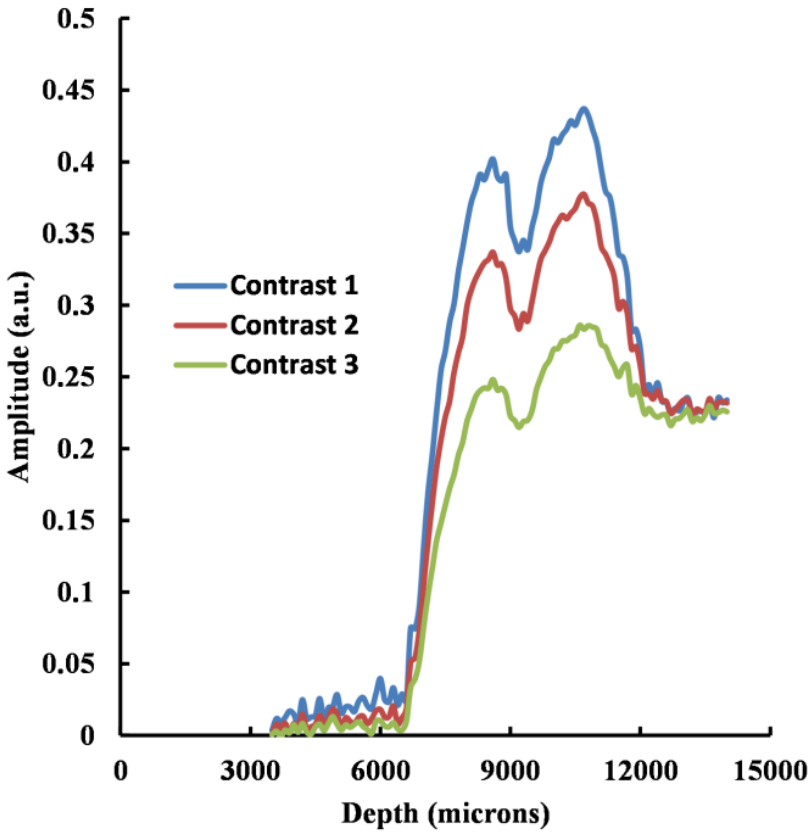

Fig. 5.20 Profile NMR data of cylinder without adhesive liner having de-bond within the rubber layers.

Another collinear defect de-bond between composite cylinder and rubber interface is also observed. As stated earlier, glass epoxy composite layer has thickness of 5000 microns, whereas rubber signature was noticed from 7000 microns, this indicates an air-gap of about 2000 microns. Also, there was no adhesive layer signature observed at this inspected zone indicating absence of adhesive liner at the interface. Thus, presence or absence of adhesive liner material within multi-layered structure has been ascertained using low field NMR. With single profile NMR data, it was possible to identify the nature of materials, air-gap between constituent layers of multi-layered composite structure as well as presence or absence of materials at the interface.

The experimental results were further verified at another zone identified on the same composite cylinder. X-ray CT scan data revealed presence of all the constituent materials including glass epoxy composite layer, rubber layer and propellant. However, presence of adhesive liner bonding rubber and propellant could not be identified. X-ray CT scan also revealed air-gap

within the rubber layers and air gap between GFRP composite and rubber. Low field NMR profile data was obtained in the same zone in which X-ray CT scan observations were recorded.

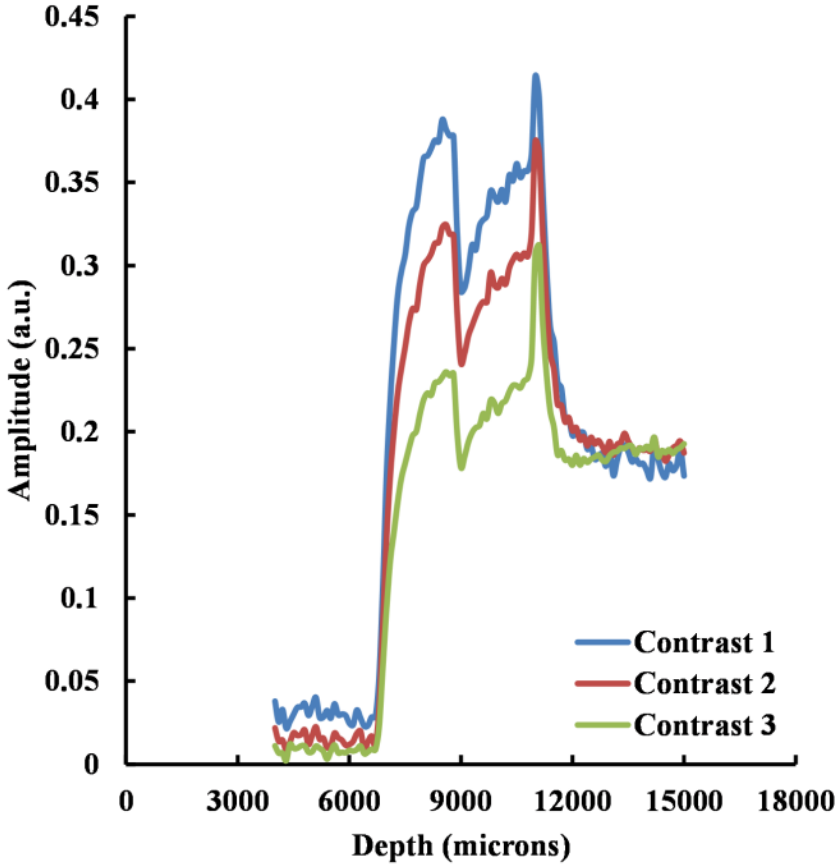

Fig. 5.21 Profile NMR data of GFRP cylinder-rubber-adhesive liner-propellant having collinear defects

From the profile NMR data as shown in Figure 5.21, it is observed that rubber signature is obtained from 7000 microns as against 5000 microns considering the thickness of composite layer as 5000 microns. The shift in the start of rubber signal corresponds to air-gap at the zone between composite layer and rubber. It is estimated from experimental data that air-gap could be 2000 microns. The presence of air-gap is also observed in CT scan data as well as AUS inspection already discussed earlier. NMR profile data showed a dip in the data at around 9000 microns depth indicating presence of air-gap at that location. CT scan for the corresponding zone shows air-gap within rubber layers. Thus, profile NMR data further confirms presence of de-bond within rubber layers. All collinear defects (i) rubber-rubber de-bond and (ii) composite to rubber interface de-bond were observed in both CT scan as well as profile NMR data. In

addition to the presence of defect, profile NMR also shows characteristic signature of adhesive liner material (sharp peak between rubber layers and propellant). Absence of this peak in NMR profile data in the earlier Figure 5.20 and presence of peak between rubber and propellant in Figure 5.21 is attributed to adhesive liner. The adhesive liner peak as seen in Figure 5.21 is clear and distinguishable from other constituent materials. Thus, low field NMR profile data reveals information about presence or absence of thin (about 150 micron thick) adhesive liner material whereas X-ray CT scan and AUS method could not detect the adhesive liner material. It is also observed that signal intensity of constituent materials is varying with curvature; however, it has no bearing on the defect detection. The technique is able to distinguish different materials of multi-layered structure based on their chemical constituents. Free induction decay (FID) curves for rubber, adhesive liner and propellant were obtained separately at the locations identified earlier from profile NMR data as shown in Figure 5.21. Probe was moved to the corresponding depth of rubber, adhesive liner and propellant. FID data was captured for all the three materials separately using low field (12.88 MHz) single sided NMR. Figures 5.22 to 5.24 show FID curves for rubber, adhesive liner and propellant respectively.

5.5. Evaluation of Transverse Relaxation Time

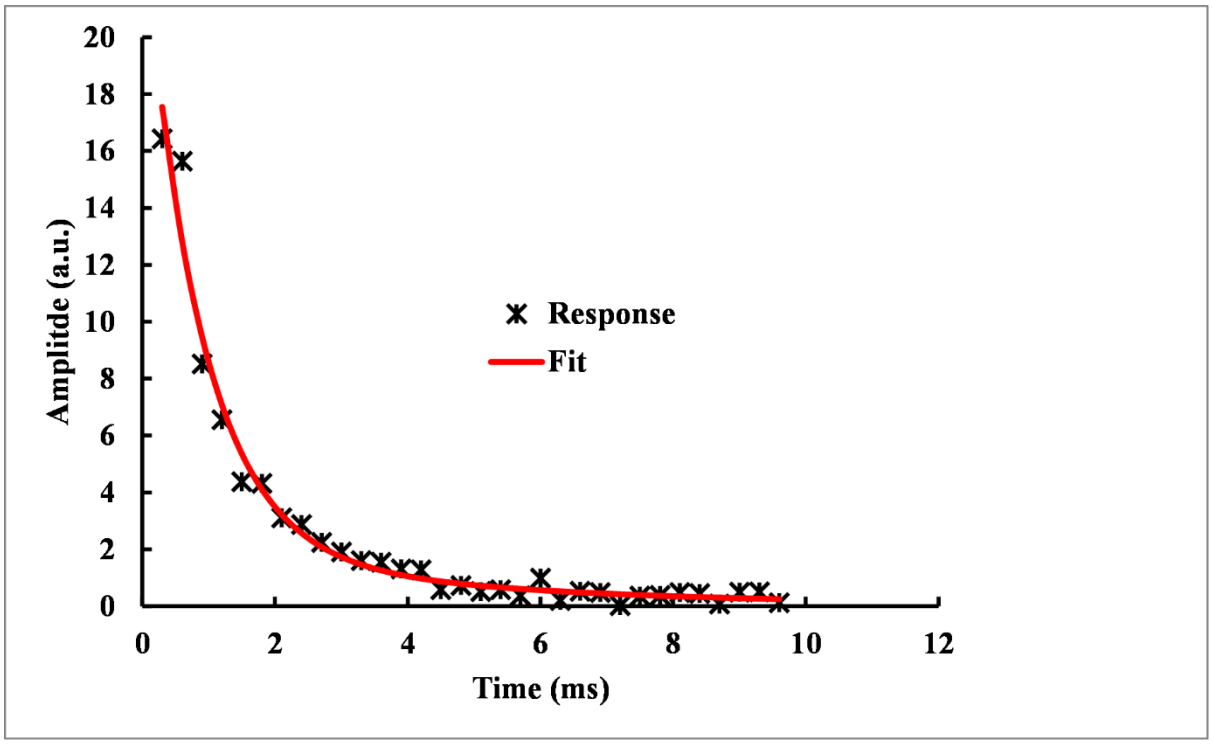

Fig. 5.22 FID data of rubber (Bi-exponential fit)

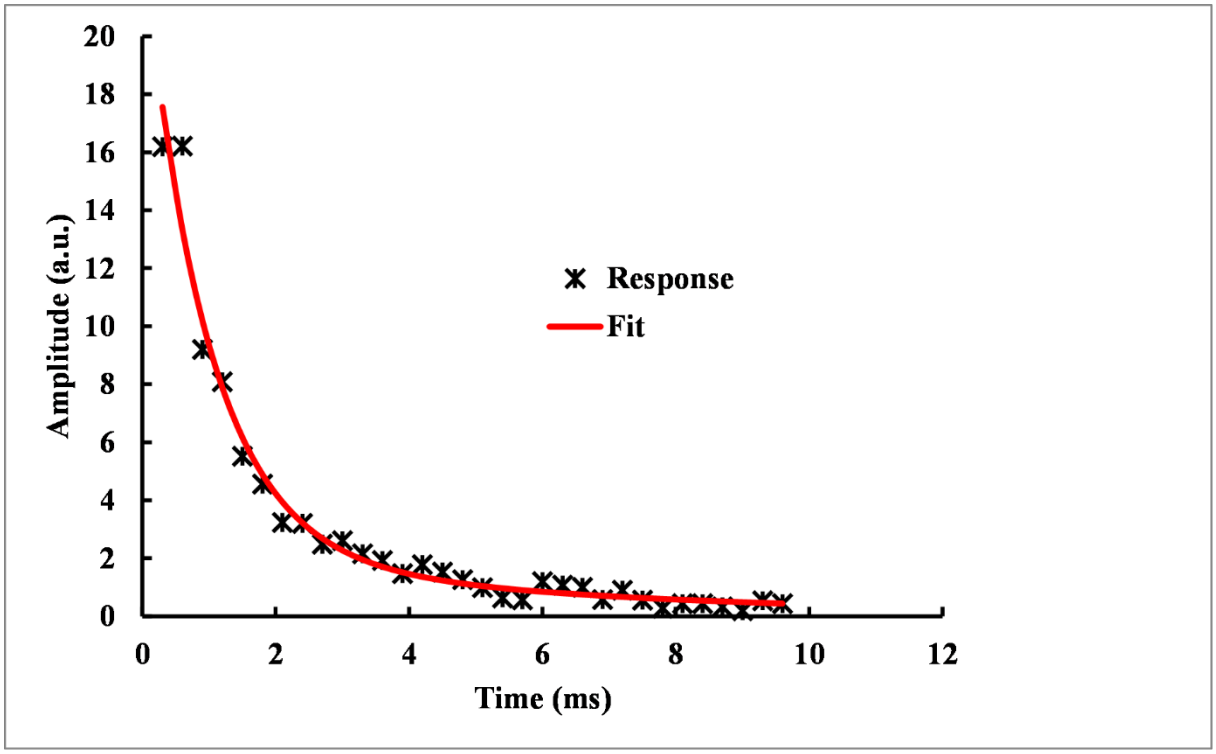

Fig. 5.23 FID data of adhesive liner (Bi-exponential fit)

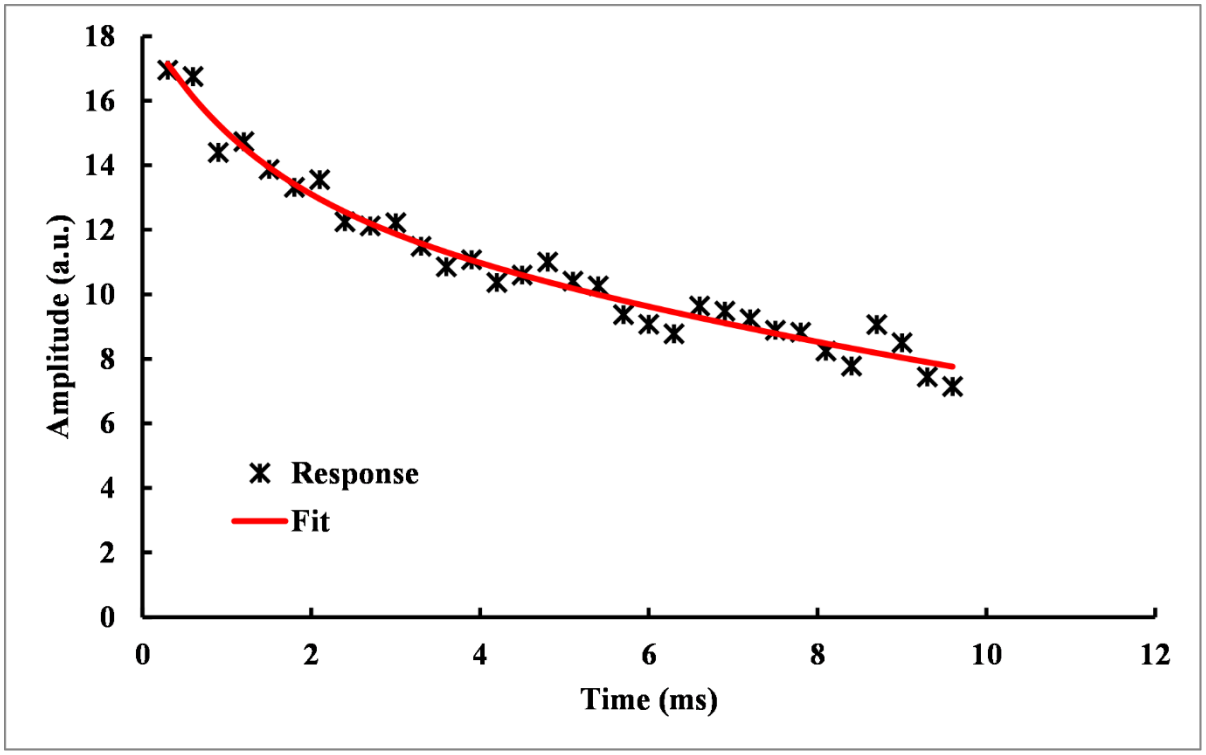

Fig. 5.24 FID data of propellant (Bi-exponential fit)

On fitting exponential decay of FID data to bi-exponential function, two transverse relaxation times (T_{2short} and T_{2long}) were obtained. Table 5.1 shows the transverse relaxation times (T_{2short} and T_{2long}) obtained for rubber, adhesive liner and propellant after bi-exponential fitting of the FID data. The values of transverse relaxation times may be used for identifying chemical nature of the constituent materials and distinguishing them. All the three materials have distinct relaxation times unique to their chemical signature. Transverse relaxation time T_{2long} is observed to be 2.3 ms, 5.9 ms and 14.5 ms for rubber, adhesive liner and propellant respectively.

Table 5.1 Transverse relaxation times of constituent materials rubber, adhesive liner and propellant captured using low field NMR @12.88 MHz

Material	Transverse relaxation times			
	A_{short}	T_{2short} (ms)	A_{long}	T_{2long} (ms)
Rubber	0.8	0.7	0.2	2.3
Adhesive liner	0.9	1	0.1	5.9
Propellant	0.5	13.1	0.5	14.5

5.6. Summary

The cylindrical GFRP composite structure with defects was tested using single sided low field NMR technique and the results are compared with the results obtained from the AUS and X-ray radiography. The results are summarized in this section. Low field NMR profile data is useful for localising defects in multi-layered cylindrical GFRP composite structures. Distinct peaks/signal intensity values and transverse relaxation times were observed for each constituent material. Air-gaps at the interfaces of (i) GFRP-rubber, (ii) within rubber layers were all detectable. There is no effect of curvature on air-gap detection at the interfaces using low field NMR single sided inspection. Low field NMR is observed to be useful over other NDE techniques in characterising materials based on their chemical signatures. Presence or absence of thin adhesive liner between rubber and propellant was detectable using NMR profile data and was not possible even with X-ray CT. Collinear defects which are at multiple interfaces were all detectable.

6. Comparison of Flat and Cylindrical Composite Structures

The present chapter aims to compare the results obtained from the flat and cylindrical multi-layered composites with the similar defects. The effect of shape of the structure on the interference with the results from NMR are reported.

6.1. Samples for Testing

GFRP flat and cylindrical structure is fabricated by filament winding process. Composite surface is prepared, followed by application of primer and rubber solution. Solid propellant in slurry form is cast on GFRP-rubber lined flat and curved structure. To retain rubber insulation to propellant bond intact, a carbon black based adhesive liner compatible to both rubber insulation and propellant is applied before propellant casting. Interfacial bond properties between propellant and rubber like peel strength between rubber-adhesive liner-propellant were evaluated destructively with an aim of cohesive failure within propellant.

Elastic properties were studied using universal testing machine (UTM) whereas NMR relaxometry data was studied using a commercially available single sided low field proton NMR system (Commercial name: NMR MOUSE PM 25, Manufactured by M/s Magritek GmbH) magnetic field @ 12.88 MHz RF frequency, spectrometer Kea^2, (M/s Magritek GmbH). Profile NMR-MOUSE (PM 25) as shown in Figure 6.1 is a simple portable NMR system consisting of sensor and permanent magnet (B_o equivalent to 0.3T) having uniform gradient perpendicular to the scanning surface outside the magnets along with the Data Acquisition to the PC connected (Figure 6.2) to NMR system. CPMG (Carr-Purcell-Meiboom-Gill) pulse sequences were used for generating the relaxometry data. Automated incremental motion with an accuracy of 50 µm using high precision lift is attached to the permanent magnets (B_o). Depth profile is obtained by moving the precision lift in increments of 50 µm or more and relaxometry data is collected at each of the location. Normalized amplitude of the test sample is further processed to arrive at the value for plotting profile data.

Fig. 6.1 Profile NMR-MOUSE (PM 25)

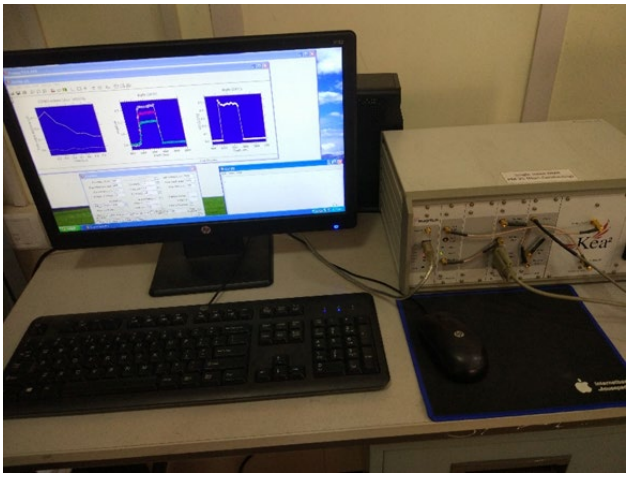

Fig. 6.2 Data Acquisition from the Profile NMR

The low field NMR system model PM25 is a single sided NMR sensor that allows to measure spin densities, transverse and longitudinal relaxation times through objects with a high spatial resolution (in this case 100 microns). It is also delivered with additional set of spacers to adjust the maximum penetration depth to allow the user to achieve best sensitivity for a selected task. Rubber (co-polymer of acrylonitrile and polybutadiene), which is commonly used for industrial applications, has been selected for the current studies. Rubber of about 2.2 mm thickness was selected for initial studies on the low field NMR system.

The rubber surface is abraded and then cleaned by Tri-Chloro-Ethylene (TCE) to remove oily and greasy substances from the surface and dried in an oven at 105 ^{O}C for 5 hours to evaporate the solvent and moisture. Thin layer of adhesive liner is applied by using spray gun. Casting of composite solid propellant is carried out on peel strength test cartons at regular intervals of 48, 120 and 160 hrs after liner application. After Propellant was cast under vacuum, cartons were sent for curing at 60^{0}C for 5 days.

Peel strength test samples of width of 25mm was cut from cured cartons with slicing machine. The finished samples maintain dimensions of Ø100 x Ø 60 x 25 mm. One set of samples is identified for peel strength evaluation immediately after curing, while other samples were kept for accelerated aging in thermocouple-controlled oven at age temperature of 60^{0}C for 15, 30, 45 & 60 days. Samples aged at 60^{0}C for 60 days are thermally equivalent to natural age of 4 years as per ASTM F1980 with accelerated aging factor of 2. Samples were desiccated in $CaCl_2$

atmosphere for 48 hrs prior to testing. Testing of samples was carried out using UTM with cross head speed of 300mm/min.

6.2. Peel strength studies

Peel strength studies are indicative of bond quality and adhesion properties of adhesive. Over a period of time or during processing, adhesion becomes poor due to changes in elastic properties of adherend/adhesive or both. NMR relaxation time is inversely related to cross link density which in turn indicates changes in elastic properties. Poor interfacial properties can result in poor peel strength. Interfacial properties were estimated from the relaxation times of the interface.

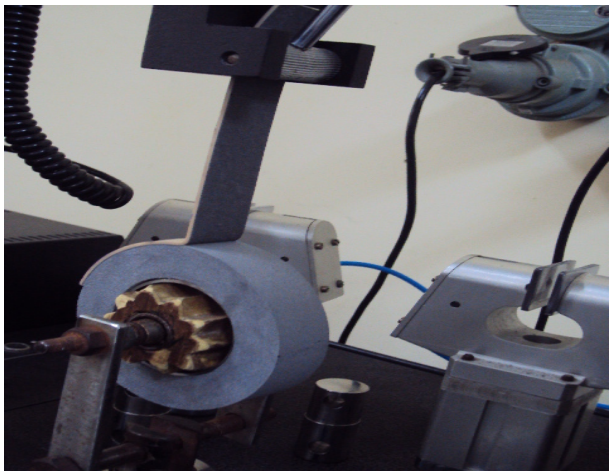

Fig. 6.3 Specimen under test for peel strength properties

Peel strength studies of test samples were carried out as per DIN 53357 using standard UTM. Tests were conducted at constant speed of 300mm/min for assessing peel strength properties. Test is continued until cohesive failure within propellant is observed as shown in Figure 6.3.

Peel strength of the samples was obtained using the test procedure described above. Several sets of the samples were subjected to aging at different conditions and tested as described earlier. Figure 6.4 shows peel strength values of test sample of propellant with adhesive liner coated over insulation layer as a function of aging done over 0 to 60 days. Each test sample is different with adhesive liner curing for 48 hrs, 120 hrs and 160 hrs before propellant casting. This is the duration after adhesive liner application and before propellant casting, so that we achieve different tackiness values. Each sample is subjected to isothermal aging at 60^0C for 15

days, 30 days, 45 days and 60 days. Aged samples were separately evaluated for peel strength. From the Figure 6.4, it is observed that peel strength of test sample for interface of adhesive liner–propellant decreases with aging. Also peel strength values increase with duration of adhesive liner cure due to increased tackiness from 48 hrs to 120hrs. However, beyond 120 hrs adhesive liner cure results in irregular peel strength values due to uncontrolled processes which need further investigation using NMR. The peel strength values fall within experimental error of 0.2 Kgf/cm.

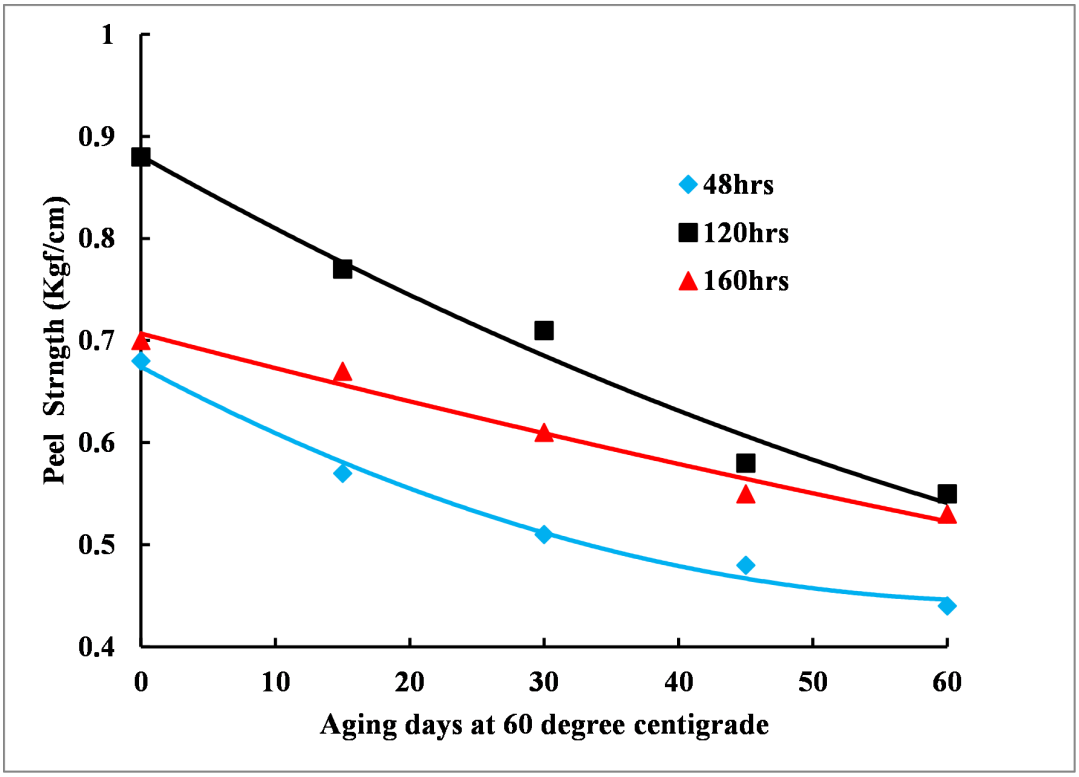

Fig. 6.4 Peel strength studies of samples aged at 60 ^{0}C.

Since the samples are multi-layered in configuration, conventional NMR cannot be used. Out of three sets of samples, one set of samples was cured for 48hrs at 60^{0}C has been chosen for present studies, which is supposed to be the optimum process conditions. This sample has been taken to prove or establish portable NMR as viable NDE tool to study adhesive interface properties as an alternative method to destructive tests. Moreover, the application of portable NMR is for practical samples, which are cylindrical in shape. In this scenario, it is pertinent to study the effect of shape of samples on the NMR results. Hence both flat and cylindrical samples have been studied for their depth profile using portable single sided NMR. However, before

studying the interface for mechanical properties, sample has been systematically studied using NMR at each step.

6.3. Adhesively Bonded Sample and Rubber

Figure 6.5 shows depth profile NMR data of flat GFRP laminate over which rubber of 2 layers is adhesively bonded. The amplitude from rubber is shown to rise sharply with increasing depth indicating response due to magnetization of material with the applied magnetic field within the sensitive volume. As the depth of sensitive volume increased, the response from rubber molecules remained high until the sensitive volume reached end of rubber layer thickness. At the boundary of rubber layer and air the response falls sharply due to absence of rubber molecules beyond its thickness. Thereafter the signals value reached plateau and remains closer to baseline noise. From the Figure 6.5, it is observed that the amplitude values raise to about 0.35 value at 4000 microns and remained high before falling to zero at 8000 microns. The amplitude value remained high due to response of protons in the rubber layer due to magnetization. In the absence of the proton chemical signatures, the response to magnetic field falls to zero. Hence, it may be estimated that the rubber thickness is shown in the response to the sensitive volume. In this case rubber thickness on flat GFRP composite is observed to be about 4000 microns. The undulations in the peak amplitude value may be due to in-homogeneity of rubber material within its thickness.

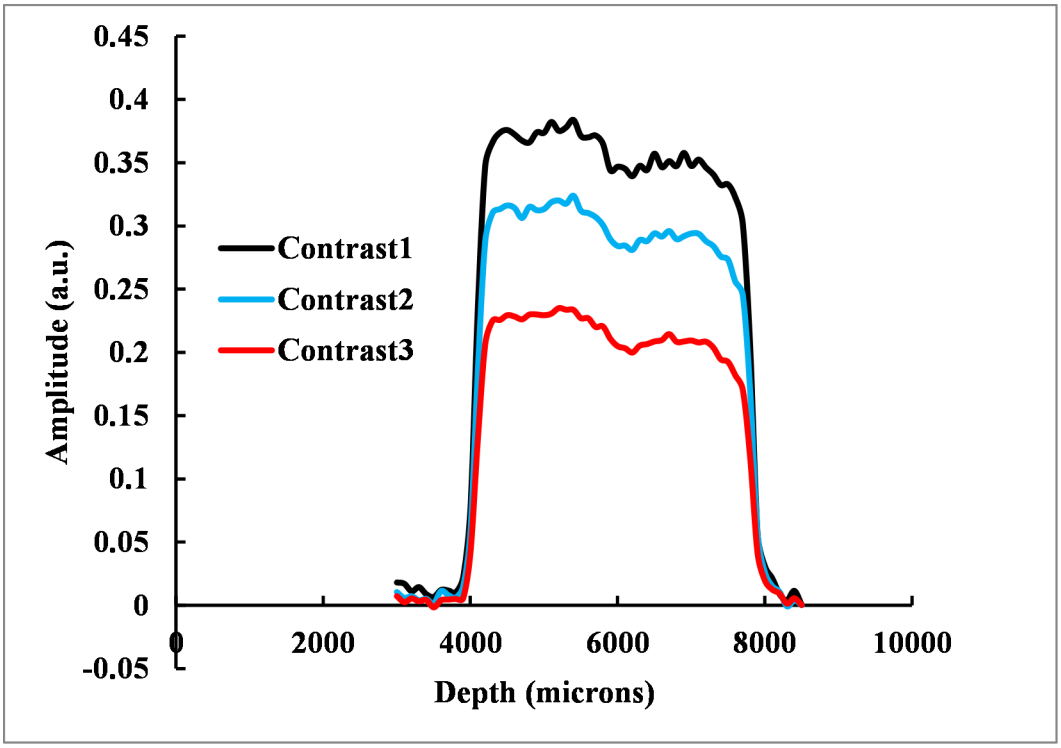

Fig. 6.5 Profile NMR data of flat test sample adhesively bonded with rubber

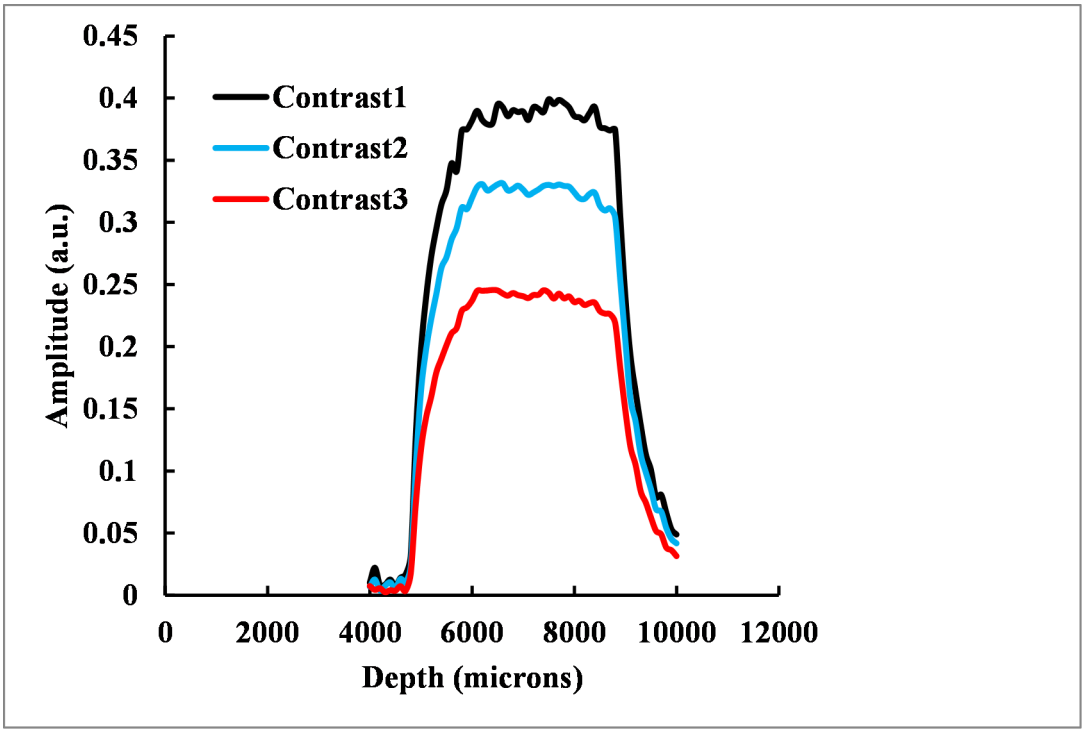

Fig. 6.6 Profile NMR data of cylindrical test sample adhesively bonded with rubber

Figure 6.6 shows depth profile NMR data of composite test sample with rubber lining. Profile data shows rubber thickness is about 4000 microns. The data is shown with three contrasts blue, red and green which correspond to initial 1-4 peak amplitudes, 1-8 peak amplitudes and 1-16 peak amplitudes and their summation respectively. The order of peak intensities is higher to lower from 1-4 to 1-16 as seen above. However, the peak rise and fall are gradual due to cylindrical shape of the structure. As estimated earlier for flat samples, the rubber thickness estimation will be erroneous if one takes the peak rise point and peak fall point. The peak rise and peak fall are not sharp due to the curvature of the cylindrical sample. Hence the plateau of the profile data after reaching the peak is taken for estimation. This is due to the center of sensitive volume interacting with the thickness of the rubber within cylindrical structure. By gradually moving the location of the sensitive volume within the rubber layer, we continue to receive higher amplitude signal. By drawing two vertical lines across the plateau of the rubber signal we can estimate the rubber layer thickness inside the cylindrical sample.

6.4. Adhesive Liner Coating

It is well known that chemical signatures of each of the materials are captured from NMR relaxometry data. In this case, samples of both flat and cylindrical have same configuration of GFRP composite, rubber liner, adhesive liner and propellant. Figure 6.7 shows profile NMR data of flat test sample adhesively bonded to composite structure with adhesive liner coated (about 400 microns) over it. Adhesive liner has distinct peak and clearly distinguishable. It is observed that amplitude rises to 0.4 when the depth of sensitive volume reaches rubber layer. Amplitude of the chemical signature from rubber remained at 0.4 until the profile reached 8000 microns. The plateau of amplitude 0.4 is due to rubber layer alone. The difference in peak rise at 4000 microns and end of plateau at 8000 microns is approximately the thickness of rubber layer which is about 4000 microns. Sharp peak observed at 8000 microns is due to adhesive liner coated over rubber layer. The peak raise at 8000 microns from the plateau to peak fall at 8400 microns is due to adhesive liner material alone. The width of peak gives the adhesive liner response alone. From this, the estimated peak width of adhesive liner is about 400 microns which is equivalent to the thickness of the coated adhesive liner material. Figure 6.7 shows depth profile NMR data of GFRP cylindrical sample adhesively bonded with rubber and coated with adhesive liner material.

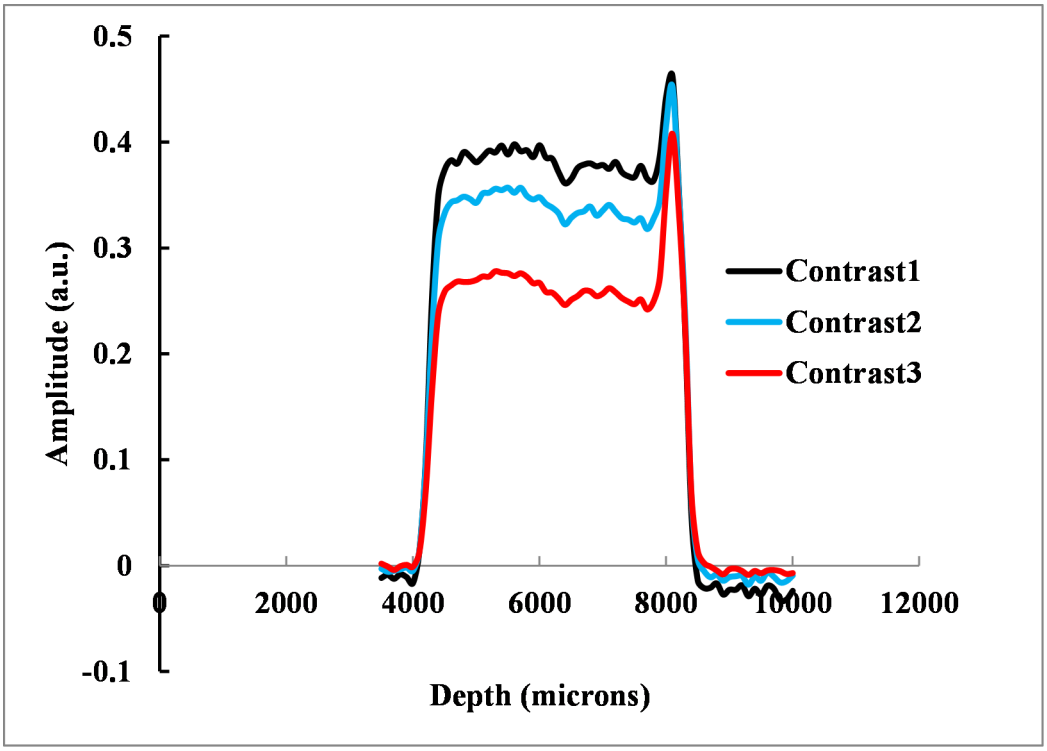

Fig. 6.7 Profile NMR data of flat test sample adhesively bonded with rubber and coated with adhesive liner.

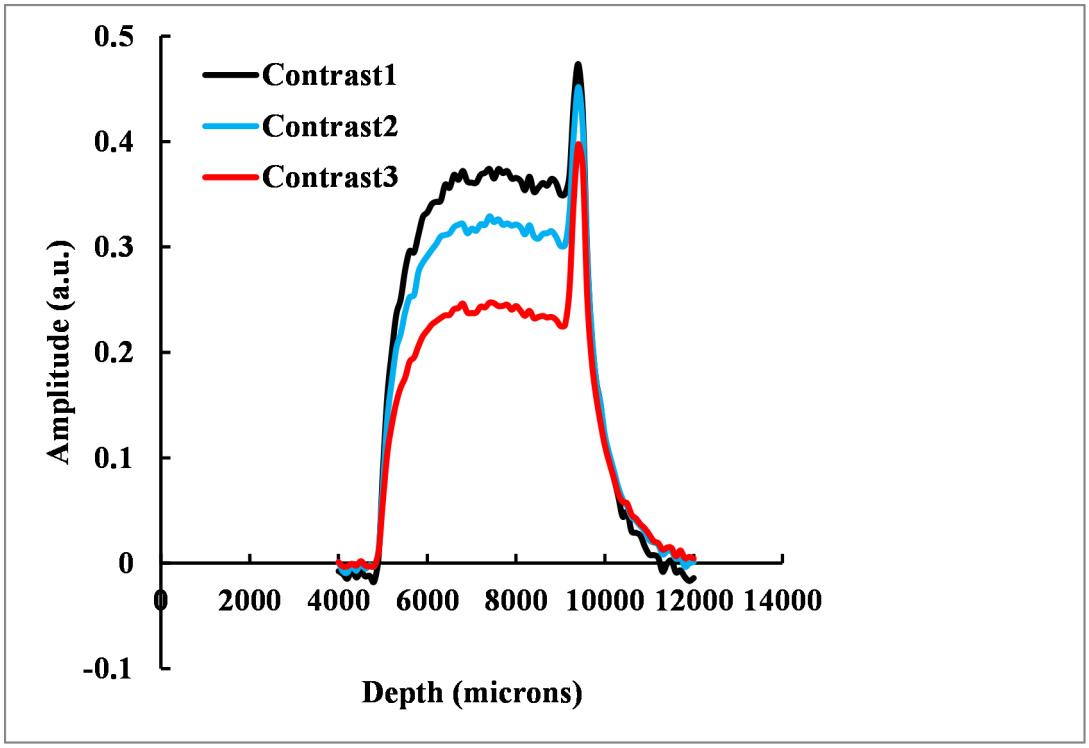

Fig. 6.8 Profile NMR data of cylindrical GFRP test sample adhesively bonded with rubber and coated with adhesive liner.

From the Figure 6.8, it is observed that the rise and fall in amplitude due to protons inside rubber layer is gradual and not as sharp as that of flat sample. The gradual rise or fall of amplitudes may be attributed to the interaction of sensitive volume with the curved part of the sample. As the sensitive volume edge encounters the curved part of the sample, signal is observed but not as high as the interaction of center portion of the sensitive volume when it interacts with rubber material. Figure 6.9 shown depicts the movement of sensitive volume (flat slice) within the curved test sample.

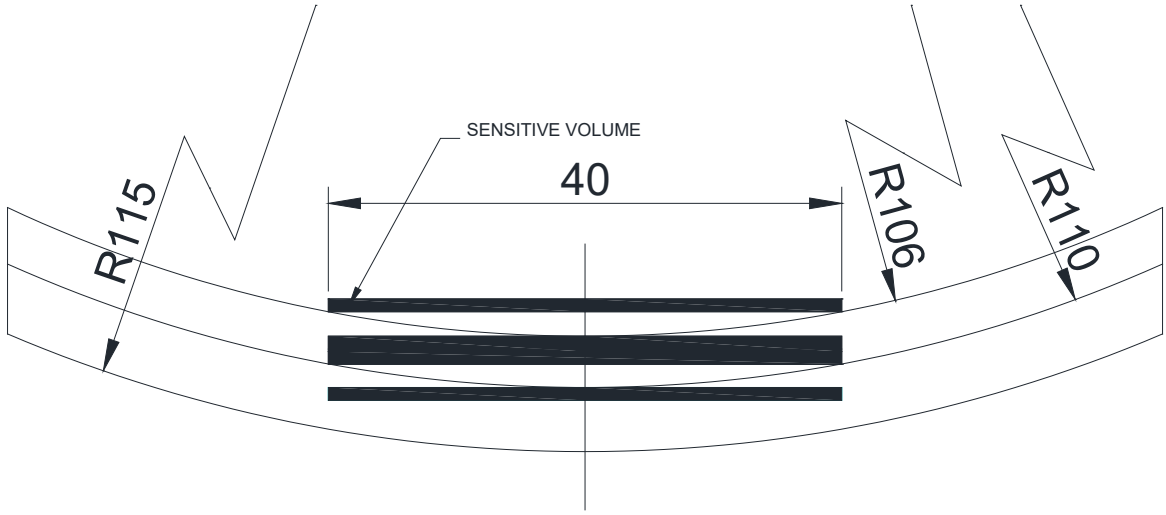

Fig. 6.9 Schematic of sensitive volume of the profile NMR system within the curved /cylindrical test sample at various depths.

As long as the edges of the sensitive volume magnetizes the rubber within cylindrical sample, response signal amplitude keeps increasing (when sensitive volume is moving towards cylindrical sample) or decreasing (when sensitive volume is moving away from the cylindrical sample). The gradual rise in the signal amplitude in the cylindrical sample as compared to flat sample is profound and may vary with cylinder diameter. In case of small diameters, sensitive volume being larger than cylinder diameter, sample is always partially covering the sensitive volume, hence multiple responses in profile data may be observed. However, when cylinder diameter is larger than the sensitive volume, the rise in signal amplitude may be gradual and very sharp in case of flat samples.

6.5. With Propellent

The profile NMR data of flat test sample adhesively bonded with rubber is shown in Figure 6.10. Profile NMR data has been taken over entire thickness of the sample i.e., 4000 microns to 15000 microns. Data has been collected with an aim to separate the contributions of rubber, adhesive liner and propellant. As seen from the figure, data from all the three regions of the test sample are distinct and clear.

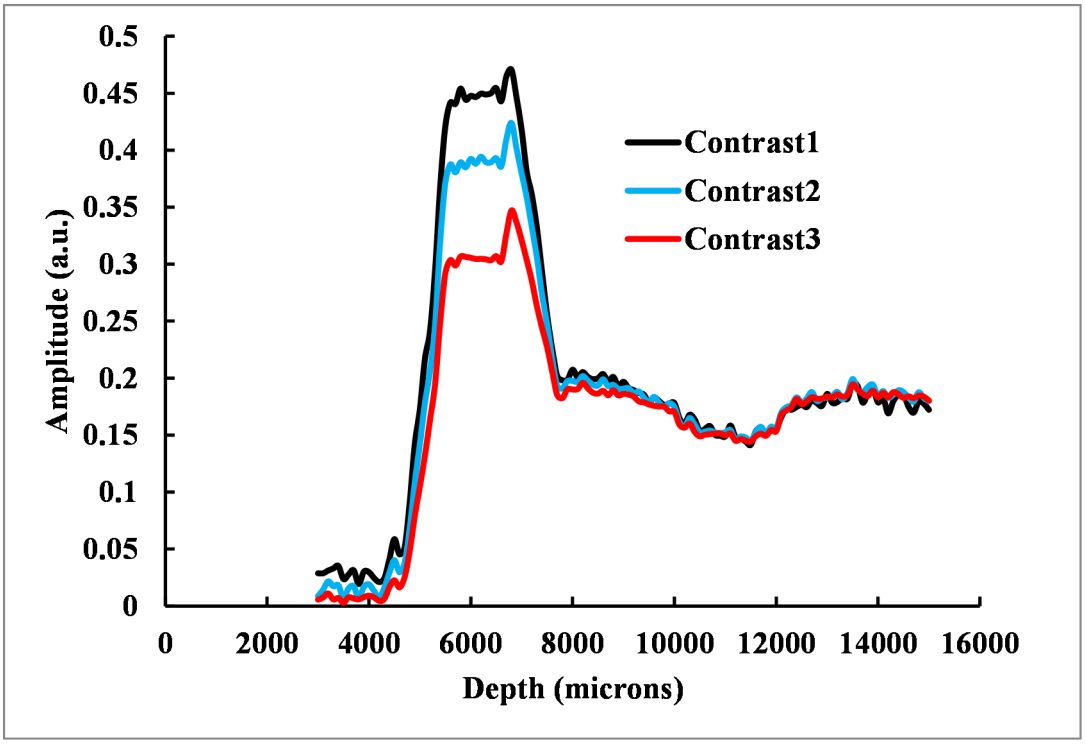

Fig. 6.10 Profile NMR data of flat test sample adhesively bonded with rubber and coated with adhesive liner with propellant

Figure 6.11 shows depth profile NMR data of cylindrical sample at one of the locations. As the sensitive volume is moved into the thickness of the sample, the response from the protons present in the material is observed due to their magnetization. The rise in magnetization is observed from 5000 microns onwards until entire thickness of rubber is covered. As the adhesive liner interface is encountered by sensitive volume, a sharp peak in the amplitude is observed at that instant. When amplitude of each step of thickness is plotted, the depth profile of the sample is obtained as shown in the Figure 6.11. The sharp rise in amplitude at 9000 microns is due to the presence of adhesive liner interface at that point. The depth profile of cylindrical test sample shown in Figure 6.11 is similar to the depth profile of flat test sample. However, the rise in the amplitude for cylindrical sample is not as sharp as flat sample and more gradual. This is due to the flat nature of the sensitive volume in presence of curved sample. The nature of the curve is more due to the way the sensitive volume is interacting with the curved material of cylindrical sample as explained above. All the constituent materials of the cylindrical composite sample were distinguished from their response to magnetization. This is similar to the nature of response in case of flat composite sample. Hence, it may be concluded

that irrespective of the shape, profile NMR is able to distinguish the materials based on their response to the external magnetic fields.

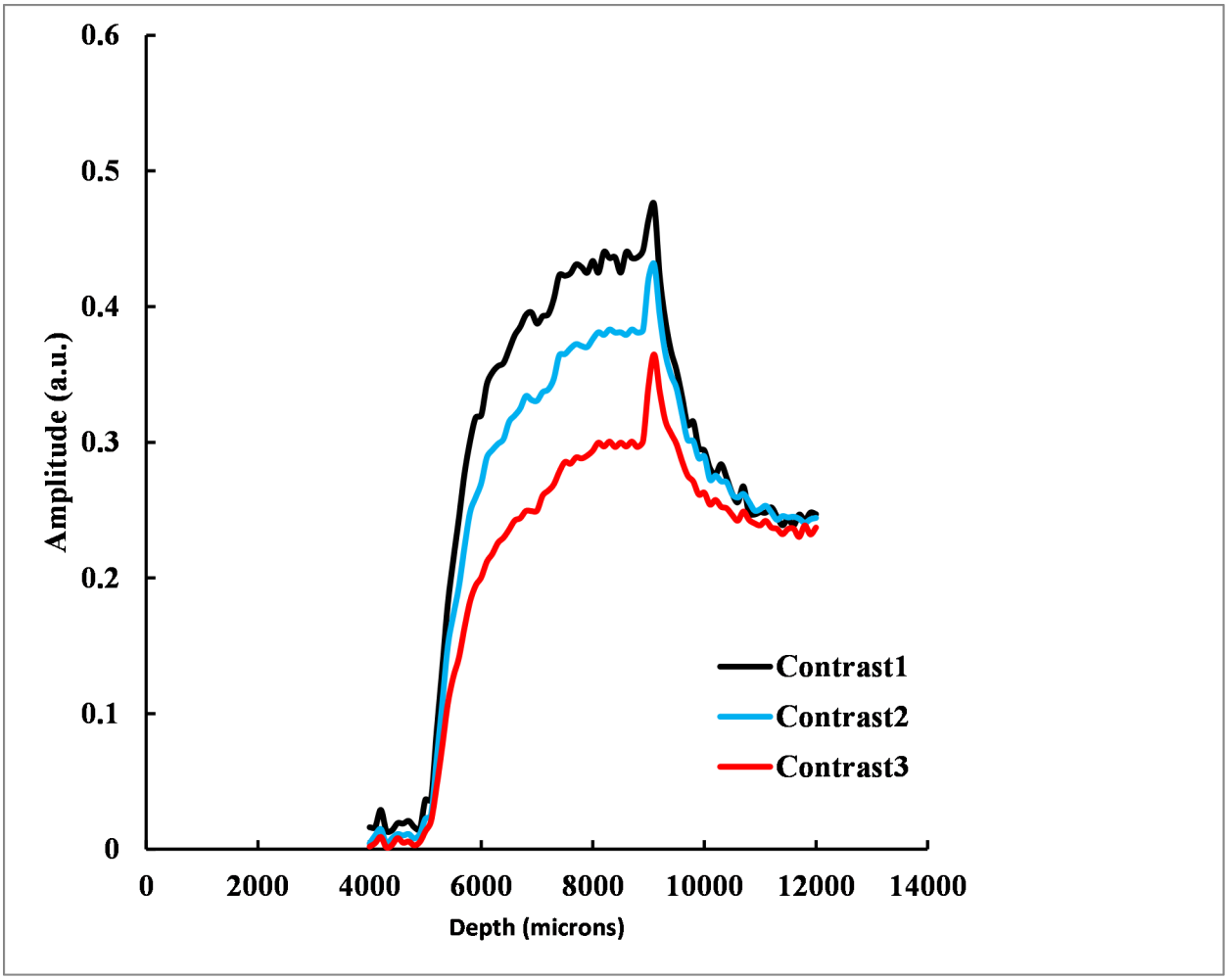

Fig. 6.11 Profile NMR data of cylindrical test sample adhesively bonded with 4 mm rubber and coated with adhesive liner with propellant

6.6. Transverse Relaxation Times

It is well known that the nature of the material can be distinguished from their response to external magnetic field. In this study, spin-spin relaxation times of the samples were compared with each other and effect of the shape factor has been analyzed. Table 6.1 shows the spin-spin relaxation times of constituent materials of flat sample and cylindrical sample. It may be observed that irrespective of the shape of the material, the chemical signature of the material remained same e.g., Rubber T_2 values short and long are similar for flat and cylindrical samples. For all the three materials the spin-spin relaxation times are distinct and comparable. Also, there

is no effect of shape on the free induction decay (FID) curve of the constituent materials. Figure 6.12 shown below depicts FID curve of constituent materials of flat composite sample.

Table 6.1 Transverse relaxation times of constituent materials rubber, adhesive liner and propellant captured using low field NMR @12.88 MHz

Material	Transverse relaxation times							
	Flat Sample				Cylindrical Sample			
	A_{short}	T_{2short} (ms)	A_{long}	T_{2long} (ms)	A_{short}	T_{2short} (ms)	A_{long}	T_{2long} (ms)
Rubber	0.8	0.7	0.2	1.5	0.7	0.6	0.3	1.7
Adhesive liner	0.6	1.2	0.4	6.4	0.7	0.9	0.3	5.4
Propellant	0.5	12	0.5	11.4	0.5	11.4	0.5	13.7

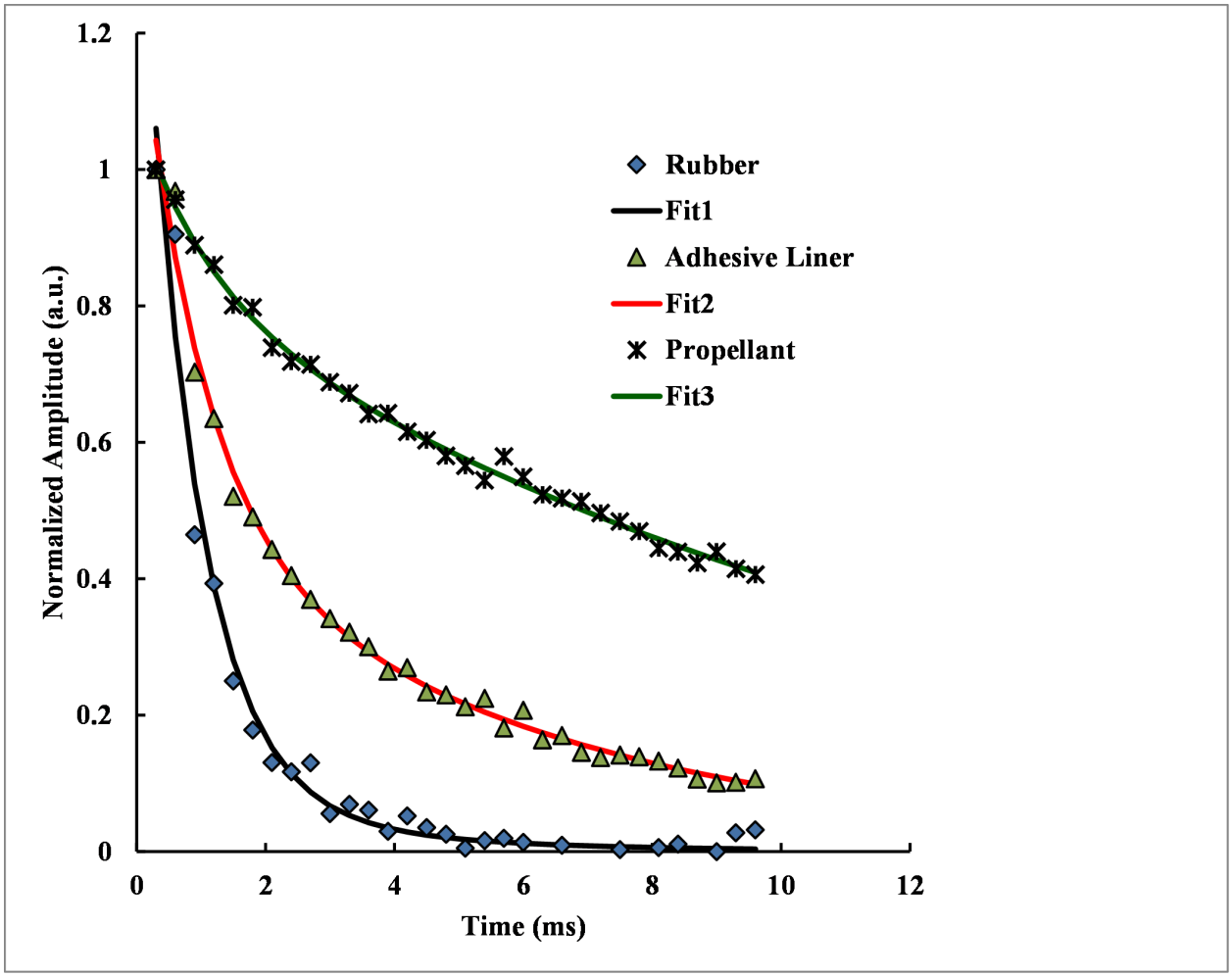

Fig. 6.12 Normalized FID curves of rubber, adhesive liner and propellant samples over flat composite laminate

Data has been captured at one location of the large sample. Figure 6.12 shows normalized FID curves of rubber, adhesive liner and propellant and they are distinct, with different slope indicating the molecular state of the material. It may be concluded that propellant has similar molecular state whereas rubber and adhesive liner has multiple molecular states within the material.

From Figure 6.12, it may be observed that FID curve of rubber is exponentially decaying faster than both adhesive liner and propellant indicating higher crosslink density of rubber as seen from their T_2 relaxation data as well shown in Table 6.1. As reported, T_2 relaxation is inversely proportional to crosslink density. However, the results have to be compared with cylindrical structure to study the effect of shape on relaxation times.

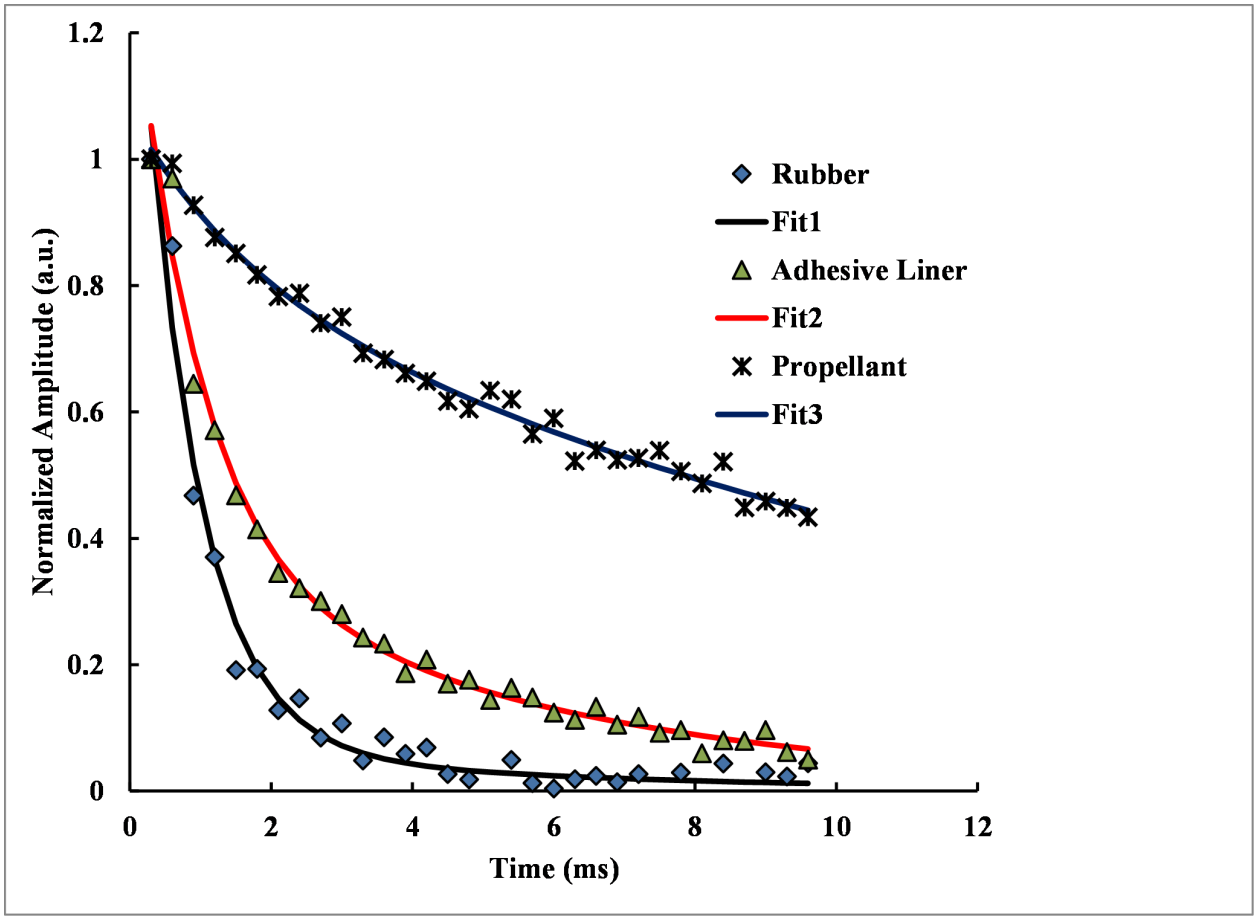

Fig. 6.13 Normalized FID curves of rubber, adhesive liner and propellant samples over cylindrical composite sample

Figure 6.13 shown above depicts normalized FID curves of rubber, adhesive liner and propellant samples of cylindrical sample. From the above figure, it may be observed that the constituent materials are distinct and has different slopes indicating nature of the constituent materials. Also, it may be concluded that the observations drawn from the NMR data of flat sample and curved sample are similar. Hence, there is no effect of shape on the NMR data either in the depth profile or in the FID curves and also there is no effect of shape factor on the estimation of spin-spin relaxation times of the constituent materials.

7. CONCLUSIONS

No perfect multi-layered composite structures can be manufactured. Rather, it is necessary to devise process and fabrication procedures to minimize the defects. Only when the role of defects in the determination of the mechanical properties is understood, attempts to control and limit their introduction into the finished article can be justified. With single sided low field NMR technique, the defects can be monitored and with appropriate mechanical testing, their role in the ultimate engineering performance of the multi-layered composite structures can be determined. The conclusions of the work are published and summarized as follows,

1. Single sided low field NMR studies are useful for assessing the soundness of constituent materials and estimation of their thicknesses with accuracies ranging from 50 microns to 200 microns.

2. Interfacial defects are detected and characterized in multi-layered GFRP composite structures.
3. Presence or absence of thin adhesive liner material between adherends is detectable.
4. Collinear defects at multiple interfaces are detectable.
5. Results obtained from the depth profile studies of multi-layered composite structures were correlated with other NDE techniques like X-ray radiography, computed tomography, microwave NDE, acousto-ultrasonic scanning for defect characterization and validation of the technique.
6. Depth profile data of flat and cylindrical composite structures indicated that the depth profile is not affected by the shape or curvature of the sample for interfacial defect detection.
7. Single sided low field NMR technique is found to be a superior NDE tool and a complete method on its own to study adhesively bonded structures as very fine flaws are detectable with better sensitivity.
8. Low field profile NMR is found to be useful for measurement of wet layers of polymer adhesive material accurately which is difficult by conventional or physical measurement methods.

8. SCOPE FOR FUTURE WORK

1. NMR imaging or tomography may be implemented as a means of detecting and imaging previously invisible imperfections to assure improved manufacture and performance of multi-layered composite structures.
2. More experimental investigation/work on depth profiling of other shaped (elliptical, parabolic, dome shaped, etc.) composite structures may be carried out for better conclusive statement regarding effect of curvature.
3. The NMR study can be extended to other Elastomeric materials like EPDM, natural rubber etc,
4. Relaxometry study may be carried out to evaluate degree of crosslinking and curing of adhesive and resin-based components as process monitoring non-destructively.

5. NMR imaging may be implemented as a structural health monitoring tool in studying the physical aging and degradation of crosslinked structures.
6. Single sided NMR as an onsite NDE tool for inspection of large size composite structures should be attempted.
7. Attempt should be made to implement low field profile NMR system with automation using AI and Mathematical models as an in-situ quality control tool in polymer, defense and aerospace sectors.

REFERENCES

1. McMaster Robert C, Nondestructive Testing, Vol. 2, 2nd Edition, ASTM and ASM, 1982.
2. McMaster Robert C, Nondestructive Testing Hand Books, Ronald Press Company, 1991.
3. McGonnagle Warren J, Nondestructive Testing, Gorden and Breach, 1971.
4. Swarup S, Jain V K, NDT standards an aid for inspection and quality assurance, Journal of Nondestructive Evaluation, Vol. 10(2), 1990.
5. Gardner W E, Improving the Effectiveness and Reliability of Nondestructive Testing, 1st Edition, Pergamon Press Limited, Oxford, UK, 1992.
6. Rummel W D, Matzkanin G A, Non Destructive Evaluation (NDE) capabilities Data Book, NTLAC :DB-97-02, Nondestructive Testing Information Analysis Centre, Texas Research institute Austin Inc., 1997.
7. Krautkramer J, Krautkramer H, Ultrasonic Testing of Materials, 3rd Edition, springer-Verlag Berlin Heidelberg, 1983.
8. Forli O, Pettersen B, The performance of conventional ultrasonic and radiographic examination, British Journal of NDT, Vol. 27(6), 1985.
9. Halmshaw R, Industrial Radiology Techniques, Wykenham Publishers, 1971.
10. Schneeman Justin G, Industrial X-ray Interpretation, Index Publishing Company, 1968.
11. Venkat Rao K, Munirathnam B, Subbiah C, Sai Suryanarayana P V, Viswanathan K, characterization of defects in large solid propellant rocket motors, 2000, 15th WCNDT, www.ndt.net.
12. Buragohain Manoj K, Composite Structures: Design, Mechanics, Analysis, Manufacturing and Testing, CRC Press, 2017.

13. Mazumdar Sanjay K, Composites Manufacturing: Materials, Product and Process Engineering, CRC Press, 2002, ISBN 0-8493-0585-3.

14. Isaac M Daniel, Ori Ishai, Engineering Mechanics of Composite Materials, Oxford University Press, 2015, ISBN-13: 978-0-19-809838-6.

15. Mallick P K, Fiber-reinforced Composites: Materials, Manufacturing, and Design, Taylor & Francis Group, USA, 2008, ISBN-13: 978-0-8493-4205-9.

16. Adams R D, Cawley P, A review of defect types and nondestructive testing techniques for composites and bonded joints, NDT International 1988; 21(4), pp.208-222.

17. Cawley P, Adams R D, The location of defects in structures from measurements of natural frequencies, The Journal of Strain Analysis for Engineering Design, 1979, Vol. 14(2), pp. 49-57, https://doi.org/10.1243/03093247V142049.

18. Adams R D, Cawley P, Pye C J, Stone B J, A vibration technique for non-destructively assessing the integrity of structures, Journal of Mechanical Engineering Science, 1978, Vol. 20(2), pp. 93-100, https://doi.org/JMES_JOUR_1978_020_016_02.Raj Baldev, Jayakumar T, Thavasimuthu M, Practical Non-destructive Testing, Narosa, 2001.

19. Ibrahim M E, Nondestructive evaluation of thick-section composites and sandwich structures: A review, Composites: Part A 64, 2014, pp.36-48.

20. Schull Peter J, Nondestructive Evaluation: Theory, Techniques and Applications, CRC Press, 2002.

21. Raj Baldev, Jayakumar T, Thavasimuthu M, Practical Non-destructive Testing, 2001, Narosa.

22. Kim Jang-Kyo. Engineered interfaces in fibre-reinforced composites, Elsevier Publications, 1998, ISBN 0-08-042695-6.

23. Burnett L J, McKay D R, Magnuson E M, Solid rocket motor NDE using nuclear magnetic resonance, Review of Progress in Quantitative Nondestructive Evaluation, 1993, Vol. 12, pp. 663-670.

24. Nieminen A O K, Koening J L, NMR imaging of the interfaces of epoxy adhesive joints, Journal of Adhesion, 1989, Vol. 30, pp. 47-56.

25. Nieminen A O K, Koening J L, Chemical shift effects in NMR imaging of adhesives and adhesive joints, Applied Spectroscopy, 1989, Vol. 43, pp. 1358-1362.

26. Nieminen A O K, Liu J W, Koening J L, NMR imaging of adhesive-bonded structures, Journal of Adhesion Science and Technology, 1989, Vol. 3(6), pp. 455-462.

27. Blümich B, Haber-Pohlmeier S, Zia W, Compact NMR, Walter de Gruyter GmbH & Co KG, 2014.

28. Macomber Roger S, A complete introduction to modern NMR Spectroscopy, John Wiley & Sons, Inc., 1998.

29. Callaghan P T, Principles of Nuclear Magnetic Resonance Spectroscopy, Claredon Press, Oxford, 1993.

30. Tsutsui A, Characterizing flame-resistant polymers using single-sided NMR, 2019, BS Thesis.

31. Saalwachter K, Heuer Andreas, Chain Dynamics in elastomers as investigated by proton multiple-quantom NMR, Macromolecules, 2006, Vol. 39, pp. 3291-3303, https://doi.org/10.1021/ma052567b.

32. Casanova F, Perlo J, Blümich B, Single sided NMR, Springer-Verlag, Berlin, 2011, ISBN 978-3-642-16306-7.

33. Blümich B, Low field and benchtop NMR, Journal of Magnetic Resonance, 2019, Vol. 306, pp. 27-35, https://doi.org/10.1016/j.jmr.2019.07.030.

34. Blümich B, NMR Imaging of Materials, Oxford University Press: Oxford, 1992.

35. Blümich B, Essential NMR for Scientists and Engineers, Springer-Verlag Berlin Heidelberg, 2005.

36. Blümich B, Blümer P, Eidmann G, Guthausen A, Haken R, Schmitz U, Saito K, Zimmer G, The NMR-mouse: construction, excitation, and applications, Magnetic Resonance Imaging, Vol. 16, Nos. 5/6, 1998, pp. 479-484.

37. Blümich B, Perlo J, Casanova F, Mobile single-sided NMR, Progress in Nuclear Magnetic Resonance Spectroscopy 52 (2008) 197-269.

38. Goga N O, Non-destructive characterization of materials by single-sided NMR, PhD Thesis, 2007.

39. Voda A E, Low field NMR for analysis of rubbery polymers, PhD Thesis, 2006.

40. Somers A E, Bastow T J, Burgar M I, Forsyth M, Hill A J, Quantifying rubber degradation using NMR, Polymer degradation and stability, 2000, Vol. 70, pp. 31-37.

41. Matzkanin G A, A review of non-destructive characterization of composites using NMR, Nondestructive Characterization of Materials, Springer-Verlag, Berlin, 1989.

42. Blümich B, Singh K, Desktop NMR and its applications from materials science to organic chemistry, Angewandte Chemie International Edition, 2017, Vol. 56, pp. 2-17, https://doi.org/10.1002/anie.201707084.

43. Srinivas K, Durga Rani N, Murthy B V S R, Single sided NMR for NDE of GFRP-rubber interface, the e-Journal of Nondestructive testing, ISSN 1435-4934, Vol.20, No.6, June 2015.

44. Halmen Norbert, Kugler C, Hochrein T, Heidemeyer P, Bastian M, Determination of the degree of cross-linking and curing with single-sided NMR, AMA Conferences 2017-Sensor 2017 and IRS^2 2017, pp. 561-566.

45. Halmen Norbert, Kugler C, Kraus E, Baudrit B, Hochrein T, Bastian M, Single -sided NMR for the measurement of the degree of cross-linking and curing, Journal of Sensors and Sensor Systems, Vol. 7 (2018), pp. 21-30.

46. Kelley M, Abdol N, Soroushian P, Keating K, Balachandra A M, Meldrum T, Monitoring real-time curing of epoxies in situ using single-sided NMR, Journal of Polymer Science, 2020, pp. 1-8, https://doi.org/10.1002/pol.20190117.

47. Blümich B, Teymouri Y, Clark R, NMR on the road: Non-destructive characterization of the crumb-rubber fraction in asphalt, https://doi.org/10.1007/s00723-018-1097-8.

48. Busse F, Rehorn C, Küppers M, Ruiz N, Stege H, Blümich B, NMR relaxometry of oil paint binders, Magn Reson Chem, 2020; 1-10. https://doi.org/10.1002/mrc.5020.

49. Tortora M, Sfarra S, Casieri C, NMR relaxometry and IR thermography to study ancient cotton paper bookbinding, Applied Sciences, 2019, https://doi.org/10.3390/app9163406.

50. Blümich B, Anferova S, Sharma S, Segre A L, Federici C, Degradation of historical paper: Nondestructive analysis by the NMR-MOUSE, Journal of Magnetic Resonance, 2003, Vol. 161, pp. 204-209.

51. Anferova S, Anferov V, Adams M, Blümler P, Routley N, Hailu K, Kupferschläger, Mallet M J D, Schroeder G, Sharma S, Blümich B, Construction of a NMR-MOUSE with short dead time, Concepts in Magnetic Resonance (magnetic Resonance Engineering), 2002, Vol. 15(1), pp.15-25.

52. Balibanu F, Hailu K, Eymael R, Demco D E, Blümich B, NMR in inhomogeneous magnetic fields, Journal of Magnetic Resonance, 2000, Vol. 145, pp. 246-258.

53. Tarpani J R, Portela A M A, Magnetic resonance imaging of contaminated and damaged core cells in polymer composite sandwich panels, Journal of Sandwich Structures and Materials, 2017, pp. 1-30, DOI:10.1177/1099636216681698.

54. Ibarra-Castanedo C, Tarpani J R, Maldague X P V, Non-destructive testing with thermography, European Journal of Physics, 2013, Vol. 34(6), https://doi.org/10.1088/0143-0807/34/6/S91.

55. Alves C L, Oliveira J S, Tannus A, Tarpani A C S P, Tarpani J R, Detection and imaging of damages and defects in fibre-reinforced composites by resonance magnetic technique, Preprints 2019, 2019120295, DOI:10.20944/preprints201912.0295.v3.

56. Souza G, Tarpani J R, Distributed fiber optics sensing applied to laminated composites: embedding process, strain field monitoring with OBR and fracture mechanisms, Journal of Nondestructive Evaluation, 2020, Vol. 39(4), pp. 1-15.

57. LaPlante G, Marble A E, MacMillan B, Lee-Sullivan P, Colpitts B G, Balcom B J, Detection of water ingress in composite sandwich structures : A magnetic resonance approach, NDT&E International, 2005, Vol. 38, pp. 501-507.

58. Eidmann G, Savelsberg R, Blümler P, Blümich B, The NMR MOUSE, a mobile universal surface explorer, Journal of Magnetic Resonance A, 1996, Vol. 122, pp. 104-109.

59. Marble A E, LaPlante G, Mastikhin I V, Balcom B J, Magnetic resonance detection of water in composite sandwich structures, NDT&E International, 2009, Vol. 42, pp. 404-409.

60. Alston S, Arnold C, Swan M, Stone C, The use of single-sided NMR to study moisture behaviour in an activated carbon fibre/phenolic composite, Applied Magnetic Resonance, 2020, https://doi.org/10.1007/s00723-020-01273-3.

61. Köller E, Dobmann G, Kuhn W, Non-destructive characterization of prepreg aging using nuclear magnetic resonance techniques, Research in Non-destructive Evaluation, 1990, Vol. 2, pp. 187-194.

62. Xu Z, Li L, Guo P, Ji Y, Wu J, He C, Portable unilateral NMR measuring system for assessing the ageing status of silicon rubber insulators, Applied Magnetic Resonance, 2018, https://doi.org/10.1007/s00723-018-1061-7.

63. Siegfried J, Marion I M, Dagmar V D, Gerhard W R, Jonas B, Senay M, Blümler P et al, Combined MRI–PET dissects dynamic changes in plant structures and functions, The Plant Journal, 2009, Vol. 59(4), pp. 634-644.

64. Windt C W, Helmut S, Dagmar V D, Blümler P, A portable Halbach magnet that can be opened and closed without force: the NMR-CUFF, Journal of Magnetic Resonance, 2011, Vol. 208(1), pp. 27-33.

65. Guthausen A, Zimmer G, Blümler P, Blümich B, Analysis of polymer materials by surface NMR via the MOUSE, Journal of Magnetic Resonance, 1998, Vol. 130(1), pp. 1-7.

66. Anferova S, Anferov V, Rata D G, Blümich B, Arnold J, Clauser C, Blümler P, Raich H, A mobile NMR device for measurements of porosity and pore size distributions of drilled core samples, Concepts in Magnetic Resonance Part B: Magnetic Resonance Engineering: An Educational Journal, 2004, Vol. 23(1), pp. 26-32.

67. Blümler P, Blümich B, Aging and phase separation of elastomers investigated by NMR imaging, Macromolecules, 1991, Vol. 24(9), pp. 2183-2188.

68. Anferova S, Anferov V, Arnold J, Talnishnikh E, Voda M A, Kupferschläger K, Blümler P, Clauser C, Blümich b, Improved Halbach sensor for NMR scanning of drill cores, Magnetic Resonance Imaging, 2007, Vol. 25(4), pp. 474-480.

69. Blümich B, Casanova F, Dabrowski M, Danieli E, Evertz L, Haber A, Landeghem M V, Haber-Pohlmeier S, Olaru A, Perlo J, Sucre O, Small-scale instrumentation for nuclear magnetic resonance of porous media, New Journal of Physics, 2011, Vol. 13, 015003 (15pp), https://doi.org/10.1088/1367-2630/13/1/015003.

70. Oliveira-Silva R, Lucas-Oliveira E, Araujo-Ferreira A G, Trevizan W A, Vidoto E L G, Sakellariou D, Bonagamba T J, A benchtop single-sided magnet with NMR well-logging tool specifications – Examples of application, Journal of Magnetic Resonance, 2021, https://doi.org/10.1016/j.jmr.2020.106871.

71. Danieli E, Blümich B, Single-sided magnetic resonance profiling in biological and materials science, Journal of Magnetic Resonance, 2012, https://dx.doi.org/10.1016/j.jmr.2012.11.023.

72. Mauler J, Casanova F, Blümich B, Shaping the sensitive volume of a single-sided NMR-sensor to profile cylindrical samples with high resolution, Applied Magnetic Resonance, 2013, https://doi.org/10.1007/s00723-013-0484-4.

73. Halmshaw R, Industrial Radiology : Theory and Practice, 2nd edition, Chapman and Hall, 1996.

74. Raju P K, Acousto-ultrasonic technique for non-destructive evaluation of composites and structures, Journal of Acoustical Society of America, Vol. 102, November 1997, pp. 3082.

75. Mareeswaran S, Sasikumar T, The Acousto-Ultrasonic Technique : A review, International Journal of Mechanical Engineering and Technology, 8(6), June 2017, pp. 418-434.

76. Srivastava V K, Acousto-ultrasonic evaluation of interface bond strength of coated glass fibre-reinforced epoxy resin composites, Composite structures, 30 (1995), pp. 281-285.

77. Vary A, The acousto-ultrasonic approach, NASA Lewis Research Centre, Cleveland, Ohio 44135.

78. Natraj S, Ravindran V K, Somanathan S, Rajkumar N, Manna S S, Sumangali R, Valsa B, Ultrasonic and Acousto-ultrasonic evaluation of polyimide pipes and its interface for cryogenic rocket stages for space launch vehicles, NDE 2016, http://www.ndt.net/?id=21202.

79. Somanathan S, Ravindran V K, Natraj S, Rajkumar N, Manna S S, Sumangali R, Valsa B, Method for evaluation of bond between acoustic attenuation foam and composite panels of payload fairings of large launch vehicle, NDE 2016, http://www.ndt.net/?id=21205.

80. Kwon Oh-Yang, Lee Seung-Hwan, Acousto-ultrasonic evaluation of adhesively bonded CFRP-aluminum joints, NDT& E International, 32 (1999), pp. 153-160.

81. Daniel I M, Luo J J, Hsiao H M, Acousto-ultrasonic techniques for evaluation of bond integrity of composite repair patches, Review of progress in quantitative non-destructive evaluation, Vol. 17, 1998, pp. 1331-1338.

82. Moon S M, Jerina K L, Hahn H T, Acousto-ultrasonic wave propagation in composite laminates, Springer US, 1988, pp. 111-125.

83. Tiwari Anil, Edmund G, Henneke II, Duke John C, Acousto-ultrasonic (AU) technique for assuring adhesive bond quality, The Journal of Adhesion, 1991, Vol. 34, pp. 1-15.

84. Ibrahim M E, Smith R A, Wang C H, Ultrasonic detection and sizing of compressed cracks in glass and carbon fibre reinforced plastic composites, NDT & E International, 2017, Vol. 92, pp. 111-121.

85. Ibrahim M E, Headland D, Withayachumnankul W, Wang C H, Nondestructive Testing of Defects in Polymer–Matrix Composite Materials for Marine Applications Using Terahertz Waves. Journal of Nondestructive Evaluation, 2021, Vol. 40(2), pp. 1-11.

86. Ibrahim M E, Phillips A W, Ditchburn R J, Wang C H, Nondestructive evaluation of mechanically loaded advanced marine composite structures, In Advanced materials research, 2014, Vol. 891, pp. 594-599.

87. Mukherjee S, Tamburrino A, Haq M, Udpa S, Udpa L, Far field microwave NDE of composite structures using time reversal mirror, NDT & E International 2018, Vol. 93, pp. 7-17.

88. Mukherjee S, Tamburrino A, Udpa l, Udpa S, NDE of composite structures using microwave time reversal imaging, In AIP Conference Proceedings, 2016, Vol. 1706(1), pp. 100002.

89. Green G A, Campbell P, Zoughi R, An investigation into the potential of microwave NDE for maritime application, In 16th World Conference of Non-Destructive Testing, 2004, Vol. 30.

90. Hughes D, Kazemi M, Marler K, Zoughi R, Myers J, Nanni A, Microwave detection of delaminations between fiber reinforced polymer (FRP) composite and hardened cement paste, In AIP Conference Proceedings, 2002, Vol. 615(1), pp. 512-519.

91. Bharath A, Hughes D, Zoughi R, Myers J, Nanni A, Near-field microwave detection of disbond in carbon fiber reinforced polymer composites used for strengthening cement-based structures and disbond repair verification, Journal of materials in civil engineering, 2004, Vol. 16(6), pp. 540-546.

92. Mahmut E, Stephen V, Myers J, ZoughiR, Microwave NDE of RC beams strengthened with CFRP laminates containing surface defects and tested under cyclic

loading, Electrical and Computer Engineering, University of Missouri-Rolla, Rolla MO 65409, 2004, pp. 1-8.

93. Khousa A, Mohamed A, Ryley A, Kharkovsky S, Zoughi R, Daniels D, Kreitinger N, Steffes G, Comparison of X-ray, millimeter wave, shearography and through-transmission ultrasonic methods for inspection of honeycomb composites, In AIP Conference Proceedings, 2007, Vol. 894(1), pp. 999-1006.

94. Garcea S C, Wang Y, Withers P J, X-ray computed tomography of polymer composites, Composites Science and Technology, 2018, Vol. 156, pp. 305-319.

95. Katunin A, Wronkowicz-Katunin A, Dragan K, Impact damage evaluation in composite structures based on fusion of results of ultrasonic testing and X-ray computed tomography, Sensors, 2020, Vol. 20(7), pp. 1867.

96. Senck S, Scheerer M, Revol V, Dobes K, Plank B, Kastner J, Non-destructive evaluation of defects in polymer matrix composites for aerospace applications using X-ray Talbot-Lau interferometry and micro CT, In 58th AIAA/ASCE/AHS/ASC Structures, Structural Dynamics, and Materials Conference, 2017, pp. 0355.

97. Gokul Asha, Srinivas K, Dhanasekaran J, Inspection of profiled FRP composite structures by microwave NDE, International Journal of Microwave Engineering, Vol. 5, January 2020.

98. Gokul Asha, Srinivas K, Dhanasekaran J, Bond quality inspection of bonded surfaces using microwave NDE, International Journal of Advances in Microwave Technology, Vol. 4, November 2019.

99. Zoughi R, Microwave Non-Destructive Testing and Evaluation, Springer Netherlands, 2000.

100. Ida N, Microwave NDT, Developments in Electromagnetic Theory and Applications, Vo. 10, Kluwer Academic Publishers, 1992.

Publications

Articles in Peer Reviewed Journals

1. Sanjaya K. Sahoo, Srinivas Kuchipudi, R. Narasimha Rao, Manoj K. Buragohain, Ch Sri Chaitanya, Application of low field magnetic resistance for defect detection in multi-layered cylindrical composite structures, Nondestructive Testing and Evaluation. https://doi.org/10.1080/10589759.2021.1889549. Impact Factor: 1.424 **[SCI]**
2. Sanjaya K. Sahoo, Srinivas Kuchipudi, R. Narasimha Rao, Manoj K. Buragohain, Ch Sri Chaitanya, Detection of planar defects in multi-layered GFRP composite structures using low field NMR, Materials Evaluation. Impact Factor: 0.772 **[SCI]**
3. Sanjaya K. Sahoo, Srinivas Kuchipudi, Deo Kumar Verma, R. Narasimha Rao, Manoj K. Buragohain, A study on effect of shape on depth profile NMR data of multi-layered composite structure. (under review)
4. S. K. Sahoo, R. N. Rao, K. Srinivas, M. K. Buragohain, NDE of glass fiber reinforced composite structures using single sided solid-state proton NMR, Materials Today: Proceedings 21 (2020) 1239-1243. Impact Factor: 0.576 **[SCOPUS]**
5. S. K. Sahoo, R. N. Rao, Asha Gokul, K. Srinivas, M. K. Buragohain, Comparison of NMR and microwave NDE methods for defect detection in composite structures, Materials Today: Proceedings 18 (2019) 4074-4081. Impact Factor: 0.576 **[SCOPUS]**
6. S. K. Sahoo, R. N. Rao, K. Srinivas, M. K. Buragohain, Application of single sided NMR and Acousto-Ultrasonic methods for NDE of composite structures, Lecture Notes in Mechanical Engineering, Lecture Notes in Mechanical Engineering, https://doi.org/10.1007/978-981-15-1201-8_61 547-555. **[SCOPUS]**
7. S. K. Sahoo, R. N. Rao, Y. L. V. D. Prasad, K. Srinivas, M. K. Buragohain, NDE of GFRP composite laminates using single sided NMR and Acousto-Ultrasonic methods, Journal of NDE (ISNT), 17(17), June 2019, pp. 26-29.
8. S. K. Sahoo, R. N. Rao, K. Srinivas, M. K. Buragohain, Ch Sri Chaitanya, A novel NDE approach towards evaluating adhesive bonded interfaces, Materials Today: Proceedings 26 (2020) 1191-1197, https://doi.org/10.1016/j.matpr.2020.02.240. Impact Factor: 0.576 **[SCOPUS]**

Conferences

1. S. K. Sahoo, R. N. Rao, Y. L. V. D. Prasad, K. Srinivas, M. K. Buragohain, Study of single sided solid-state proton NMR for NDE of glass/epoxy composite and rubber bonded interface, ETME-2019, 9-10 Jan 2019, NIT Warangal.

2. S. K. Sahoo, R. N. Rao, Y. L. V. D. Prasad, K. Srinivas, M. K. Buragohain, NDE of GFRP composite laminates using single sided NMR and Acousto-Ultrasonic methods, ICAFMD-2019, 26-28 Feb 2019, NIT Warangal.

Bio Data

Name: Sanjaya Kumar Sahoo

Contact: +91 4024309222

Email: sahoosanjayk@rediffmail.com

Address: Advanced Systems Laboratory, DRDO,
Kanchanbagh, Hyderabad-500058,
Telangana, India

Area of Research: Non-destructive Evaluation, Composite Materials, High-energy Radiography, Ultrasonic Testing, Single-sided NMR.

Educational Qualification:

Degree	Institute	Specialization	Graduated
H. S. C.	Nilamadhaba Vidyapitha, Kantilo	Mathematics, Science and Social Studies	1992
Diploma	Uma Charan Patnaik Engineering School, Berhampur	Mechanical Engineering	1995
B. E.	Regional Engineering College, Rourkela	Mechanical Engineering	1999
M. Tech	Indian Institute of Technology, Kanpur	Solid Mechanics and Design	2002
Ph. D.	National Institute of Technology, Warangal	Mechanical Engineering	Present

Work Experience

1. 1999-2000 – Graduate Operators Trainee, TATA Steel
2. 2001-Present – Scientist, Defence R & D Organisation (DRDO)

Publications: 18

1. Peer Reviewed Journals: 5

2. Conference Publications in Peer Reviewed Journals: 3
3. Conference Publications as Book Chapters: 1
4. Invited Conference Proceedings: 1
5. Conference Proceedings: 8

Memberships

1. Life Member – Indian Society for Non-destructive Testing (ISNT)
2. Life Member – High Energy Materials Society of India (HEMSI)

Reviewer Service

1. Nondestructive Testing and Evaluation (Taylor & Francis)